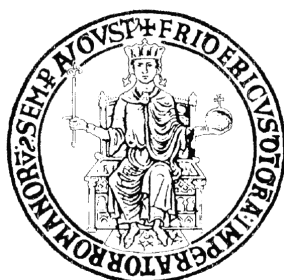


UNIVERSITA' DEGLI STUDI DI NAPOLI FEDERICO II



FACOLTA' DI SCIENZE MATEMATICHE FISICHE E NATURALI

PhD IN CHEMISTRY

XXIII CYCLE

SCREENING OF BACTERIAL  
MOLECULES WITH ANTAGONISTIC OR  
ADJUVANT ACTIVITY

Eleonora Fregolino

TUTOR

Dott.ssa  
Cristina De Castro

SUPERVISOR

Prof.ssa  
Paola Giardina

**Abstract**

v

**PART I: INTRODUCTION*****Chapter I: Structures and functions of polysaccharide components of the Gram-negative bacteria Outer Membrane***

1.1 Bacterial Cell Envelope	1
1.2 General architecture, function and biosynthesis of the Lipopolysaccharide (LPS)	2
1.3 The Core oligosaccharide and O-Specific Side Chain	5
1.4 Structure and biological activity of Lipid A	6
1.5 Capsular polysaccharides (CPSs) and glycoconjugate vaccines	10

***Chapter II: General aspects***

2.1 <i>Rhizobium radiobacter</i> RV3 as a source of oligosaccharide with potential use for HIV vaccine production	12
2.2 <i>Cupriavidus necator</i>	13
2.3 <i>Acinetobacter baumannii</i>	13
2.4 Virulence factors of <i>Escherichia coli</i> and the <i>Enterobacterial common antigen</i>	14

**PART II: RESULTS AND DISCUSSION*****Chapter III: Synthesis of new neoglycoprotein using mannan oligosaccharide from Rhizobium radiobacter RV3***

3.1 LOS chemical analyses	16
3.2 NMR analysis of Core oligosaccharide	17
3.3 Characterization of OS-BSA conjugate	22
3.4 Conclusions	27

***Chapter IV: Characterization of the O-Chain and Lipid A portions of the LPS from Cupriavidus necator DSM 13523***

4.1 Chemical analyses of the Lipopolysaccharide	28
4.2 Structural characterization of Lipid A	29
4.3 Spectroscopic analysis of the O-Chain	32
4.4 Conclusions	36

***Chapter V: Lipooligosaccharide structural characterization of a clinical isolate of Acinetobacter baumannii, strain SMAL***

5.1 Chemical analyses of the Lipooligosaccharide	37
5.2 Mass spectrometry analysis of the intact and ammonia-deacylated Lipid A from the growth in Luria Broth at 28 °C	38
5.3 Structural variation of Lipid A under different growth conditions	42
5.4 Spectroscopic characterization of Core oligosaccharide from the growth in Luria Broth at 28 °C	44
5.5 Conclusions	47

**Chapter VI: Identification and structural determination of the Capsular polysaccharides from two clinical isolates of *Acinetobacter baumannii*, strains SMAL and MG1**

6.1 Isolation and chemical analyses of ultracentrifuge supernatants and sediment	49
6.2 Electrophoretic and Western blot analysis of ultracentrifuge supernatant and sediment	50
6.3 Spectroscopic characterization of the CPS from <i>A. baumannii</i> strain MG1	51
6.4 Spectroscopic characterization of the CPS from <i>A. baumannii</i> strain SMAL	55
6.5 Conclusions	59

**Chapter VII: LPS analysis and isolation of two forms of cyclic Enterobacterial common antigen (ECA) from the enterohaemorrhagic *Escherichia coli* O157:H**

7.1 Screening of phenol and water extracts of <i>E. coli</i> O157:H at 37°C and 20°C	60
7.2 Purification and immunodetection analysis of LPS in water extracts	62
7.3 Characterization of the two cyclic forms of the <i>Enterobacterial common antigen</i>	65
7.4 Conclusions	68

**PART III: MATERIALS AND METHODS**

**Chapter VIII: Isolations of Lipopolysaccharides and Capsular Polysaccharides**

8.1 <i>Rhizobium radiobacter</i> RV3	70
8.2 <i>Cupriavidus necator</i> DSM 13513	70
8.3 <i>Acinetobacter baumannii</i> clinical isolates SMAL and MG1	71
8.4 <i>Escherichia coli</i> O157:H	72

**Chapter IX: General and analytical methods**

9.1 Electrophoretic and chemical analyses	73
9.2 Immunodetection analyses	74
9.3 Isolation of oligosaccharides from LOS of <i>Rhizobium radiobacter</i> RV3	75
9.4 Preparation of the carbohydrate component of the neoglycoprotein	75
9.5 Synthesis and characterization of OS-BSA conjugate	75
9.6 Isolation of the 4-deoxy-β-D-arabinohexose	77
9.7 Isolation of oligosaccharides from LOS of <i>A. baumannii</i> strain SMAL	77
9.8 Chemical treatments on CPSs from <i>A. baumannii</i> strains SMAL and MG1	77
9.9 LPS purification and isolation of the <i>Enterobacterial common antigen</i> from <i>E. coli</i> O157:H	78

**Chapter X: Mass Spectrometry**

10.1 Preparations of Lipid As	79
10.2 Electrospray Ionization Fourier-Transform Ion Cyclotron Resonance Mass Spectrometry	79
10.3 MALDI-TOF Mass Spectrometry	80

**Chapter XI: NMR spectroscopy**

11.1 Oligosaccharides from <i>Rhizobium radiobacter</i> Rv3	81
11.2 O-Chain from <i>Cupriavidus necator</i>	81
11.3 Oligosaccharides from <i>Acinetobacter baumannii</i> SMAL and MG1	81
11.4 Capsular polysaccharides from <i>Acinetobacter baumannii</i> SMAL and MG1	82
11.5 O-Chain and the <i>Enterobacterial common antigen</i> from <i>E. coli</i> O157: H	82

## **PART IV: STRUCTURAL CHARACTERIZATION OF MENB OMVs MEMBRANE CONSTITUENTS<sup>1</sup>**

<b>1 Introduction</b>	83
1.1 <i>Neisseria meningitidis</i> and the new vaccine approach against group B based on Outer Membrane Vesicles (OMVs)	83
<b>2 Results and discussions</b>	85
2.1 Structural characterization of the polysaccharide components on Outer Membrane Vesicles (OMVs) of <i>Neisseria meningitidis</i> serogroup B (MenB)	85
2.1.1 NMR analyses of native Capsular polysaccharide and of intact OMVs	86
2.1.2 Electrophoretic and Spectroscopic analyses of LOS and CPS extracted from OMVs	87
2.1.3 GC-MS quantification of LOS immunotypes	89
2.1.4 MALDI MS spectrometry characterization of Lipid A	94
2.1.5 Chemical and electrophoretic analyses to determine the content of LOS and CPS outside the OMVs	98
<b>3 Materials and Methods</b>	100
3.1 Isolations of Lipopolysaccharide and Capsular polysaccharide	100
3.1.1 Outer Membrane vesicles of <i>Neisseria meningitidis</i> serogroup B	
3.2 General and analytical methods	101
3.2.1 SDS-PAGE and chemical analyses of LOS and CPS from OMVs	
3.3 Preparations and Mass Spectrometry of Lipid A	102
3.3.1 MALDI MS spectrometry of intact Lipid A from <i>N. meningitidis</i> serogroup B	
3.4 NMR spectroscopy	102
3.4.1 Capsular polysaccharide of <i>Neisseria meningitidis</i> serogroup B	
<b>References</b>	103

---

<sup>1</sup> This part of the thesis regards a project developed in collaboration with the Novartis Vaccines Diagnostic of Siena and it is reported as accepted by a clearance process.



## Abstract

The Lipopolysaccharides (LPSs) are the major constituents of the outer membrane of Gram-negative bacteria and the interest in their chemical characterization is motivated by the close correlation existing between the structure and the biological activity of these molecules.<sup>1</sup> In particular, the glycolipid portion of the LPS, the Lipid A, is the real endotoxic principle since it triggers the innate immune system of infected organism.<sup>2</sup> The intrinsic structural variability of the Lipid A is on the basis of its different biological activity, ranging from the activation to the inhibition of an inflammatory process, and for this reason a Lipid A is classified as agonist or antagonist.<sup>3</sup> The ability of Lipid A to stimulate the innate immune system that in turn activates the adaptive immunity, makes this molecule a useful vaccine adjuvant.

The present thesis deals with the structural study of Lipopolysaccharides and Capsular polysaccharides (CPSs) from different Gram-negative bacteria:

The Lipooligosaccharide (LOS) structure produced by *Rhizobium radiobacter* Rv3 was determined through spectroscopic studies. It shows the occurrence of a mannose oligosaccharide analogue to the D1 arm of the gp120 oligosaccharide shield, recognized by the broadly neutralizing human anti-HIV antibody 2G12.<sup>4</sup> This discovery opened the attractive way to the use of this bacterium for potential HIV vaccine development: a new neoglycoprotein was realized, possessing as antigen portion the modified LOS linked, through a spacer, to the commercial Bovine Serum Albumin (BSA).

In order to find a Lipid A with a potential antagonistic activity, structural features of this molecule, produced by the non-pathogen *Cupriavidus necator*<sup>5</sup> DSM 13523, were explored. This choice starts from the assumption that structural moieties of organisms that do not enter in contact with humans, may be not or poorly recognized by the immune system; so it is likely that they have low, no toxic or antagonistic activity. *Cupriavidus necator* produces mainly a symmetric hexa-acyl Lipid A made up of a diphosphorylated disaccharide glucosamine backbone, peculiarly substituted only by fourteen carbons chains: the tetradecanoic, the 2- and 3- hydroxytetradecanoic acid. Different Lipid As from non-pathogenic bacteria as *Rhodobacter capsulatus*, *Rhodobacter spheroids* and *Chromobacter violaceum* were described as antagonists;<sup>3</sup> in particular, the Lipid A from *Chromobacter violaceum* possessed an hexa-acyl symmetric structure, similarly to that found for *Cupriavidus necator*. These assumptions increase the interest to the investigation of the biological activity of *Cupriavidus necator* Lipid A. The O-polysaccharide repeating unit produced by *Cupriavidus necator*<sup>6</sup> DSM 13523 was

---

<sup>1</sup> Raetz, C.R.H and Whitfield, C. *Ann. Rev. Biochem.*, 2002, **71**, 635.

<sup>2</sup> Miyake, K. *Trends Microbiol.* 2004, **12**, 186.

<sup>3</sup> Seydel, U.; Oikawa, M.; Koichi Fukase, K.; Kusumoto, S. and Brandenburg, K. *Eur. J. Biochem.*, 2000, **267**, 3032.

<sup>4</sup> Pantophlet, R. and Burton, D. *Ann. Rev. Immunol.*, 2006, **24**, 739.

<sup>5</sup> Zeph, L. R. and Casida, Jr. *Appl. Environ. Microbiol.*, 1986, **52**, 819.

also disclosed through spectroscopic analyses and it consisted only of deoxy sugars: four rhamnose units and one 4-deoxy- $\beta$ -D-*arabino*hexose unit.

The complete structural characterization of the Lipooligosaccharide produced by a clinical isolate of *Acinetobacter baumannii* strain SMAL was determined to provide valuable information on the mechanism activity adopted by this emerging pathogen. The Core oligosaccharide is formed of twelve sugar residues, organized in a highly branched inner Core moiety. It was found to be similar to that of *Acinetobacter baumannii* ATCC 19606,<sup>7</sup> although the LOS from the strain SMAL presented an enhanced zwitterionic character. The features presented by this structure, might reflect the adaptation of the bacterium to the host environment; in particular, the presence of cationic amino sugars decrease the net negative charge of the Core region and thus might shield the bacterial membrane from the effect of host defence agents, like the cationic antimicrobial peptides. Regarding to the Lipid A structure, mass spectrometry experiments revealed that it is composed of a heterogeneous blend of molecules differing for type and degree of acylation. The proportion among the differently acylated species changed in response to the growth conditions: predominance of the hepta-acylated species was observed when the bacterium was grown in Fetal Bovine Serum at 37°C (chosen as a mimic of the host environment), whereas the hexa-acylated molecular species resulted more abundant using Luria Broth as growth medium. The results would suggest that the production of the hepta-acyl Lipid A is a mechanism of adaptation to the mammalian host, and also able to confer antibiotic resistance to the bacterium.

The structure of Capsular Polysaccharides by two clinical isolates of *A. baumannii* strains SMAL and MG1 was elucidated. Hot phenol/water extractions of the dry biomasses, followed by enzymatic digestions and repeated ultracentrifugations led to the isolation of capsular material: these polysaccharides were negative to Western Blot analysis with anti-lipid A antibodies, and their structures were established through spectroscopic and chemical analyses. The *A. baumannii* MG1 CPS consisted of a linear aminopolysaccharide and it is quite similar to the *O*-Chain of the LPS from *A. baumannii* strain 24.<sup>8</sup> The repeating unit of the CPS produced by strain SMAL comprised a branched pentasaccharide backbone, which was previously described as the *O*-antigen of another *Acinetobacter baumannii* species (strain ATCC 17961)<sup>9</sup>, while here it occurs as a capsule. These results highline that care must be taken in the development of these diagnostic devices, because similar if not identical polysaccharides might be constituents of the Lipopolysaccharides *O*-antigen or of the bacterial envelope capsule, as reported for *A. baumannii* SMAL and MG1. Furthermore, this study may contribute significantly to the establishment of serotyping scheme for this bacterium.

The study conducted on the LPS produced by the enterohaemorrhagic *E. coli* O157:H<sup>-</sup>, subject of a collaboration, demonstrated that it is was not affected by the phenomenon of the phase variation but

---

<sup>7</sup> Vinogradov, E. V.; Duus, J. Ø.; Brade, H. and Holst, O. *Eur. J. Biochem.*, 2002, **269**, 422.

<sup>8</sup> Vinogradov, E. V.; Brade, L.; Brade H. and O. Holst. *Carbohydr. Res.*, 2003, **338**, 2751.

<sup>9</sup> MacLean, L.; Perry, M. B.; Chen, W. and Vinogradov, E. V. *Carbohydr. Res.*, 2009, **344**, 474.

also that it produced two cyclic forms of the *Enterobacterial common antigen*:<sup>10</sup> the tetrameric ECA<sub>CYC</sub> and the pentameric ECB<sub>CYC</sub>. The presence of ECA<sub>CYC</sub> for a pathogenic strain of *E.coli* together with the pentameric form, ECB<sub>CYC</sub>, represents a new datum and further studies will be focused on the study of biological functions of these molecules and eventually on their implication as a virulence factor.

The last part of the thesis is the result of a collaboration with the Novartis Vaccines Diagnostic of Siena concerning the analyses of the polysaccharide components on the Outer Membrane Vesicles (OMVs) of *Neisseria meningitidis* group B (MenB). In particular, one of the target was focused on the isolation and structural characterization of the Lipooligosaccharide in order to define the LOS immunotypes of the strain used for vaccine production. The Lipid A family of the strain was also structurally defined through MALDI mass spectrometry and the penta-acyl Lipid A resulted the predominant specie. Finally, the content of LOS and CPS outside vesicles was determined, as well.

Parts of this thesis has been adapted from the following articles:

Fregolino, E.; Fugazza, G.; Galano, E.; Gargiulo, V.; Landini, P.; Lanzetta, R.; Lindner, B.; Pagani, L.; Parrilli, M.; Holst, O. and De Castro, C. Complete Lipooligosaccharide Structure of the Clinical Isolate *Acinetobacter baumannii*, Strain SMAL. *Eur. J. Org. Chem.* **2010**, 7, 1345-1352

Fregolino E., Gargiulo V., Lanzetta R., Parrilli M., Holst O., De Castro C. Identification and structural determination of the capsular polysaccharides from two *Acinetobacter baumannii* clinical isolates, MG1 and SMAL. (Submitted to *Organic & Biomolecular Chemistry* in September 2010).

---

<sup>10</sup> Erbel, P.J; Barr, K.; Gao, N.; Gerwig, J.G.; Rick, P.D. and Gardner, K.H. *J. Bacteriol.*, 2003,**185**, 1995.



## PART I: INTRODUCTION

### CHAPTER I

#### STRUCTURES AND FUNCTIONS OF POLYSACCHARIDE COMPONENTS OF THE GRAM-NEGATIVE BACTERIA OUTER MEMBRANE

##### 1.1 Bacterial Cell Envelope

Bacteria have evolved a sophisticated cell envelope or membrane that protects the cytoplasm and contains a wide variety of biological molecules involved in many cellular processes. Cell envelope is composed by a series of layers, and their organization allows the distinction of two different families of bacteria: Gram-positives and Gram-negatives (figure 1.1.1).

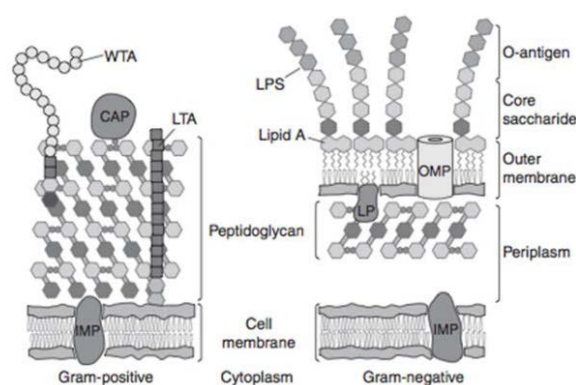


Figure 1.1.1: Depiction of the cell envelope in Gram-positive and Gram-negative bacteria

Three principal layers are individuated in Gram-negative cell envelope: the outer membrane (OM), the periplasm and the inner membrane (IM). The OM has a peculiar asymmetrical organization, it consists of glycerophospholipids and lipoproteins in the inner leaflet and of Lipopolysaccharides (LPSs) in the outer leaflet. The OM contains several integral, transmembrane proteins, outer membrane proteins (OMPs), and some of these such as the porins allow the passive diffusion of small molecules such as mono-, disaccharides and amino acids across the OM.

The OM is stapled to underlying Peptidoglycan layer by peculiar lipoprotein called Braun's lipoproteins or murein lipoproteins. Peptidoglycan is made up of repeating units of the disaccharide *N*-acetyl- glucosamine and *N*-acetyl muramic acid cross-linked by tetrapeptide side chains (Vollmer *et al.*, 2008) and because of its rigidity, it determines the cell shape. The IM is made up of phospholipid bilayer, mainly phosphatidyl ethanolamine and phosphatidyl glycerol, arranged so that hydrophobic hydrocarbons chains are shielded from the surrounding polar fluid with polar heads oriented towards the extracellular face. Other minor lipids include polyisoprenoid carriers, whose function is the translocation of activated sugar intermediates required for envelope biogenesis.

Bacteria lack of intracellular organelles like mitochondria, smooth and rough endoplasmic reticulum that perform a number of essential cellular processes; so many of the functions of eukaryotic organelles are performed in the IM. The OM and IM delimit an aqueous cellular compartment called the periplasm, densely packed with proteins and more viscous than the cytoplasm.

The Gram-positive cell envelope differs in several key ways from that of Gram-negative. The major differences regard the absence of the outer membrane in Gram-positives and the Peptidoglycan thickness. The Gram-negative Peptidoglycan is only a few nanometers thick, the Gram-positive is 30 – 100 nm thick and the most notable structural difference relates to the peptide cross-links between glycan strands (Vollmer, 2008). The OM of Gram-negative bacteria plays a major role in protecting the organisms from the environment by excluding toxic molecules and providing an additional stabilizing layer around the cell, and because it indirectly helps to stabilize the inner membrane, the Peptidoglycan mesh surrounding Gram-negative cell is relatively thin. Threading through the Peptidoglycan layers of Gram-positive bacteria, there are long anionic polymers, called Teichoic acids (TAs), which are composed largely of glycerol phosphate, glucosyl phosphate, or ribitol phosphate. One class of these polymers, the wall Teichoic acids (WTAs), are covalently attached to Peptidoglycan; another class, the Lipoteichoic acids (LTAs), are anchored to the head groups of membrane lipids (Neuhaus, 2003). Collectively, these polymers can account for over 60% of the mass of the Gram-positive cell wall, making them major contributors to envelope structure and function. In the case of virulent Gram-positive and Gram-negative bacterial strains, the macromolecules constituting the cell envelope are strongly involved in mechanisms of adhesion, colonization, infection of host organisms. In particular Peptidoglycan, Teichoic acids for Gram positive, Lipopolysaccharides for Gram negative bacteria perform the role of antigens because they are recognized by specific receptors of system immune cells.

### ***1.2 General architecture, function and biosynthesis of the Lipopolysaccharide (LPS)***

LPS is the most abundant surface molecule and ubiquitous in all Gram negative bacteria (Alexander and Rietschel, 2001). It is schematically represented as a tripartite amphipatic molecule comprising glycolipid moiety, termed Lipid A, covalently linked to the Core oligosaccharide (OS). In the “Smooth-type” LPS (S-LPS) (figure 1.2.1) the Core is glycosylated by a polysaccharide termed the *O*-antigen or *O*-Specific Side Chain; while the “Rough-type” (R-LPS) is composed only by Lipid A and Core region, in this case LPS is also called as Lipooligosaccharide (LOS). Lipid A, is made up of 2-amino-2-deoxy-D-glucose (glucosamine, GlcN) disaccharide backbone, which is phosphorylated and acylated with a variable number of fatty and hydroxy-fatty acid chains. This hydrophobic portion is embedded in the phospholipid bilayer and forms the majority of the outer lipid leaflet of the OM providing the anchorage of the LPS to the outer membrane.

The Core is composed by one to three residues of 2-keto-3-deoxy-D-manno-octulosonic acid (Kdo), a distinctive acid monosaccharide for all bacterial Core oligosaccharide, residues of heptoses and hexoses. The O-antigen is a polymer made up of oligosaccharide repeating units whose chemical composition, structure varies widely among Gram-negative bacteria.

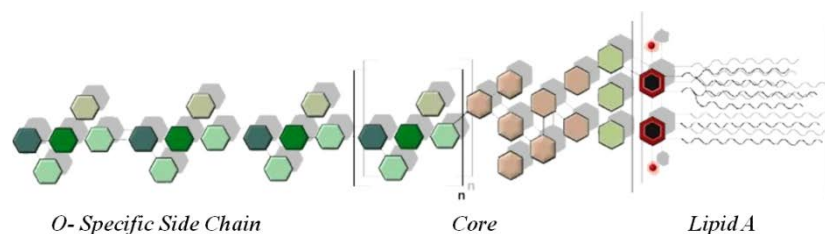


Figure 1.2.1: General structure of Smooth type LPS (S-LPS)

The LPS layer of the outer membrane represents an effective diffusion barrier toward external stress factors. This is due in part to the low fluidity state of the hydrocarbon regions of the Lipid A and to the strong lateral interactions between LPS molecules. Furthermore, the negatively charged groups carried by Lipid A (as phosphates, pyrophosphates, uronic acids) and often present on the residues of the inner Core, participate in ionic interaction with divalent cations, such as  $\text{Ca}^{2+}$  or  $\text{Mg}^{2+}$ . This contributes to create hydrophilic environment that provide a barrier preventing the passage of hydrophobic substances such as detergent or antibiotics across the outer membrane. The synergic interactions between LPS-LPS, LPS-cations, LPS-OMP play an important role in maintaining the structural integrity of the bacterial outer membrane.

The biosynthesis of LPS is a complex process involving various steps that occur at the plasma membrane followed by the translocation of the formed LPS to the bacterial cell surface (figure 1.2.3). In general, the Core oligosaccharide is assembled on a preformed Lipid A, while the O-antigen is independently assembled and then linked to the Lipid A-Core oligosaccharide (Raetz and Whitfield, 2002). The enzymology and molecular genetics of the steps of Lipid A biosynthesis are best characterized in *E. coli* (figure 1.2.2). In the first step the UDP-GlcNAc acyltransferase (LpxA) promotes the acylation of the sugar nucleotide UDP-GlcNAc. This acyltransferase is selective for 3-hydroxymyristate, consistent with the composition of *E. coli* Lipid A and it needs an acyl carrier protein (ACP) thioester as donor of substrate. In last steps, two Kdo residues are transferred to not yet complete Lipid A backbone, coherent with the structure of LPS of *E. coli* and lauroyl and myristoyl residues are added to the non reducing glucosamine unit, generating acyloxyacyl moieties. LipidA-Kdo<sub>2</sub> is the minimal Lipopolysaccharide that supports growth in most bacteria and is the acceptor on which the Core oligosaccharide is assembled via sequential glycosyl transfer from nucleotide sugar precursors.

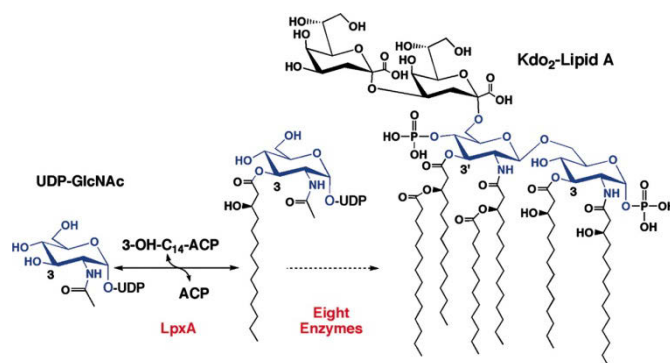


Figure 1.2.2: *LpxA* catalyzes the first step of Lipid A biosynthesis. It transfers the (*R*)-3-hydroxyacyl moiety from (*R*)-3-hydroxyacyl-ACP to the 3-position of UDP-GlcNAc. The acyl chains at the 3 and 3' positions of Kdo<sub>2</sub>-Lipid A are derived from *LpxA*.

The assembly occurs at the cytoplasmic face of the inner membrane, where acceptor and nucleotide sugars are available (figure 1.2.3).

The *O*-antigen is assembled on undecaprenyl-phosphate (Und-P), a polyisoprenoid lipid to which *O*-antigen is linked via phosphodiester bond. Different reactions involve the elongation, translocation and polymerization of *O*-repeating units leading the polymeric *O*-antigen linked to Und-PP localized to the periplasmic side of the inner membrane. These processes converge in the transfer of the *O*-antigen on the Core domain of the preformed Lipid A-Core acceptor, and the complete LPS (Lipid A-Core oligosaccharide-*O*-antigen) is further translocated to the outer membrane, becoming surface exposed (figure 1.2.3)

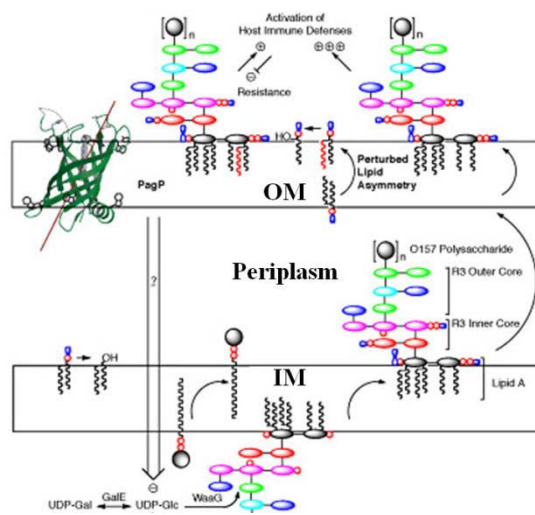


Figure 1.2.3: Depiction of LPS biosynthesis

### 1.3 The Core oligosaccharide and O-Specific Side Chain

The Core oligosaccharide is covalently linked to the O-6 of the non reducing unit of glucosamine of Lipid A (Holst *et al.*, 1999) and it is characterized by major *intra*-genus variability compared to the Lipid A portion. The Core is conceptually divided into two regions: Inner Core proximal to Lipid A and Outer Core that provides an attachment site for O-antigen. The Inner Core is more conservative and characterized by the occurrence of peculiar monosaccharides, although there is an high structural variability among the same genus. The Kdo performs the linkage between the Core and Lipid A but in some cases a derivate, D-glycero-D-talo-oct-ulosonic acid (Ko) is also present as observed in some *Acinetobacter* (Kawahara *et al.*, 1987) or *Burkholderia* (Silipo *et al.*, 2006) strains. In most cases the Core hosts additional Kdo units and other peculiar monosaccharides, the heptoses, typically L-glycero-D-manno-heptosepyranoses (L,D-Hep). Some bacteria contain D-glycero-D-manno-heptosepyranoses (D,D-Hep), biosynthetic precursor of L,D-Hep, alone or in combination with the more prevalent L,D-Hep (Ding *et al.*, 1994); while others, like *Rhizobium*, lack heptoses entirely. The base structure of Inner Core is often decorated with non-stoichiometric additions of other sugars, phosphate (P), pyrophosphoethanolamine (PEtN) or phosphorylcholine (PCho) residues. The varying extent of these modifications contributes to the heterogeneity of LPS molecules. The Outer Core shows more structural diversity as might be expected for a region with more exposure to the selective pressures of host responses and environmental stresses. It usually contains neutral and acid monosaccharides but also amino sugars. It is possible to find phosphate or pyrophosphate groups and occasionally non-glycidic substituents like aminoacids residues. The O-Chain is present only in the smooth-type LPS. This polysaccharide has an high molecular weight (10000-60000 Da) and the O-repeating units may comprise varying numbers of monosaccharides (deoxysugars, heptoses, aminosugars, uronic acids), which can form homopolymers or, more frequently, heteropolymers. The sugars can bring non stoichiometric modifications (N- or O-acetylation or glycosylation) or acyl groups like acetyl, formyl, pyruvil groups that may complicate the repeating unit structure. The location of O-polysaccharide at the cell surface places it at the interface between the bacterium and its environment; variation of the structure can be used to modulate the response of the bacterium to external factors. When the LPSs are separated by SDS-PAGE, the extensive heterogeneity in the sizes of the molecules is evident: variations in the chain length of the O-polysaccharides give the classical “ladder” patten in SDS-PAGE, where each band of the ladder represents a Lipid A-Core molecule substituted with an increment of additional O- unit.

The Core of some rough strains and the O-Chains are recognized by the acquired immune system that develops specific antibodies against epitopes localized within the oligosaccharide, leading to the rise of the immune system.

### 1.4 Structure and biological activity of Lipid A

The Lipid A is the most conservative portion of LPS: its structure is maintained, with few variation, among the genus. (Zähringer *et al.*, 1999). The base architecture is made by a disaccharide backbone of 2-amino-2-deoxy-D-glucose (GlcN) connected by a  $\beta$ -(1 $\rightarrow$ 6) glycosidic linkage. The reducing GlcN unit (GlcN I), is phosphorylated at O-1, the non reducing unit (GlcN II) is phosphorylated at O-4 and glycosylated at O-6 by Kdo. Both of GlcN units are acylated via ester and amide bonds by long chains of 3-hydroxy-fatty acids that constitute the primary fatty acids, and their the  $\beta$ -hydroxyl groups are generally esterified by the secondary fatty acids. A bacterial strain produces a family of Lipid As, because this type of molecule has an intrinsic heterogeneity due related to the acylation pattern and to the number of phosphate groups, eventually substituted, in non stoichiometric amounts, by other groups often as 2-aminoethanol (EtN), 4-deoxy-4-amino-L-arabinopyranose (Ara4N) and 2-aminoethanolphosphate (EtNP). The Lipid A is the real endotoxin principle of the LPS because it is recognized by the innate immune system of infected hosts. The innate immune (or non specific) system is the first line of defense against invading organisms (Akira *et al.*, 2006), while the adaptive immune system is composed of highly specialized cells that process and eliminate the hosts and affords protection against re-exposure to the same pathogen.

The strategy of the innate immune recognition is based on the detection, through pattern recognition receptors (PRRs), of constitutive and conserved products of microbial metabolism known as Pathogen Associated Molecular Pattern (PAMPs). These include Lipoproteins, Peptidoglycan, Lipoteichoic acids and Lipid A of LPS which represents the invariant pattern in all Gram-negatives. Most of the pathogenic phenomena associated with the infection are induced by the interaction of the Lipid A with a specific PRR receptor, the Toll-like receptors 4 (TLR4) (Takeda and Akira, 2005). Recognition of LPS by TLR-4 is complex and requires several accessory molecules (figure 1.4.1) (Miyake, 2004).

TLR4 is associated on the cell surface to a the glycoprotein MD-2, essential for the formation of LPS-TLR4 complex. LPS is first bound to a serum protein, LBP (LPS-binding protein) that removes the LPS from the outer membrane and delivers the LPS to the CD14.

This is a glycoprotein that mediates the interaction LPS-TLR4; in particular the mCD14 (membrane bound) is attached to the surface of myeloid cells via glycosylphosphatidyinositol tail.

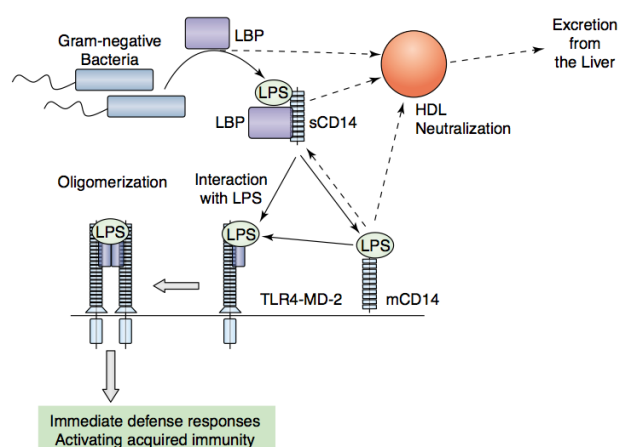


Figure 1.4.1: Processing, signalling and clearance of the LPS

The sCD14 (soluble form) occurs in the plasma and helps the LPS signalling to the cells, e.g. epithelial, endothelial cells, that have not the mCD14 form, allowing its elimination through the high density lipoprotein (HDL) (figure 1.4.1). The LPS bound to mCD14 is transferred to TLR4-MD2 complex, which undergoes oligomerization and triggers a complex series of events, the so-called inflammatory cascade, leading to the production of several effectors molecules as cytokines and interleukins. This structural variability of the Lipid A (phosphorylation and acylation pattern) is responsible for the three-dimensional changes in overall Lipid A assembly, leading to changes in the response of the innate immune system and consequently in the toxicity of Lipid A itself. This modulation of Lipid A biological activity can include both the induction and the inhibition of the inflammatory process: in the first case Lipid A acts as agonist and it is dose-dependent, in the second as antagonist (figure 1.4.3). Low concentrations of an agonistic Lipid A trigger the innate immune system to stimulate the adaptive immune system via dendritic cells differentiations; while high concentrations cause the massive production of pro-inflammatory factors resulting in septic shock with an often fatal outcome of such bacterial infection. In contrast, an antagonistic Lipid A has a low or absent toxic activity and it is able to compete with receptor sites of the agonist Lipid A without triggering the inflammatory response.

It was demonstrated that different biological activities of Lipid A are directly correlated to its intrinsic conformation (Seydel *et al.*, 2000). Orientation measurements with attenuated total reflectance (ATR) infrared spectroscopy were applied on hydrated Lipid A samples, from various sources. Lipid A molecules with an asymmetric (4/2) distribution of the acyl chains have a conical molecular shape, a large tilt angle of the diglucosamine backbone with respect to the membrane surface, and are endotoxically highly active (figure 1.4.2 **A**); the monophosphoryl hexa-acyl Lipid A has a smaller tilt angle, a conical shape deviating only slightly from the cone and it shows a decreased endotoxic activity (figure 1.4.2 **B**). Penta-, tetra-acyl Lipid As or hexaacyl Lipid A with a symmetric acyl chain distribution (3/3), present a small tilt angle, a cylindrical shape and result endotoxically inactive or antagonistic (figure 1.4.2 **C, D, E**). Some of the tested Lipid As are reported in figure 1.4.3: the highly agonistic Lipid A from *E. coli* or *Salmonella minnesota* (type **A**, figure 1.4.2), the medium endotoxically active monophosphoril Lipid A (type **B**, figure 1.4.2) and the antagonistic Lipid As from *Rhodobacter capsulatus* and *spheroides* (type **C**, figure 1.4.2), the Lipid<sub>Vla</sub>, a precursor of enteric Lipid A or isolated from *Yersinia pestis* grown at 37 °C (type **D**, figure 1.4.2) and *Chromobacter violaceum* (type **E**, figure 1.4.2).

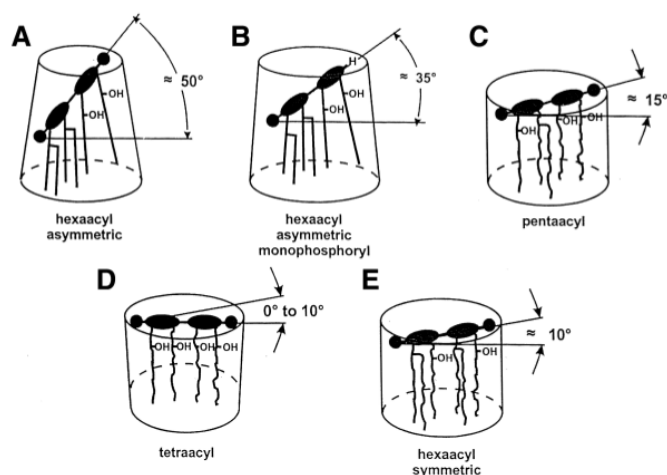


Figure 1.4.2: **A:** endotoxically highly active *E. coli*-type Lipid A; **B:** medium active MPLA; **C, D and E** inactive or antagonistic Lipid As.

Gram negative bacteria have developed mechanisms to modify the biosynthesis and consequently the structure of Lipid A in response to environmental stressing conditions (Miller *et al.*, 2005). These modifications can promote resistance to host cationic antimicrobial peptides (CAMPs) and alter the recognition by TLR4. *Yersinia pestis* is known as major pathogen due to its ability to be transmitted to humans by insect vectors. It is exposed to the innate immune system in humans and rodents at 37°C, in fleas at 21°C, and it developed the ability to regulate the Lipid A structure with changes of the temperature. At 21°C Lipid A is highly acylated and more resistant to CAMPs, whereas at 37°C is largely in Lipid<sub>IVA</sub> form (figure 1.4.3) which does not have a stimulatory effect on human innate immune signalling through TLR4. The regulation of Lipid A structure and the differential stimulation of human TLR4 might explain in part why insect-based transmission (TLR4 recognition) is much less virulent than human-to-human respiratory transmission (TLR4 invisibility), which results in severe bacteremia before septic shock (Miller *et al.*, 2005)

The ability of Lipid A to stimulate the innate immune response that in turn activates the adaptive immunity, identifies this molecule as a useful adjuvant for vaccine formulation. Adjuvants are combined with vaccine antigens to generate a faster, lasting longer response. Aluminum hydroxide (alum) is currently the dominant adjuvant for vaccines and although it is effective at boosting antibody response, repeated administration of vaccine are usually required. Monophosphoril Lipid A (figure 4.2.3) is the first low-toxicity LPS derivate to be approved for widespread human vaccine adjuvant use instead of alum, because it generates a useful immune response and has about 0.1 % of the inflammatory toxicity of its parent molecule (Mata-Haro *et al.*, 2007).

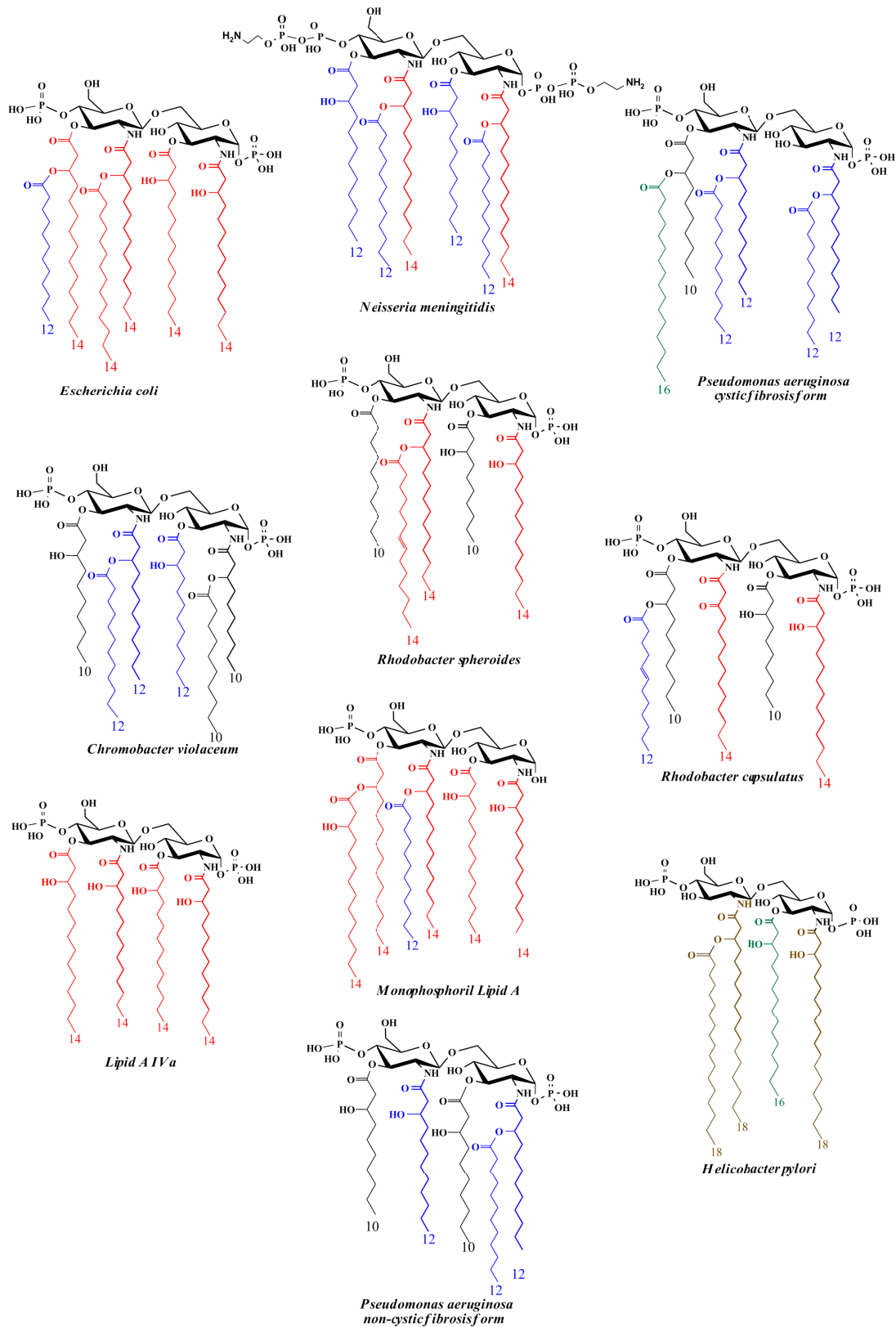


Figure 1.4.3: Agonistic Lipid As from *E. coli*, *N. meningitidis*, *P. aeruginosa* cystic fibrosis form; Antagonistic Lipid As from *R. spheroides*, *R. capsulatus*, *C. violaceum*, Lipid  $_{VIa}$  (or from *Y. pestis* grown at 37 °C); Lipid A with reduced toxicity: Monophosphoril Lipid A and inactive Lipid As from *Helicobacter pylori*, *P. aeruginosa* non-cystic fibrosis form

### 1.5 Capsular polysaccharides (CPSs) and glycoconjugate vaccines

A very broad range of bacterial species present a layer of extracellular polysaccharide: it can consist of a slime polysaccharide with little or no cell association (Exopolysaccharide, EPS) or alternatively can form an adherent cohesive layer, forming the morphological entity termed capsule (Capsular Polysaccharide, CPS). This is anchored to the outer membrane via multiple ionic interactions with LPS or covalent bonds to phospholipid or Lipid A molecules. CPS differs from *O*-antigen with respect to the mode of cell surface linkage and size, in fact it tends to be longer and to form a layer on the cell surface which often masks the underlying *O*-antigen. CPSs may themselves be released into the growth medium to form the EPS. (Roberts, 1996). Bacterial polysaccharides can be homo- or heteropolymers, branched or linear, sometimes decorated by organic or inorganic molecules. This results in the multiple serotypes established for many bacterial species. Over 80 different capsular polysaccharides (K antigens) have been described for *Escherichia coli*, and only a small fraction can be associated with specific infections (Whitfield and Roberts, 1999). Chemically identical capsular polysaccharides may be synthesized by different bacterial species. The CPS of *Neisseria meningitidis* group B is identical to the K1 polymer of *E. coli*, and the *E. coli* K18, K22, and K100 antigens have the same constituents and a structure similar to the capsule of *Haemophilus influenzae* (Jann and Jann, 1990). The apparent conservation of particular capsular polysaccharide structures between taxonomically diverse bacterial genera raises interesting questions concerning the evolution of capsule diversity and the acquisition and transmission of capsule biosynthesis genes.

The primary role of the CPS is to protect the cell from external environment. The presence of hydrated layer around the surface may avoid effects of desiccation and may be particularly relevant in aiding the transmission of encapsulated pathogens from one host to the next. Furthermore, Capsular Polysaccharides promote the formation of a biofilm that assists the colonization process and the adherence of bacteria to several surfaces. These ability can have important consequences: the colonization of hospitals can lead to serious nosocomial infections, representing often a permeability barrier to antibiotics (such as for *Pseudomonas aeruginosa* or *Acinetobacter baumannii*).

The capsular polysaccharides resulted often immunogenic in humans, so they are a good candidates for vaccines development. In addition, they are non-toxic, easily isolated and purified with high yields, and have conserved and chemically defined structures. To date, vaccines based on the capsular polysaccharides of *Neisseria meningitidis* groups A, C, W-135, Y, *Streptococcus pneumoniae*, *Haemophilus influenzae* type b have been already successfully developed (Pon and Jennings, 2008).

However, the immune response generated by CPS is T-independent (TI) with no immunological memory and produce an inadequate response in infants that are the most vulnerable to bacterial infections. To overcome this limitation of a new generation of glycoconjugate vaccines were developed in which the polysaccharide were conjugated (covalently linked) to a protein carrier, which in contrast generates a T-dependent (TD) response (Peeters *et al.*, 2003).

The strategy to realize a glycoconjugate compound includes the selection of an appropriate size of the saccharide fragment, a protein carrier and the most efficient reaction for the coupling. Bacterial antigens can include Capsular Polysaccharide as well as Lipopolysaccharide and Lipooligosaccharide. Thus, the antigen may be an oligosaccharide or a polysaccharide, in which case depolymerization if needed, can be accomplished by various means: acid or enzymatic hydrolyses, oxidations, alkaline or lyase-mediated eliminations or physical methods such as sonication. The purification and the selection of a defined range of molecular weight can be obtained by several techniques such as ultrafiltration, gel permeation, ion exchange chromatographies.

Most popular proteins carrier are tetanus toxoid (TTd), diphtheria toxoids (DTd) that are readily accessible, and licensed for human and in particular infants use. Toxoids originate from native bacterial toxins which are detoxified by the deactivation or modification of some of reactive sites on amino acids within the chains. However the use of detoxified bacterial toxins offers some disadvantages. Physical and chemical properties of the toxin are modified by the detoxification yielding to a lot-to-lot variations, in addition this procedure inactivates some of the readily accessible amino groups that could be used in coupling the polysaccharide to the carrier, reducing the conjugation efficiency. An alternative has been the use of mutant-derived diphtheria toxin (CRM<sub>197</sub>) and pertussis toxin (CRM<sub>3201</sub>) which are non toxic and antigenically equivalent to DT.

Various spacer arms have been used as a linker (adipic acid dihydrazide, glutaraldehyde, diamminobutane, 6-aminohexanoic acid) between the saccharide and the protein. The spacer may avoid the shielding of important carbohydrate epitopes by the secondary structure of the carrier protein and improve the efficiency of the coupling by increasing the steric accessibility of activated moieties.

The choice of coupling chemistry is largely driven by the model of conjugate that is needed, namely a neoglycoprotein or crosslinked lattice. The first is obtained by the activation of a single end of the saccharide that produce the simplest conjugate configuration in which the saccharide chains radiate from the individual protein molecules. It is generally more efficient for the coupling of oligosaccharides or short polysaccharides. The crosslinked lattice is obtained by random activation at several points on the saccharide chain leading to a cross-linked and not defined structure. In general, it is the more practical approach for the coupling of polysaccharides.

## CHAPTER II

### GENERAL ASPECTS

#### *2.1 Rhizobium radiobacter RV3 as a source of oligosaccharide with potential use for HIV vaccine production*

The development of an effective vaccine against HIV remains an unrealized, although still hoped, goal in the effort to contain the current pandemic. The humoral immune response to infection by HIV is characterized by the production of relative low levels of neutralizing antibodies with a broad activity against many different isolates of the virus. The identification and the extensive characterization of several monoclonal antibodies (Burton *et al.*, 1994; Corti *et al.*, 2010; Walker *et al.*, 2009; Zwick *et al.*, 2001) suggested that the vaccination is possible stimulating the adaptative immune system with an appropriate antigen. One broadly neutralizing antibody, 2G12, recognizes a high mannose carbohydrate epitope presented on the gp120 glycoprotein of the virus. In particular, it interacts with the a cluster of terminal  $\alpha$ -D-Man-(1 $\rightarrow$ 2)- $\alpha$ -D-Man residues, that comprise the D1 arm of the gp120 glycan shield, although more recent studies have shown that the binding site can also be occupied by the D3 arm (figure 2.1.1) (Pantophlet and Burton, 2006).

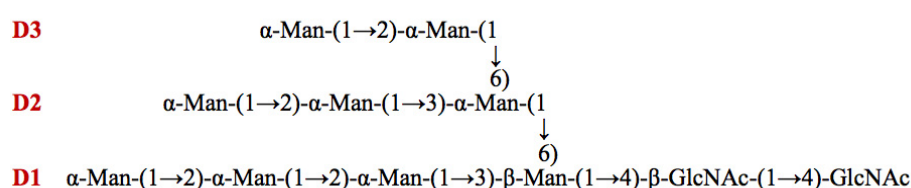


Figure 2.1.1: Structure of gp120 oligosaccharide target of the 2G12 antibody. All monosaccharides are D configured and in the pyranose form.

Furthermore, 2G12 provides an extended surface for multivalent interaction with the conserved cluster of oligomannose on the surface of gp120 (Calarese *et al.*; 2003). The crystal structure of the core of gp120 suggests that the carbohydrate attachment sites are clustered together on a part of the gp120 molecule known as the “silent face” (Kwong *et al.*, 1998; Wyatt *et al.*, 1998; Calarese *et al.*, 2005). This face is largely covered by carbohydrate and expected to be relatively weakly immunogenic and, hence, is described as immunologically silent. So far, many efforts are focused to the elaboration of a proper oligomannose antigen able to stimulate the 2G12, ranging from that present on the gp120 to more simplified structures consisting of a linear  $\alpha$ -(1 $\rightarrow$ 2)-Man oligosaccharides. These have been conjugated on different types of carrier proteins and their affinity for 2G12 analysed together with their antigenic potentials (Astronomo *et al.*, 2010).

*Rhizobium radiobacter* RV3 is a Gram negative soil bacterium and produces a Lipooligosaccharides structure closely related to the Man<sub>9</sub>GlcNAc<sub>2</sub> glycan shield of the gp120 and for this reason it was individuated as a useful source for the development of a potential vaccine for HIV (Chapter III).

## 2.2 *Cupriavidus necator*

In order to find a Lipid A with a potential antagonistic activity, structural features of this molecule, produced by the non-pathogen *Cupriavidus necator* DSM 13523, were explored (Chapter IV). This choice starts from the assumption that structural moieties of organisms that do not enter in contact with humans, may be not or poorly recognized by the immune system; so it is likely that they have low, no toxic or antagonistic activity. As reported, the innate immune system is triggered by the interaction of differently acylated Lipid A molecules to the TLR4-MD2 complex and the intensity of the response depends on the presence of phosphate groups and on the number and size of the fatty acids. So, it was established that a diphosphorylated and hexa-acylated specie, as present in *Escherichia coli* LPS, acts as agonist, whereas less acylated specie is inactive or even antagonist (section 1.4).

*Cupriavidus necator* is a Gram-negative nonobligate predator of different soil Gram-positive and negative bacteria (Sillman and Casida, 1986; Zeph and Casida, 1986) including *Agromyces ramosus*, *Arthrobacter globiformis*, *Azotobacter vinelandii*, *Bacillus subtilis*, *Bacillus thuringiensis*, *Ensifer adhaerens*, *Escherichia coli*, *Micrococcus luteus*, *Staphylococcus aureus* (Germida and Casida, 1983). *Cupriavidus necator* does not require to prey cells to grow, but if the level of available nutrients in soil decreases, it attacks other bacteria. The encounter with prey is stimulated by chemotaxis phenomenon that it is followed by the attachment and penetration of the prey outer membrane. During interperiplasmic growth phase, there is the cells differentiation and finally the prey envelope lysis. Bacteria of genus *Cupriavidus* are highly resistant to copper (Casida, 1988). They produce a peptide growth initiation factor (GIF) which, chelating copper, helps the bacterium to provide the necessary copper for its initial growth. It was observed that the growth following the initial is not influenced or inhibited by addition of extra copper and the rate of GIF production depend on which amino acid or other carbon compounds are available to the bacterium. Furthermore, *Cupriavidus* seems to use copper-GIF for delivering toxic levels of copper to its prey cells (Casida, 1988). Some of the bacteria attached are them self predators and in this cases an attack-counter attack phenomenon was described (Byrd and *et al.*, 1985).

## 2.3 *Acinetobacter baumannii*

*Acinetobacter baumannii* is an opportunistic Gram-negative bacterium considered the most common human pathogen species within its genus, followed by *A. lwoffii* and *A. haemolyticus*.

This bacterium is widely distributed in nature and is extraordinarily adaptable to a variety of environmental conditions, e.g., it may colonize a variety of hospital surfaces such as surgical drains and catheters (Peleg *et al.*, 2008). It is generally considered an opportunistic pathogen in immuno-compromised patients causing severe nosocomial, bloodstream, pneumonia, or urinary tract infections, and septicemia (Van Looveren and Goossens, 2004).

The propensity of this organism to develop drug-resistance (Fournier *et al.*, 2006) (against carbapenem, beta-lactam, and tetracycline antibiotics) and the lack of development of new drugs to treat infections have resulted in a significant increase in *Acinetobacter*-related studies (Bergogne-Berezin and Towner, 1996). The most common pathogens belong to the so-called *A. calcoaceticus* - *A. baumannii* complex (Joly-Guillou, 2005). The mechanism by which *Acinetobacter* is able to express its pathogenicity is not yet completely elucidated but a crucial role is played by components of the cell envelope outer membrane, namely the Lipopolysaccharides and Capsular Polysaccharides. These molecules act in synergy by blocking the access of human complement factors to the bacterial cell wall, thus preventing bacterial killing and lysis (Goel and Kapil, 2001). So, the establishment of the CPS and LPS structures is of importance to understand the physical assemblage of the external membrane and its properties, like adhesion to surfaces (i.e. hospital's furniture or human skin), permeability to hazardous compounds (e.g., detergents used to clean surfaces) but also can contribute to the development of new pharmacological and immunostimulatory strategies for the prevention or the therapy of the diseases (Chapters V and IV).

#### **2.4 Virulence factors of *Escherichia coli* and the Enterobacterial common antigen**

*Escherichia coli* is part of the normal micro flora of the gastrointestinal tract of mammals and birds, but certain strains have been associated with gastrointestinal diseases in both humans and animals. *E. coli* is serotyped on the basis of their O (somatic), H (flagellar), and K (capsular) surface antigen profiles (Nataro and Kaper, 1998; Lior, 1994). A specific combination of O, K and H antigens defines the serotype of an isolate. *E. coli* of specific serotype can be associated reproducibly with certain clinical syndromes, but in general the serologic antigens themselves do not confer virulence. In fact, some *E. coli* strains have been categorized into pathogenic groups, based on their virulence properties (Nataro and Kaper, 1998). One of these groups is characterized by the production of potent cytotoxins that inhibit protein synthesis within eukaryotic cells. These toxins are either termed verocytotoxins (VT), because of their activity on Vero cells, or Shiga toxins (Stx), because of their similarity with the toxin produced by *Shigella dysenteriae* (Melton-Celsa and O'Brien, 1998). Therefore, these strains are either termed Stx-producing *E. coli* (STEC) or VT-producing *E. coli* (VTEC). Enterohaemorrhagic *E. coli* (EHEC) constitutes a subset of serotypes of STEC that has been firmly associated with bloody diarrhoea and haemolytic uraemic syndrome (HUS) in industrialized countries (Griffin and Tauxe; 1991). The majority of disease worldwide is caused by strains of serotype O157:H7, but also by O26,

O111, O103, and O145 (Tozzi *et al.*, 2003). The production of Stx appears to be essential but not the only responsible for the pathogenic effects, hence many efforts in recent years have been focused on the possible involvement of other virulence factors and on the understanding of their mechanisms. Outer membrane components as OM proteins, capsules, LPSs have been extensively considered, in particular because they are subjected to the phase variation (Lukáčová *et al.*, 2008). This phenomenon is associated with reversible changes within repeated simple DNA sequence motifs that exhibit high mutation rates by loss or gain of repeating units during DNA replication. The switch can be influenced by the extracellular conditions. Such reversible changes are heritable and reversible between generations, and the switching frequency is characteristic for the gene, the bacterial species and the regulatory mechanism. Consequently, the high-frequency variation in the expression of the outer membrane components is valid strategy to overcome the immune system.

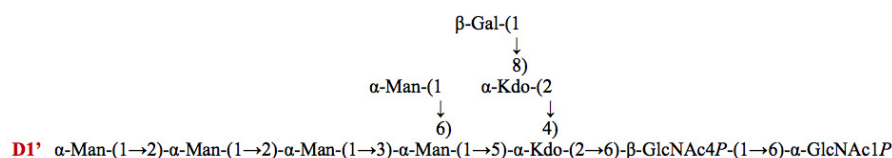
The cell surface of enteric bacteria contains an additional antigenic polysaccharide known as the *Enterobacterial common antigen* (ECA) (Kuhn *et al.*, 1988; Männel and Mayer, 1978). It is a heteropolysaccharide made up of a trisaccharide repeat unit: 3)- $\alpha$ -D-FucNAc-(1 $\rightarrow$ 4)- $\beta$ -D-ManNAcA-(1 $\rightarrow$ 4)- $\alpha$ -D-GlcNAc-(1 $\rightarrow$ ). The ubiquitous form is represented by the glycolipid ECA<sub>PG</sub> (phosphoglyceride-linked) where polysaccharide ECA chains are covalently linked to diacylglycerolphosphate via glycosidic linkage between the reducing terminal GlcN unit and the phosphate residue of the phosphoglyceride aglycone, which anchors the ECA to the outer membrane (Rick *et al.*; 1998; Rinno *et al.*; 1980). The two related forms are the ECA<sub>LPS</sub> and the ECA<sub>CYC</sub> isolated in certain *Enterobacteriaceae*. About the first, the linear ECA polysaccharide chains are covalently linked to the Core region of the LPS instead of the phosphoglyceride aglycone. In contrast, the ECA<sub>CYC</sub> is a cyclic water soluble polysaccharide that contains only the trisaccharide repeating units with different degree of *O*-acetylation (Dell *et al.*, 1984; Staaf *et al.*, 2001). Furthermore, its occurrence is quite restricted, in fact it was isolated and characterized in *Yersinia pestis* (from 3 to 5 repeating units) (Vinogradov *et al.*, 1994), *Shigella sonnei* (from 4 to 6 repeating units), *Plesiomonas shigelloides* (4 repeating units), and *E. coli* K12 ( 4 repeating units) (Erbel *et al.*, 2003; Kajimura *et al.*, 2005). Although the structure of these molecule has been characterized, there are few information about their biological role or if it is the same in all enteric bacteria. Recent studies suggested that ECA<sub>PG</sub> may be involved in the resistance of Shiga toxin production of *E. coli* O157:H7 to organic acids (Barua *et al.*, 2002). In *Salmonella enterica* serovar *Typhimurium*, the ECA<sub>PG</sub> acts as a virulence factor for oral infection in mice by rendering the organism more resistant to bile salts (Ramos-Morales *et al.*, 2003). In contrast, there are no information about the biological function of ECA<sub>CYC</sub>. It seems that the periplasmic location and cyclic structure of this molecule are similar to those of the osmoregulated periplasmic glucans synthesized by many Gram negative *Proteobacteria* (Bohin; 2000).

## PART II: RESULTS AND DISCUSSION

### CHAPTER III

#### SYNTHESIS OF NEW NEOGLYCOPROTEIN USING MANNAN OLIGOSACCHARIDE FROM *Rhizobium radiobacter* RV3

In the following investigation, the Lipooligosaccharide structure produced by *Rhizobium radiobacter* Rv3 was determined through spectroscopic studies. It shows the occurrence of a mannose oligosaccharide (**D1'**) analogue to the D1 arm of the gp120 Man<sub>9</sub>GlcAc<sub>2</sub> oligosaccharide recognized by the broadly neutralizing human anti-HIV antibody 2G12 (section 2.1).



This discovery opened the attractive way to the use of this bacterium for potential HIV vaccine development, in particular because this is a natural and available source of antigen .

Purified LOS of *Rhizobium radiobacter* Rv3 was tested, but it showed low affinity versus 2G12 antibody. On the basis of this information, a new neoglycoprotein was realized (figure 3.3.1), possessing as antigen portion the modified LOS linked, through a spacer, to the commercial Bovine Serum Albumin (BSA) as protein carrier. The molar ratio OS/BSA was determined with two independent approaches: colorimetric phenol-H<sub>2</sub>SO<sub>4</sub> test and quantitative GC-MS estimation.

#### 3.1 LOS chemical analyses

Pure LOS was extracted by PCP procedure (section 8.1) from the dry cells of *Rhizobium radiobacter* RV3. LOS SDS-PAGE profile showed the mobility typical of low molecular weight molecules, characteristic of lipooligosaccharide species. Combining the information from monosaccharide composition, methylation analysis, the LOS fraction contained mainly terminal, 2- and 3,6 substituted D-mannose , terminal D-galactose and minor amounts of 3-substituted D-mannose; acidic residues, as 3-deoxy-manno-oct-2-ulosonic acid (Kdo) and phosphorylated glucosamine were not detected with the methylation protocol used. Fatty acids analysis showed the presence of C14:0 (3-OH), C16:0 (3-OH), C18:1 (3-OH) and C28:0 (27-OH): the lipids distinctive of this bacterial family (Silipo *et al.* 2004). LOS produced from *R. radiobacter* Rv3 was totally delipidated and the oligosaccharide mixture was analysed via strong anion exchange chromatography (HPAEC) (section 9.3), leading to the separation of two different oligosaccharides, **OS1** and **OS2**, whose structure was defined via NMR analysis.

### 3.2 NMR analysis of Core oligosaccharide

The complete assignment of  $^1\text{H}$  and  $^{13}\text{C}$  resonances of each **OS1** and **OS2** was achieved ( $^1\text{H}$ -NMR spectra in figure 3.2.1), combining the information obtained from 2D homo- and heteronuclear spectra.

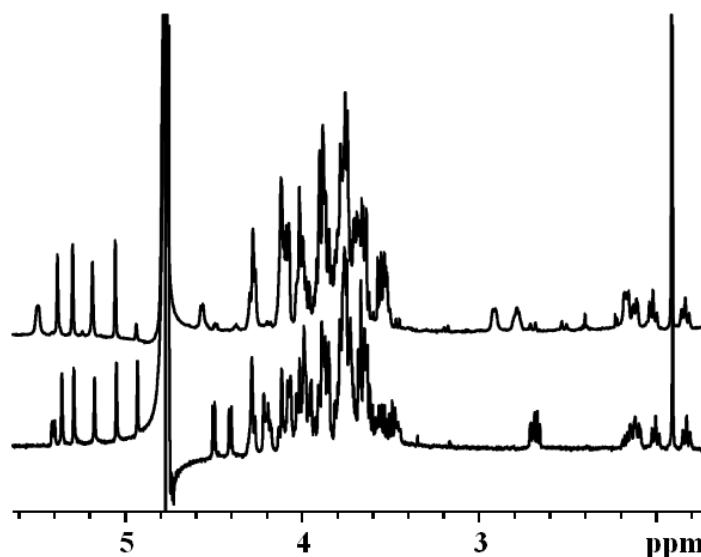


Figure 3.2.1: (600 MHz, 303 K),  $^1\text{H}$ -NMR spectra of **OS1** (bottom, NaOD 10 mM in  $\text{D}_2\text{O}$ ) and **OS2** (up,  $\text{D}_2\text{O}$ )

With regard to **OS1** spectra attribution (table 3.2.1, figure 3.2.2), the eight anomeric protons were labelled with a capital letter in decreasing order of chemical shifts, whereas two couples of the diastereotopic methylene signals were observed in the high field region of the proton spectrum, due to the presence of two Kdo residues,  $\mathbf{K}_{\text{int}}$  and  $\mathbf{K}_{\text{ext}}$ . Thus, a deca-saccharide structure was identified in the deacylated LOS. With regard to residues **A** and **H**, their anomeric protons showed six different correlations, and on the basis of their ring proton and carbon resonances, these residues were recognized as the two conserved glucosamine moieties constructing the lipid A moiety of the oligosaccharide. With regard to residues **B-F**, the TOCSY and gHSQCTOCSY (this last in figure 3.2.2) spectra of the anomeric region (figure 3.2.2) could not establish any connectivity after the H-2 proton, due to the small  $^3J_{\text{H1,H2}}$  and  $^3J_{\text{H2,H3}}$  coupling constants values; on the other hands, magnetization was propagated from H-2 proton up to H-6s, therefore these residues were recognized as mannose, all  $\alpha$  configured at the anomeric centre due to the value displayed from their C-5.



The two Kdo residues were  $\alpha$  configured on the basis of the chemical shift values of their H-3<sub>eq</sub> protons (Birnbaum *et al.*, 1987) and **K<sub>ext</sub>** was located at O-4 of **K<sub>int</sub>** on the basis of the characteristic NOE between H-3<sub>eq</sub> of **K<sub>int</sub>** and H-6 of **K<sub>ext</sub>**, observed in the TROESY spectrum (Holst *et al.*, 1995). **OS1** sequence was completed placing **K<sub>int</sub>** at O-6 of glucosamine **H**, the distal unit of the Lipid A segment of the molecule. With regard to **OS2**, spectra interpretation followed the same approach shown above, and analysis was simplified due to the lower number of residues constituting the molecule. Complete spectra attribution (table 3.3.2), identified a structure differing from that of **OS1** for the absence of both **F** and **G** units, namely the terminal mannose and galactose residues.

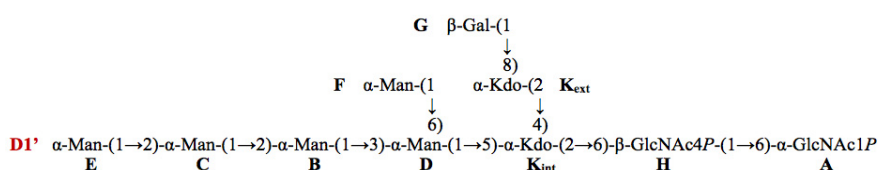


Figure 3.2.3: Oligosaccharides structure from *Rhizobium radiobacter* Rv3. All residues are D configured and in pyranose form. Residues are labelled according to the NMR attribution in tables 3.2.1 and 3.2.1. **OS1** is the major fraction, **OS2** differs from **OS1** for the lack of residues **F** and **G**.

	<b>1</b>	<b>2</b>	<b>3</b>	<b>4</b>	<b>5</b>	<b>6-6'</b>
<b>A</b>	5.41	2.7	3.62	3.49	4.09	3.78-4.28
<b>6)-<math>\alpha</math>-GlcN1P</b>	95.8	56.8	74.7	71.1	72.8	70.6
<b>B</b>	5.36	4.08	3.99	3.69	3.8	3.88-3.66
<b>2)-<math>\alpha</math>-Man</b>	102.1	79.8	71.6	68.3	74.8	62.3
<b>C</b>	5.29	4.12	3.98	3.67	3.76	3.89 x 2
<b>2)-<math>\alpha</math>-Man</b>	101.9	79.7	71.3	68.3	74.6	62.3
<b>D</b>	5.18	4.28	3.99	3.98	4.2	4.12-3.66
<b>3,6)-<math>\alpha</math>-Man</b>	102.3	71.1	80.4	66.5	72.9	66.4
<b>E</b>	5.05	4.07	3.86	3.63	3.76	3.75 x 2
<b><i>t</i>-<math>\alpha</math>-Man</b>	103.4	71.3	71.6	68.1	74.5	62.4
<b>F</b>	4.93	4.03	3.88	3.66	3.67	3.77 x 2
<b><i>t</i>-<math>\alpha</math>-Man</b>	101	71.2	71.9	68.1	74	62.4
<b>G</b>	4.5	3.54	3.72	3.95	3.76	3.80 x 2
<b><i>t</i>-<math>\alpha</math>-Gal</b>	104.6	72.2	73.9	69.9	76.4	62.2
<b>H</b>	4.41	2.67	3.57	3.64	3.64	3.78-3.46
<b>6)-<math>\beta</math>-GlcN4P</b>	104.2	57.5	77.3	74.5*	75.6*	70.5
	<b>3<sub>eq</sub>-3<sub>ax</sub></b>	<b>4</b>	<b>5</b>	<b>6</b>	<b>7</b>	<b>8</b>
<b>K<sub>ext</sub></b>	2.13-1.83	4	4.01	3.86	4.3	4.19-3.93
<b>8)-<math>\alpha</math>-Kdo</b>	36	67.4	68.5	73	70.8	72.1
<b>K<sub>int</sub></b>	2.10-2.00	4.05	4.22	3.73	3.74	3.86-3.76
<b>4,5)-<math>\alpha</math>-Kdo</b>	35.8	72.6	75.4	73	70.9	64.4

\*These signals can be interchanged

Table 3.2.1:  $^1\text{H}$  (regular) and  $^{13}\text{C}$  (italic) chemical shifts at 303 K in 10 mM NaOD in  $\text{D}_2\text{O}$ , measured for **OSI** (figure 3.2.3). For **K<sub>ext</sub>** and **K<sub>int</sub>** C-2 were identified in the HMBC spectrum at 103.5 and 100.8 ppm respectively; while C-1 were not detected. All residues are D configured and in pyranose form.

	<b>1</b>	<b>2</b>	<b>3</b>	<b>4</b>	<b>5</b>	<b>6-6'</b>
<b>A'</b>	5.49	2.92	3.71	3.54	4.12	4.29-3.81
<b>6)-<math>\alpha</math>-GlcN1P</b>	<i>94.85</i>	<i>56.51</i>	<i>73.9<sup>†</sup></i>	<i>71.2</i>	<i>72.3*</i>	<i>70.7</i>
<b>B'</b>	5.38	4.09	4.00	3.69	3.8	3.88 x 2
<b>2)-<math>\alpha</math>-Man</b>	<i>102.2</i>	<i>80.1</i>	<i>71.6</i>	<i>68.5</i>	<i>74.9</i>	<i>62.4</i>
<b>C'</b>	5.3	4.12	3.97	3.68	3.76	3.88 x 2
<b>2)-<math>\alpha</math>-Man</b>	<i>102.1</i>	<i>79.9</i>	<i>71.5</i>	<i>68.5</i>	<i>74.6</i>	<i>62.4</i>
<b>D'</b>	5.18	4.28	4.01	3.9	4.09	3.86 x 2
<b>3)-<math>\alpha</math>-Man</b>	<i>102.1</i>	<i>71.3</i>	<i>80.2</i>	<i>66.9</i>	<i>74.3</i>	<i>61.8</i>
<b>E'</b>	5.06	4.07	3.86	3.64	3.78	3.65-3.56
<b><i>t</i>-<math>\alpha</math>-Man</b>	<i>103.7</i>	<i>71.5</i>	<i>71.8</i>	<i>68.3</i>	<i>74.7</i>	<i>63.9</i>
<b>H'</b>	4.57	2.79	3.67	3.7	3.66	3.52-3.76
<b>6)-<math>\beta</math>-GlcN4P</b>	<i>103.5</i>	<i>57.4</i>	<i>75.6<sup>‡</sup></i>	<i>74.6<sup>†</sup></i>	<i>76.4<sup>‡</sup></i>	<i>64.2</i>
	<b>3<sub>eq</sub>-3<sub>ax</sub></b>	<b>4</b>	<b>5</b>	<b>6</b>	<b>7</b>	<b>8</b>
<b>K'<sub>ext</sub></b>	2.17-1.83	4.02	4.02	3.84	4.11	3.79-3.92
<b>8)-<math>\alpha</math>-Kdo</b>	35.9	67.3	68.3	73.4	73.2*	63.8
<b>K'<sub>int</sub></b>	2.12-1.88	4.12	4.26	3.75	3.75	3.87-3.77
<b>4,5)-<math>\alpha</math>-Kdo</b>	35.8	72.3	75.0	73.4 <sup>l</sup>	70.8 <sup>l</sup>	64.6

<sup>\*</sup>, <sup>†</sup>, <sup>‡</sup>, <sup>l</sup> These signals can be interchanged

Table 3.2.2. <sup>1</sup>H (regular) and <sup>13</sup>C (italic) chemical shifts, at 303 K in D<sub>2</sub>O, measured for **OS2** (figure 3.2.3). C-2 for **K<sub>ext</sub>** and **K<sub>int</sub>** could not be established because gHMBC was not measured due to the low amount of material available. All residues are D configured and in pyranose form.

### 3.3 Characterization of OS-BSA conjugate

Free amino groups present on the deacylated, dephosphorylated and reduced mixture of oligosaccharides (section 9.4) were linked to the lysines residues of BSA using glutaraldehyde as linker (figure 3.3.1).

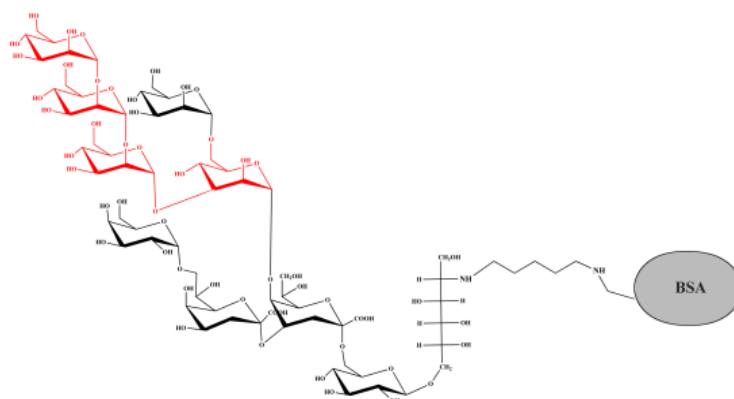


Figure 3.3.1: Neoglycoprotein obtained by the conjugation of the deacylated, dephosphorylated and reduced OS from *R. radiobacter* RV3 with BSA, mediated by glutaraldehyde. Residues in red represent the carbohydrate moiety analogue to the gp120 D1 arm (section 2.1)

Before the addition of OS substrate, the formation of Schiff bases between the BSA lysines and glutaraldehyde was estimated with the TNBS test (section 9.5).

A BSA standard solution ( $1 \text{ mg ml}^{-1}$ ) was used to build a calibration curve (figure 3.3.2), measuring the  $UV_{440}$  absorbance of known quantities of protein.

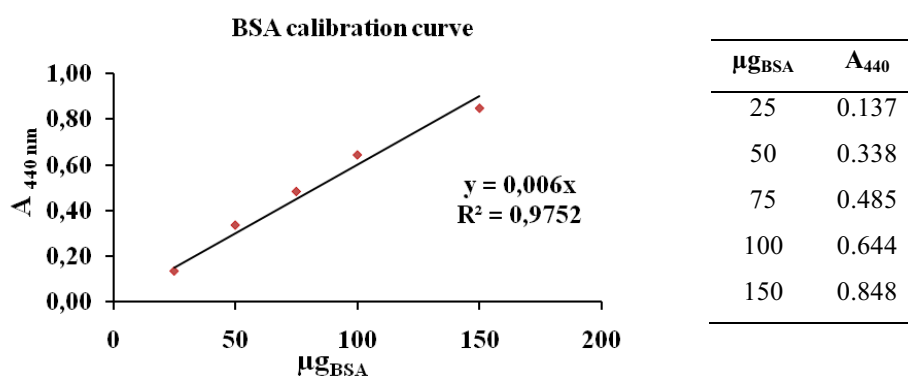


Figure 3.3.2: BSA calibration curve

The linear regression returned an interpolating straight line equation:  $A_{440} = 0.006 \mu\text{g}_{\text{BSA}}$  with a good sample correlation coefficient ( $R^2 = 0.975$ ). The measures performed on BSA conjugated with glutaraldehyde are reported in table 3.3.1

$\mu\text{g}_{\text{BSA-glut}}$	$A_{440}$	$\mu\text{g}_{\text{BSA-glut}}$ from TNBS test	% $\text{NH}_2\text{-BSA}$
15	0.058	9.72	64.78
25	0.062	10.28	41.13
50	0.112	19.98	39.97
75	0.218	36.33	48.44
100	0.326	54.32	54.32
			49.7

Table 3.3.1: Estimation of free BSA aminogroups

Where:

$$\mu\text{g}_{\text{BSA-glut}} \text{ from TNBS test} = (A_{440} / 0.006)$$

$\%_{\text{NH}_2\text{-BSA}} = [(\mu\text{g}_{\text{BSA-glut}}) \text{ from TNBS test} / (\mu\text{g}_{\text{BSA-glut}})] \cdot 100 = 49.7 \%$  in average value represents the quantity of  $\epsilon$ -amino groups of BSA lysines free after reaction with glutaraldehyde.

The OS-BSA conjugate was chromatographed on Sephacryl HR-100 and, on the basis of the chromatographic profile, fractions proximal to the void volume were divided in three groups: **OS-BSA<sub>A</sub>**, **OS-BSA<sub>B</sub>**, **OS-BSA<sub>C</sub>**, further visualized through SDS-PAGE (figure 3.3.3).

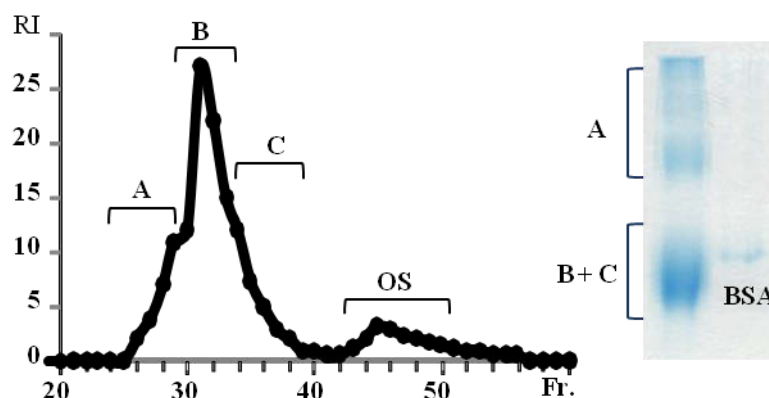


Figure 3.3.3: Sephacryl HR-100 chromatogram of the OS-BSA conjugate purification. The unreacted oligosaccharides (OS) eluted after an almost one column volume. The mixture of OS-BSA conjugate was divided into three fractions A, B, C and further analyzed via SDS-PAGE (8% separating gel, 16  $\mu\text{g}$ ) using BSA as standard.

An estimation of molecular weight of the OS-BSA conjugates was determined through GPC on TSKG5000PW<sub>XL</sub> with respect to commercial protein standards (section 9.5, table 3.3.2)

Protein	MW(Da)	LogMW	Time (min)
Tyroglobulin	669000	5.82	7.95
Apoferritin	443000	5.65	8.04
BSA	66000	4.82	9.14

Table 3.3.2: Calibration with standard proteins

The equation of the interpolating straight line:  $\text{LogMW} = -0.8057\text{min} + 12.18$  was used to calculate the molecular weight (MW) of the OS-BSA conjugates through the introduction of measured elution times (table 3.3.3, figure 3.3.4).

	Time (min)	LogPM	MW (Da)
<b>OS-BSA<sub>A</sub></b>	8.50	5.33	216000
<b>OS-BSA<sub>B</sub></b>	8.98	4.95	88300
<b>OS-BSA<sub>C</sub></b>	9.02	4.91	81500

Table 3.3.3: Estimation of OS-BSA conjugates molecular weights

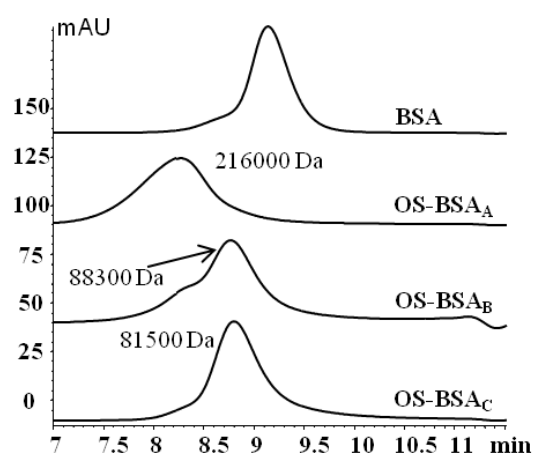


Figure 3.3.4: TSK G5000PW<sub>XL</sub> gel permeation chromatography of OS-BSA<sub>A-C</sub> fractions and BSA. Calibration was performed using protein standards (table 3.3.2)

The molecular weight of the OS-BSA<sub>A-C</sub> conjugates was major than that of BSA (66000 Da), as expected (figure 3.3.4).

The determination of the carbohydrate load of the protein was performed on the most abundant fraction OS-BSA<sub>B</sub> using the colorimetric phenol-H<sub>2</sub>SO<sub>4</sub> method and a quantitative GC-MS estimation (section 9.5).

#### Phenol-H<sub>2</sub>SO<sub>4</sub> method:

The exact concentration of the BSA component of the neoglycoprotein (0.68 mg ml<sup>-1</sup>) was estimated measuring the UV<sub>280</sub> absorbance of the solution and using the BSA extinction coefficient ( $\epsilon = 0.670$ ). The estimation of the carbohydrate content of the synthetic glycoprotein, was performed through the phenol - sulfuric acid test, calibrated with an OS solution (1.9 mg ml<sup>-1</sup>). The interpolating straight line obtained by linear regression resulted:  $A_{490\text{nm}} = 0.021 \mu\text{g}_{\text{OS}}$  (figure 3.3.5).

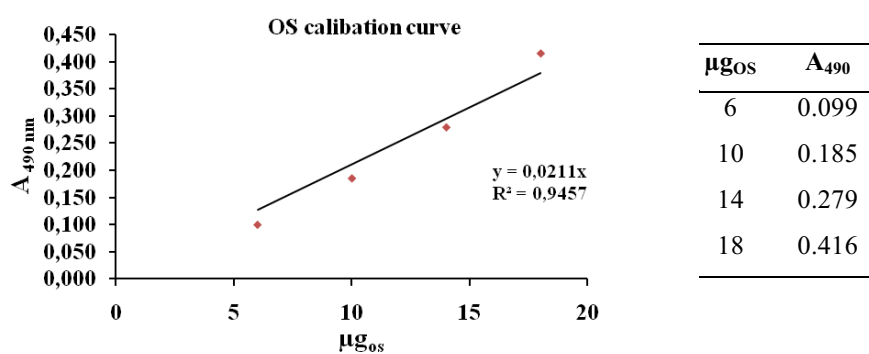


Figure 3.3.5: Oligosaccharide calibration curve

The values relative to the sample are reported in table 3.3.4:

$\text{mg}_{\text{BSA}}$	$A_{490}$	$\mu\text{gos}_{\text{BSA}}$	$\mu\text{gos}/\text{mg}_{\text{BSA}}$
0.072	0.052	2.48	34.44
0.096	0.063	3.00	31.25
0.120	0.081	3.86	32.17
			32.62

Table 3.3.4: Quantification of the ratio OS/BSA

Where:

$$\text{mg}_{\text{BSA}} = (\mu\text{l}_{\text{OS-BSA}} \cdot C_{\text{BSA}}) / 1 \cdot 10^{-3}; \text{ where } C_{\text{BSA}} = 0.68 \mu\text{g } \mu\text{L}^{-1}$$

$$\mu\text{gos}_{\text{BSA}} = A_{490} / 0.021$$

It is possible to estimate:

$$\mu\text{gos}/\text{mg}_{\text{BSA}} = \mathbf{32.62} \text{ in average value}$$

From these calculations:

$$\mu\text{mol}_{\text{OS}}/\text{mg}_{\text{BSA}} = (\mu\text{gos}/\text{mg}_{\text{BSA}})_{\text{average}} / \text{MW}_{\text{OS}} = \mathbf{0.018 \mu\text{mol}/\text{mg}_{\text{BSA}}}$$

$$\mu\text{mol}_{\text{BSA}} = 1000 \mu\text{g}/\text{MW}_{\text{BSA}} = \mathbf{0.015 \mu\text{mol}}$$

Where:  $\text{MW}_{\text{BSA}} = 66\,000 \text{ Da}$  and  $\text{MW}_{\text{OS}} = 1770 \text{ Da}$

It was concluded that:

$$\mu\text{mol}_{\text{OS}}/\mu\text{mol}_{\text{BSA}} = \mathbf{1.2}$$

Quantitative GC-MS estimation:

Mannose monosaccharide was detected as acetylated *O*-methyl glycoside and its response factor was calculated with respect to inositol as internal standard (table 3.3.5):

Mannose ( $\mu\text{g}$ )	Inositol ( $\mu\text{g}$ )	Mannose/Inositol
10	50	0.2
30	50	0.6
50	50	1
100	50	2

Table 3.3.5: Quantities of mannose monosaccharide with respect to inositol standard

A known amount of **OS-BSA<sub>B</sub>** (13.5  $\mu\text{g}$ ) was treated as the mannose monosaccharide standard and its content estimated with respect to internal inositol (0.5  $\mu\text{g}$ ), as well. The areas relative to the content of mannose and inositol were estimated through GC-MS (table 3.3.6) and used for the construction of the calibration curve (figure 3.3.6).

	OS-BSA <sub>B</sub>	Mannose/Inositol			
		0.2	0.6	1	2
$A_{\text{Man}}$	9457161	116388	278657	1499047	5720929
$A_{\text{In}}$	1654527	1829203	1541492	3284902	8416895
$A_{\text{Man}}/A_{\text{In}}$	0.175	0.064	0.181	0.456	0.680

Table 3.3.6: Areas of the mannose and inositol relative to the sample and standards

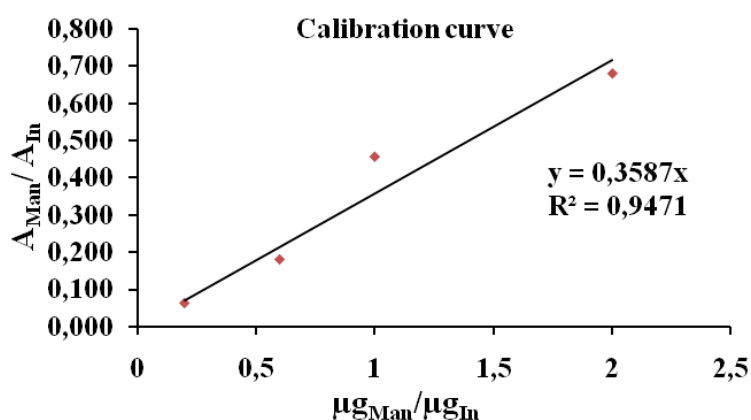


Figure 3.3.6: Mannose/inositol calibration curve

The linear regression returned a response factor  $(A_{\text{Man}}/A_{\text{In}}) = 0.359$  ( $\mu\text{g}_{\text{Man}}/\mu\text{g}_{\text{In}}$ )

Hence:

$$(\mu\text{g}_{\text{Man}}/\mu\text{g}_{\text{In}})_{\text{OS-BSA}} = (A_{\text{Man}}/A_{\text{In}})_{\text{OS-BSA}}/0.359 = 0.49$$

Where  $(A_{\text{Man}}/A_{\text{In}})_{\text{OS-BSA}} = 0.175$  (table 3.3.6)

The quantity of mannose in the sample with respect to the internal inositol (0.5  $\mu\text{g}$ ) resulted:

$$\mu\text{g}_{\text{Man}} = (\mu\text{g}_{\text{Man}}/\mu\text{g}_{\text{In}})_{\text{OS-BSA}} \cdot \mu\text{g}_{\text{In}} = 0.24 \mu\text{g}$$

$$\mu\text{mol}_{\text{Man}} = \mu\text{g}_{\text{Man}}/MW_{\text{Man}} = 1.36 \cdot 10^{-3} \mu\text{mol}$$

The quantity of OS, considering the five mannose units in the structure, resulted:

$$\mu\text{mol}_{\text{OS}} = \mu\text{mol}_{\text{Man}}/5 = \mathbf{2.7 \cdot 10^{-4} \mu\text{mol}}$$

$$\mu\text{g}_{\text{OS}} = \mu\text{mol}_{\text{OS}} \cdot MW_{\text{OS}} = 0.48 \mu\text{g}$$

The quantity of BSA of the glycoconjugate with respect to the OS-BSA quantity (13.5  $\mu\text{g}$ ) resulted:

$$\mu\text{g}_{\text{BSA}} = \mu\text{g}_{\text{OS-BSA}} - \mu\text{g}_{\text{OS}} = 13.02 \mu\text{g}$$

$$\mu\text{mol}_{\text{BSA}} = \mu\text{g}_{\text{BSA}}/MW_{\text{BSA}} = \mathbf{1.97 \cdot 10^{-4} \mu\text{mol}}$$

It was calculated that the molar ratio resulted:

$$\mu\text{mol}_{\text{OS}}/\mu\text{mol}_{\text{BSA}} = \mathbf{1.37}$$

### 3.4 Conclusions

The neoglycoprotein synthesized possessed as antigen the LOS produced by the prokaryote *Rhizobium radiobacter* RV3 opportunely derivatized, and the BSA as protein carrier. The approach used for the their linkage followed the protocol described by Holst *et al.*, 1991 that suggested a cross reaction of the glutaraldehyde linker between the lysines amino groups of the BSA and free amino group of the oligosaccharide. About the 50% of the  $\epsilon$ -amino groups of the BSA available resulted linked to the glutaraldehyde. The methods used for the quantification of OS/BSA, the colorimetric phenol- $\text{H}_2\text{SO}_4$  test and quantitative GC-MS estimation, returned a molar ratio average to 1.3. The independence of the approaches was considered a validation of the result.

However the broadly neutralizing antibody 2G12 resulted not affine to this neoglycoprotein, these studies represented a starting point to the further exploration of *Rhizobium radiobacter* Rv3 for new HIV vaccine productions.

## CHAPTER IV

### CHARACTERIZATION OF THE *O*-CHAIN AND LIPID A PORTIONS OF THE LPS FROM *Cupriavidus necator* DSM 13523

The structure of the glycolipid and *O*-antigenic portions of the LPS produced by *Cupriavidus necator* DSM 13523 (section 2.2) was elucidated. The *O*-polysaccharide repeating unit was disclosed through spectroscopic analyses, and it was constituted by five deoxy sugars, one of which is the rare 4-deoxy- $\beta$ -D-*arabino*hexose. The definition of the Lipid A moiety required the use of mass spectrometry and chemical investigations. It presented a conserved biposphorylated disaccharide backbone peculiarly substituted only by 14 carbons fatty acids and the symmetric hexa-acylated specie appeared the most abundant.

#### 4.1 Chemical analyses of the Lipopolysaccharide

Cells of *Cupriavidus necator* DSM 13523 were extracted according to the phenol-water protocol and the LPS was recovered only in the water phase, which was purified by enzymatic treatments and ultracentrifugation (section 8.2). SDS-PAGE analysis showed the characteristic ladder pattern of the LPS (figure 4.1.1, line C). Monosaccharides analysis of the LPS showed the presence of L-rhamnose (L-Rha) as main component, D-mannose (D-Man), D-glucose (D-Glc), 2-amino-2-deoxy-D-glucose (D-GlcN), L-*glycero*-D-*manno*-heptose (L,D-Hep), 3-deoxy-D-*manno*-oct-2-ulosonic acid (Kdo) and 4-deoxy-D-*arabino*hexose (D-ara4dHex) residue. This last residue was identified through NMR analysis (section 4.3).



Figure 4.1.1: SDS-PAGE (stacking gel 5 %, separating gel 12 %) stained with silver nitrate of water extract (C, 6  $\mu$ g) from *Cupriavidus necator* DSM 13523. R: standard of *E. coli* O55:B5 (6  $\mu$ g)

Methylation analysis detected the presence of 2-, 3- and 3,4- substituted rhamnose units, terminal 4-deoxy-*arabino*hexose and 2- and 4- substituted hexoses. The Kdo, heptose, and phosphorylated glucosamine were not detected with the methylation protocol used. Fatty acids methyl esters analysis showed the presence only of 14 carbons fatty acids: tetradecanoic (14:0), 3- hydroxytetradecanoic [14:0(3-OH)] and the 2-hydroxytetradecanoic [14:0(2-OH)] acid.

#### 4.2 Structural characterization of Lipid A

The Lipid A of *Cupriavidus necator* was structurally defined through MALDI-TOF mass spectrometry (chapter X). Ion negative spectrum (figure 4.2.1) of intact Lipid A showed two main groups of signals **A-B** and **C-D** corresponding respectively to hexa- and penta-acyl substitution on biphosphorylated glucosamine disaccharide backbone. The base peak **B** ( $m/z$  1821.7) was composed of four 14:0(3-OH), two 14:0, while **A** ( $m/z$  1837.52) presented the replacement of the secondary 14:0 with the 2-hydroxylated form, since it differed from **B** of 16 u. The replacement of the 14:0 unit by one 14:0(2-OH) is only possible for a secondary fatty acid since the primary are always hydroxylated at C-3. The same pattern was verified for the penta-acylated species **C-D**, differing from **A** and **B** for the lack of a 14:0 (3-OH) (figure 4.2.2, table 4.2.1). Less intense **A<sub>1</sub>**, **B<sub>1</sub>**, **C<sub>1</sub>** and **D<sub>1</sub>** signals were originated by the loss of a phosphate group from the parental species **A**, **B**, **C** and **D** (table 4.2.1).

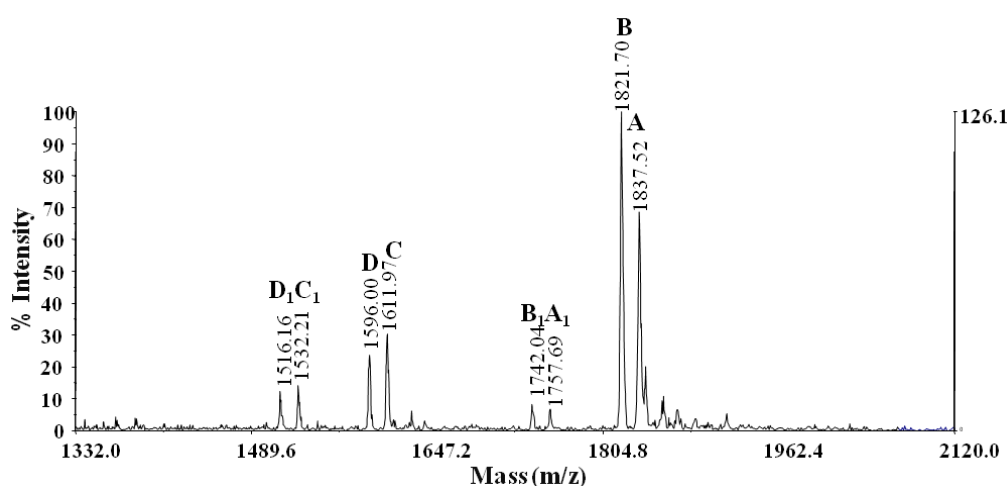


Figure 4.2.1: Linear ion negative MALDI spectrum of intact Lipid A from *C. necator* DSM 13523. Peaks attributions are reported in table 4.2.1, structures in figure 4.2.2

Specie	Rel. Int. (%)	n. acyl	Phosphate and fatty acids composition	Ion (m/z)
<b>A</b>	73.2	6	4 x 14:0(3-OH), 14:0(2-OH), 14:0, 2 x P	1837.5
<b>B</b>	100	6	4 x 14:0(3-OH), 2 x 14:0, 2 x P	1821.7
<b>A<sub>1</sub></b>	6.3	6	4 x 14:0(3-OH), 14:0 (2-OH), 14:0, P	1757.7
<b>B<sub>1</sub></b>	6.3	6	4 x 14:0(3-OH), 2 x 14:0, P	1742.0
<b>C</b>	31.7	5	3 x 14:0(3-OH), 14:0 (2-OH), 14:0, 2 x P	1611.9
<b>D</b>	24.6	5	3 x 14:0(3-OH), 2 x 14:0, 2 x P	1596.0
<b>C<sub>1</sub></b>	13.4	5	3 x 14:0(3-OH), 14:0(2-OH), 14:0, P	1532.2
<b>D<sub>1</sub></b>	10.6	5	3 x 14:0(3-OH), 2 x 14:0, P	1516.2

Table 4.2.1: Hexa- and penta-acylated species of Lipid A from *C. necator* DSM 13523 identified in the ion negative MALDI-TOF spectrum (figure 4.2.1) The two glucosamine units have been omitted for clarity.

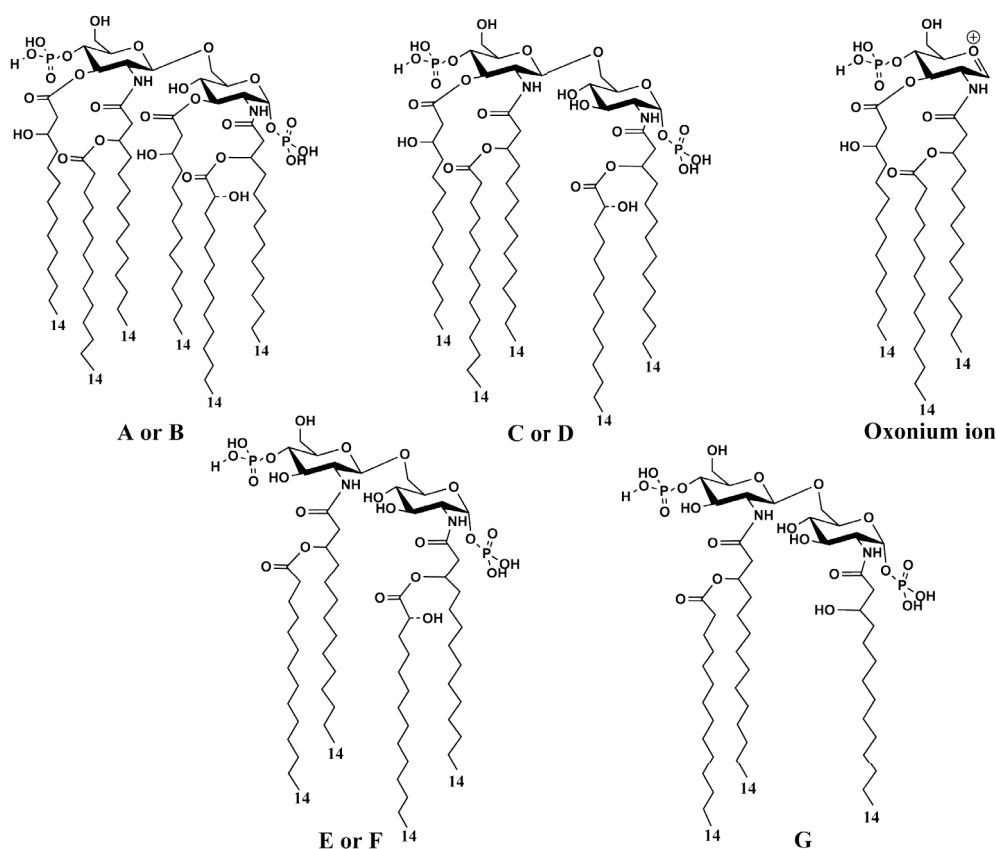


Figure 4.2.2: Structures of the Lipid A molecules from *C. necator*. Species **A** and **B**, **C** and **D** were detected in the intact Lipid A spectrum, while **E**, **F**, **G** were obtained from ammonia-treated Lipid A. The species **A-D** yielded the same oxonium ion. The broken line in the structures indicates the non stoichiometric presence of hydroxyl group (table 4.2.1)

The first information about the distribution of fatty acids was provided by the ion positive MALDI-TOF spectrum of intact Lipid A. The ion at  $m/z$  906.81 (figure 4.2.3) was consistent with a phosphorylated oxonium ion, substituted by two 14:0(3-OH) and one secondary 14:0 (figure 4.2.2). The absence of other species related to the substitution of the secondary 14:0 with the 14:0(2-OH), suggested that this heterogeneity is located on the reducing unit of GlcN (GlcN I). In order to favorite the ionization in positive mode, Lipid A was dephosphorylated. The oxonium ion signal at  $m/z$  824.15 in the ion positive MALDI-TOF spectrum (figure 4.2.4) was consistent with the composition of fatty acids structure proposed above.

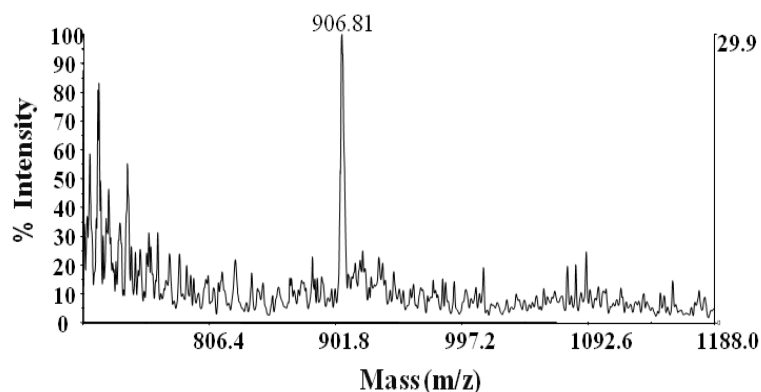


Figure 4.2.3: Expansion of the linear ion positive MALDI spectrum of the intact Lipid A. The structure of the oxonium ion ( $m/z$  906.81) is reported in figure 4.2.2.

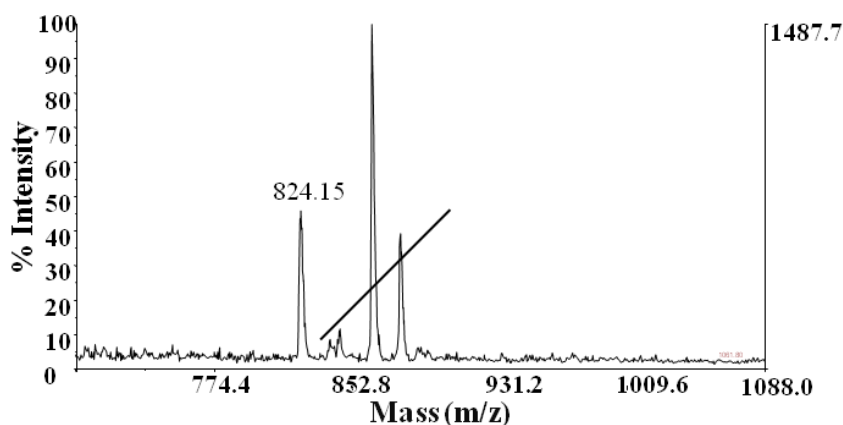


Figure 4.2.4: Expansion of the linear ion positive MALDI spectrum of the dephosphorylated Lipid A. The structure of the oxonium ion ( $m/z$  824.15) is consistent with the fatty acids composition reported in figure 4.2.2.

The position of the ester-linked fatty acids was determined analyzing the ion negative MALDI spectrum of Lipid A subjected to mild alkaline hydrolysis with ammonium hydroxide (Silipo *et al.*, 2002). The treatment removes preferentially the ester-linked acyloxyacyl esters leaving the amide-linked ones together with their acyloxy substituents. The spectrum (figure 4.2.5) showed the occurrence of a main tetra-acylated specie **F** ( $m/z$  1371.7) carrying two 14:0(3-OH), two (14:0). It was accompanied by specie **E** ( $m/z$  1387.75) that differs from **F** for the replacement of a 14:0 with a 14:0 (2-OH). Very less intense peaks **E**<sub>1</sub> and **F**<sub>1</sub> corresponded to **E** and **F** species missing of a phosphate group. The tri-acyl specie **G** ( $m/z$  1161.73) was also recorded, consistent with the presence of two 14:0(3-OH) and one 14:0 (table 4.2.2 and structures in figure 4.2.2).

These information together with that provided by the oxonium ion (figure 4.2.2) led to the conclusion that the secondary ester-linked fatty acids were located on the primary amide-linked chains and that the reducing unit of the glucosamine (GlcN D) accommodated the microheterogeneity related to the presence or not of an hydroxyl group on the secondary 14:0.

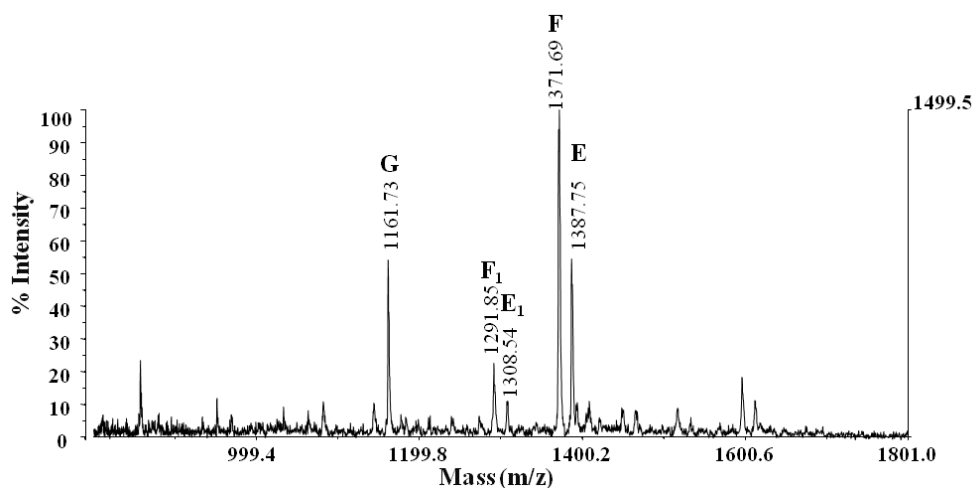


Figure 4.2.5: Linear ion negative MALDI spectrum of ammonia-treated Lipid A of *C. necator* DSM 13523  
Composition of species is reported in table 4.2.2, structures in figure 4.2.2

Specie	Rel. int.(%)	n. acyl	Phosphate and fatty acids composition	Ion (m/z)
E	53.1	4	2 x 14:0(3-OH), 14:0(2-OH), 14:0, 2 x P	1387.7
F	100	4	2 x 14:0(3-OH), 2 x 14:0, 2 x P	1371.7
E <sub>1</sub>	8.6	4	2 x 14:0(3-OH), 14:0(2-OH), 14:0, 2 x P	1308.5
F <sub>1</sub>	19.5	4	2 x 14:0(3-OH), 2 x 14:0, 2 x P	1291.8
G	51.8	3	2 x 14:0(3-OH), 14:0, 2 x P	1161.7

Table 4.2.2: Molecular species after ammonia treatment of Lipid A of *C. necator* DSM 13523 (figure 4.2.5). The two glucosamine units have been omitted.

### 4.3 Spectroscopic analysis of the O-Chain

<sup>1</sup>H NMR of the purified LPS contained the diagnostic signals relative to the repeating unit of the O-Chain (figure 4.3.1): five anomeric signals (5.09 - 4.99 ppm), several overlapped doublets at 1.3 ppm due to the methyl groups of rhamnose units, and two signals at 1.77 and 1.54 ppm corresponding to the axial and equatorial protons respectively of the 4-deoxy sugar. All residues were labelled in order of decreasing chemical shift with a letter (A-E), and the analysis of the homo- and heteronuclear 2D spectra led to the assignment of all proton and carbon chemical shifts (table 4.3.1)

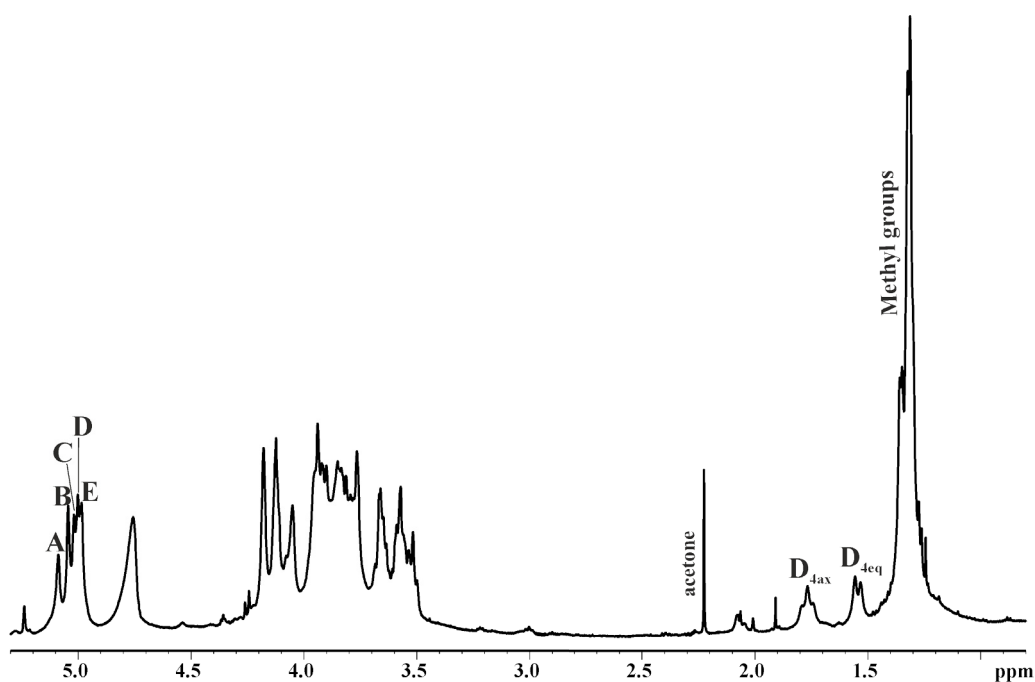


Figure 4.3.1: (600 MHz, 303 K,  $D_2O$ ),  $^1H$  NMR of the O-Chain repeating unit of *C. necator* DSM 13523. Letters are referred to the NMR attribution in table 4.3.1

	1	2	3	4	5	6-6'
<b>A</b>	5.09	4.05	3.95	3.51	3.86	1.32
<b>2)-<math>\alpha</math>-L-Rhap</b>	<i>102.6</i>	<i>80.3</i>	<i>71.1</i>	<i>73.4</i>	<i>70.7</i>	<i>17.9</i>
<b>B</b>	5.05	4.18	3.91	3.57	3.88	1.32
<b>3)-<math>\alpha</math>-L-Rhap</b>	<i>103.3</i>	<i>71.2</i>	<i>80.1</i>	<i>72.5</i>	<i>70.6</i>	<i>17.9</i>
<b>C</b>	5.02	4.14	4.06	3.82	3.97	1.35
<b>3,4)-<math>\alpha</math>-L-Rhap</b>	<i>103.6</i>	<i>71.03</i>	<i>81.43</i>	<i>78.4</i>	<i>69.4</i>	<i>18.3</i>
<b>D</b>	5.00	3.77	4.12	1.77(ax)-1.55(eq)	3.94	3.67-3.65
<b>t-<math>\beta</math>-D-4dAraHexp</b>	<i>100.6</i>	<i>69.9</i>	<i>69.1</i>	<i>29.7</i>	<i>73.1</i>	<i>65.4</i>
<b>E</b>	4.99	4.19	3.84	3.79	3.79	1.31
<b>3)-<math>\alpha</math>-L-Rhap</b>	<i>103.6</i>	<i>71.2</i>	<i>79.1</i>	<i>70.6</i>	<i>70.6</i>	<i>18.2</i>

Table 4.3.1:  $^1H$  (regular) and  $^{13}C$  (italic) chemical shifts at 303 K in  $D_2O$ , measured for the O-chain of *C. necator* DSM 13523 (proton spectrum in figure 4.3.1, structure in figure 4.3.2).

Residues **A**, **B**, **C** and **E** were classified as  $\alpha$ -Rha (6-deoxy-mannopyranose); the *manno* configuration was explained by the weak scalar correlation in the DQ-COSY spectrum relating H-2 to its vicinal protons (H-1 and H-3) and one strong between H-3 and H-4. H-1 of the spin system **D** correlated via H-2 and H-3 with high field signals linked to non hydroxylated C-4 and it was identified as a 4-deoxy-arabinohexose on the base of literature data (Katzenellenbogen *et al.*, 2003; Gamian *et al.*, 1985).



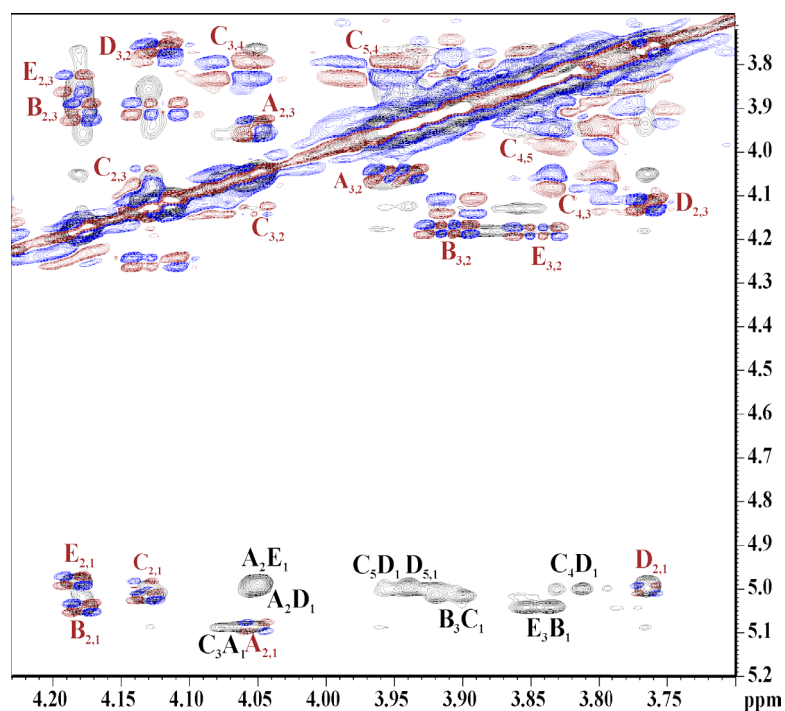


Figure 4.3.4: (600 MHz, 303 K,  $D_2O$ ) Attribution of the anomeric region of the NOESY (black) and COSY (blue and red) (table 4.3.1)

The presence of the rare sugar 4-deoxy- $\beta$ -arabinopyranose, was confirmed by the spectroscopic analysis of the monosaccharide isolated from LPS by acid hydrolysis and GPC chromatography (section 9.6). The proton spectrum (figure 4.3.5) showed the occurrence of three anomeric signals (A-C) where **B** resulted the most intense. The proton and carbon chemical shifts were assigned through the use of COSY, TOCSY, TROESY and HSQC bidimensional spectra.

Residues **B** and **C** resulted  $\beta$  and  $\alpha$  configured according to the values of  $^3J_{1,2}$  coupling constant of 0.87 Hz for **B**, 3.89 Hz for **C**. Residue **A** was identified as 1,6-anhydro-4-deoxy-arabinopyranose, because of the downfield glycosylation shifts of the *C*-1 and *C*-6.

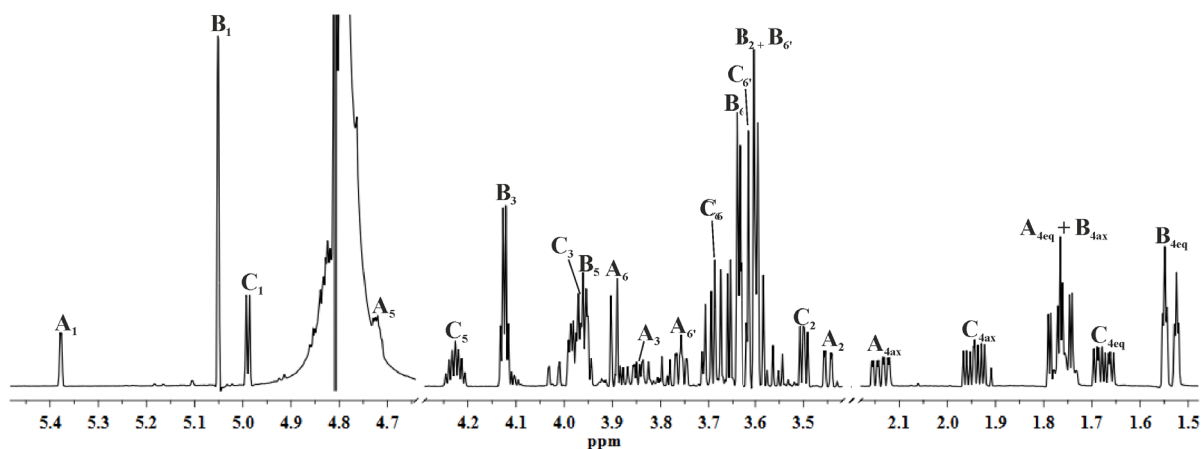


Figure 4.3.5: (600 MHz, 298 K,  $D_2O$ ),  $^1H$  NMR of the mixture of 4-deoxy-arabinopyranose monosaccharides isolated from the LPS of *C. necator* DSM 13523. Letters and numbers on the signals are referred to the NMR attribution in table 4.3.2

	1	2	3	4ax-4eq	5	6-6'
<b>A</b>	5.38	3.46	3.85	2.14-1.76	4.72	3.90-3.77
<b>1,6-anhydro-4dAraHexp</b>	<i>102.8</i>	<i>76.1</i>	<i>69.2</i>	<i>37.3</i>	<i>74.8</i>	<i>69.3</i>
<b>B</b>	5.05	3.59	4.12	1.76-1.54	3.97	3.64-3.60
<b><math>\alpha</math>-D-4dAraHexp</b>	<i>93.2</i>	<i>70.1</i>	<i>69.2</i>	<i>29.2</i>	<i>72.9</i>	<i>65.4</i>
<b>C</b>	4.99	3.50	3.96	1.95-1.67	4.23	3.68-3.63
<b><math>\beta</math>-D-4dAraHexp</b>	<i>95.0</i>	<i>71.9</i>	<i>68.4</i>	<i>30.9</i>	<i>68.6</i>	<i>64.3</i>

Table 4.3.2:  $^1\text{H}$  (regular) and  $^{13}\text{C}$  (italic) chemical shifts at 298 K in  $\text{D}_2\text{O}$ , measured for the mixture of 4-deoxy-arabinopyranose monosaccharides

#### 4.4 Conclusions

*Cupriavidus necator* produces mainly a symmetric hexa-acyl Lipid A made up by the conserved biphosphorylated disaccharide glucosamine backbone, substituted by tetradecanoic acid and the respective 3- and 2- hydroxylated forms. The amide-linked fatty acids carried the acyloxy substituents and the microheterogeneity given by the non stoichiometric substitution of a secondary 14:0 with 14:0 (2-OH) was on the reducing glucosamine (figure 4.2.2). The fatty acid pattern seems closely related to that of the highly agonistic Lipid A of *E. coli*, which has an asymmetric distribution of the acyl chains and a secondary dodecanoic acid. Different Lipid As from non-pathogenic bacteria as *Rhodobacter capsulatus*, *Rhodobacter spheroides* and *Chromobacter violaceum* were described as antagonists (Seydel *et al.*, 2000, section 1.4); in particular, the Lipid A from *Chromobacter violaceum* has an hexa-acyl symmetric structure, similar to that found for *Cupriavidus necator*. These assumptions increase the interest to the investigation of the biological activity of Lipid A of *Cupriavidus necator*.

NMR analysis allowed the establishment of the *O*-polysaccharide repeating unit. It is completely formed by deoxy sugars, four rhamnose units and one of the 4-deoxy-*arabinopyranose* as terminal unit of the chain. This last sugar is rare and identified only in certain *Citrobacter* strains (Katzenellenbogen *et al.*, 2003; Romanowska *et al.*, 1987, Gagian *et al.*, 1985; Romanowska *et al.*, 1981). The neutral and lipophilic feature of the *O*-polysaccharide is shared by the Lipopolysaccharides and Capsular polysaccharides of many other soil bacteria, most of the members of the *Rhizobiaceae* family (De Castro *et al.*, 2008; De Castro, Fregolino *et al.*, 2008), or other genera as *Azospirillum* (Fedonenko *et al.*, 2008) and *Kaistella* (Gargiulo, De Castro *et al.*, 2008). Next studies will address the Core oligosaccharide structure, and the understanding of LPS involvement in the environmental adaptation process of this bacterium or in its predatory activity.

## CHAPTER V

### LIPOOLIGOSACCHARIDE STRUCTURAL CHARACTERIZATION OF A CLINICAL ISOLATE OF *Acinetobacter baumannii*, STRAIN SMAL

The complete structural characterization of the Lipooligosaccharide produced by a clinical isolate of *Acinetobacter baumannii* strain SMAL was determined to gain valuable information that will provide an understanding of the mechanism activity adopted by this emerging pathogen (section 2.3). In particular, the characterization of the Lipid A moiety of the LPS is important since it plays a crucial role in the pathogenesis of this bacterium and give rise to the innate immune response of the patient. The sequence of the Core oligosaccharide was achieved through the combined use of the chemical and spectroscopic techniques, and it was found to be similar to that of *Acinetobacter baumannii* ATCC 19606 (Vinogradov *et al.*, 2002), although the LOS from the strain SMAL presented an enhanced zwitterionic character. Regarding the Lipid A structure, mass spectrometry experiments revealed that it is composed of a heterogeneous mixture of molecules differing for type and degree of acylation. The proportion among the differently acylated species changed in response to the growth conditions: predominance of the hepta-acylated species was observed when the bacterium was grown in Fetal Bovine Serum (FBS) at 37°C, whereas the hexa-acylated molecular species resulted more abundant using Luria Broth (LB) as growth medium. The results would suggest that hepta-acylation of Lipid A is a mechanism of adaptation to the mammalian host by *A. baumannii*.

#### 5.1 Chemical analyses of the Lipooligosaccharide

Freeze-dried bacterial cells were grown in LB at 28 °C and extracted according to PCP method (section 8.3). The LOS was found to be composed of D-glucose (D-Glc), 2-amino-2-deoxy-D-galactose (D-GalN), 3-deoxy-manno-oct-2-ulosonic acid (Kdo) and 2-amino-2-deoxy-D-glucuronic acid (D-GlcNA). Fatty acids were analysed via GC-MS as methyl ester derivatives. The combined information from total and O-linked composition identified the following ester-linked fatty acids: dodecanoic (12:0), 2-hydroxydodecanoic [12:0(2-OH)], and 3-hydroxydodecanoic [12:0(3-OH)] acid; 3-hydroxytetradecanoic acid [14:0(3-OH)] appeared as an amide-linked residue. The 3-hydroxy fatty acids possessed the (*R*)- and the 2-hydroxy fatty acid the (*S*)-configuration (Rietschel, 1976). Location of acyl substituent was determined via ESI MS spectrometry, analysing the intact and ammonia-treated Lipid A. Finally, in order to verify the influence of the environment on the bacterial Lipid A structure, *Acinetobacter baumannii* strain SMAL was grown in LB and in FBS media at 37°C (sections 8.3 and 5.3).

### 5.2 Mass spectrometry analysis of the intact and ammonia-deacylated Lipid A from the growth in Luria Broth at 28 °C

The intact and ammonia deacylated Lipids A were analysed by the Electrospray Ionization Fourier-Transform Ion Cyclotron Resonance Mass Spectrometry (ESI-FT-ICR MS) (Chapter X). The charge-deconvoluted negative ion mass spectrum of native Lipid A (figure 5.2.1) showed five groups of pseudomolecular ions, that originate from intrinsic heterogeneity caused by the type and the number of fatty acids linked to the disaccharide backbone. Each set of signals was labelled with a letter, and within each set, the different peaks were distinguished by numbers. Accordingly, group **A** was composed from hepta-acylated species, **B** from hexa-acylated, **C** from penta-acylated, **D** from tetra-acylated and **E** from tri-acylated species (table 5.2.1).

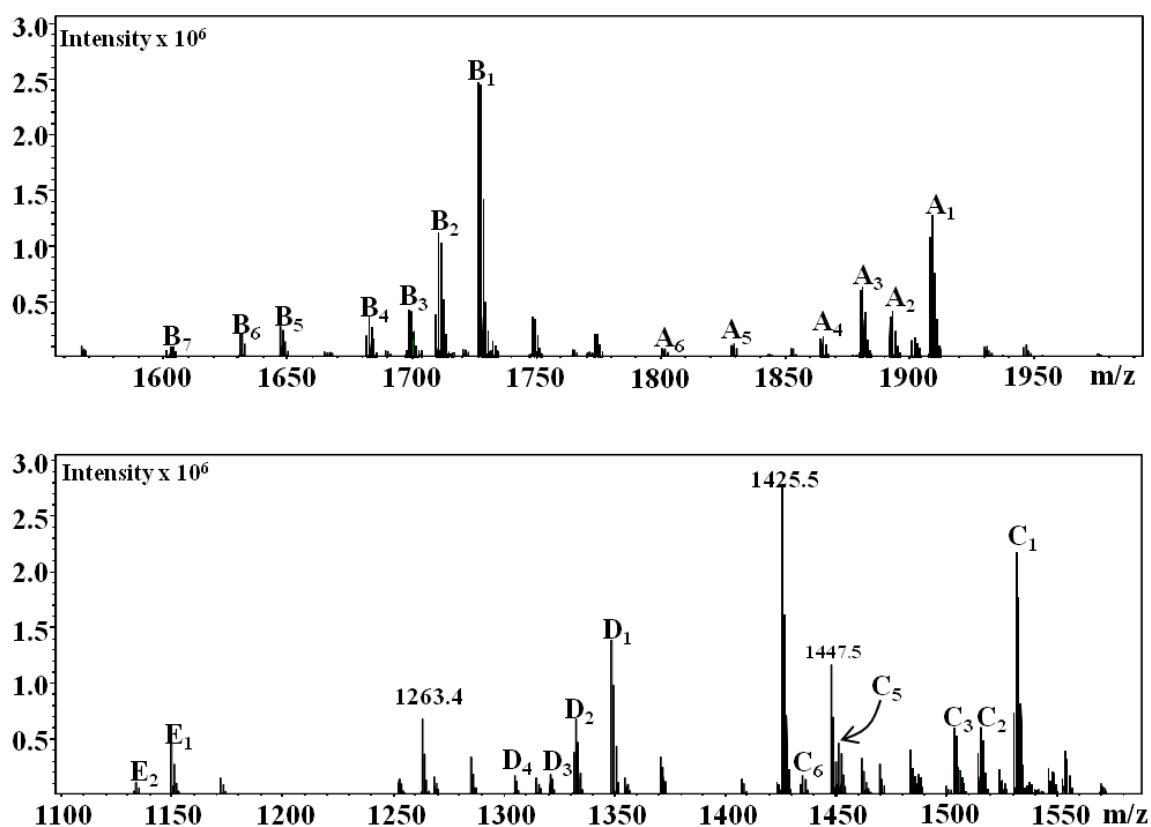


Figure 5.2.1: Pseudomolecular peaks measured by ESI-FT-ICR MS of Lipid A family produced by *Acinetobacter baumannii* strain SMAL (structures in figure 5.2.2). The peaks at  $m/z = 1447.5$  and  $1236.4$  and other minor peaks are impurities not related to Lipid A.

Ion ( <i>m/z</i> )	Rel. Int. (%)	Species	n-Acyl	Proposed fatty acid/phosphate composition
1911.3	51.8	<b>A<sub>1</sub></b>	7	2 x 14:0(3-OH), 2 x 12:0(3-OH), 12:0(2-OH), 2 x 12:0, 2 x P
1895.3	17.0	<b>A<sub>2</sub></b>	7	2 x 14:0(3-OH), 2 x 12:0(3-OH), 3 x 12:0, 2 x P
1883.3	28.0	<b>A<sub>3</sub></b>	7	14:0(3-OH), 3 x 12:0(3-OH), 12:0(2-OH), 2 x 12:0, 2 x P
1867.3	8.0	<b>A<sub>4</sub></b>	7	14:0(3-OH), 3 x 12:0(3-OH), 3 x 12:0, 2 x P
1831.3	4.8	<b>A<sub>5</sub></b>	7	2 x 14:0(3-OH), 2 x 12:0(3-OH), 12:0(2-OH), 2 x 12:0, P
1803.3	3.2	<b>A<sub>6</sub></b>	7	14:0(3-OH), 3 x 12:0(3-OH), 12:0(2-OH), 2 x 12:0, P
1729.1	100	<b>B<sub>1</sub></b>	6	2 x 14:0(3-OH), 2 x 12:0(3-OH), 12:0(2-OH), 12:0, 2 x P
1712.1	46.2	<b>B<sub>2</sub></b>	6	2 x 14:0(3-OH), 2x 12:0(3-OH), 2 x 12:0, 2 x P
1700.1	17.5	<b>B<sub>3</sub></b>	6	14:0(3-OH), 3x 12:0(3-OH), 12:0(2-OH), 12:0, 2 x P
1684.1	14.3	<b>B<sub>4</sub></b>	6	14:0(3-OH), 3x 12:0(3-OH), 2 x 12:0, 2 x P
1649.2	11.4	<b>B<sub>5</sub></b>	6	2 x 14:0(3-OH), 2 x 12:0(3-OH), 12:0(2-OH), 12:0, P
1633.2	8.5	<b>B<sub>6</sub></b>	6	2 x 14:0(3-OH), 2x 12:0(3-OH), 2 x 12:0, P
1605.1	3.6	<b>B<sub>7</sub></b>	6	14:0(3-OH), 3x 12:0(3-OH), 2 x 12:0, P
1530.0	86.9	<b>C<sub>1</sub></b>	5	2 x 14:0(3-OH), 12:0(3-OH), 12:0(2-OH), 12:0, 2 x P
1514.0	24.6	<b>C<sub>2</sub></b>	5	2 x 14:0(3-OH), 12:0(3-OH), 2 x 12:0, 2 x P
1501.9	24.1	<b>C<sub>3</sub></b>	5	14:0(3-OH), 2 x 12:0(3-OH), 12:0(2-OH), 1 x 12:0, 2 x P
1485.9	7.2	<b>C<sub>4</sub></b>	5	14:0(3-OH), 2 x 12:0(3-OH), 2 x 12:0, 2 x P
1451.0	18.3	<b>C<sub>5</sub></b>	5	2 x 14:0(3-OH), 12:0(3-OH), 1 x 12:0(2-OH), 12:0, P
1434.0	7.0	<b>C<sub>6</sub></b>	5	2 x 14:0(3-OH), 12:0(3-OH), 2 x 12:0, P
1347.8	55.8	<b>D<sub>1</sub></b>	4	2 x 14:0(3-OH), 12:0(3-OH), 12:0(2-OH), 2 x P
1331.8	15.5	<b>D<sub>2</sub></b>	4	2 x 14:0(3-OH), 12:0(3-OH), 12:0, 2 x P
1319.8	7.5	<b>D<sub>3</sub></b>	4	14:0(3-OH), 2 x 12:0(3-OH), 12:0(2-OH), 2 x P
1303.8	7.0	<b>D<sub>4</sub></b>	4	14:0(3-OH), 2 x 12:0(3-OH), 12:0, 2 x P
1149.6	18.0	<b>E<sub>1</sub></b>	3	2 x 14:0(3-OH), 12:0(2-OH), 2 x P
1133.6	1.2	<b>E<sub>2</sub></b>	3	2 x 14:0(3-OH), 12:0, 2 x P

Table 5.2.1: Molecular species of intact Lipid A from *A. baumannii* strain SMAL identified by ESI-FT-ICR MS (spectrum in figure 5.2.1, structures in figure 5.2.2). The two glucosamine units have been omitted.

In particular, the composition of the predominant species **B<sub>1</sub>** (figure and table 5.2.1), was consistent with the occurrence of two 14:0(3-OH), two 12:0(3-OH), one 12:0(2-OH), one 12:0 and two phosphate units; **B<sub>2</sub>** was related to **B<sub>1</sub>** since 12:0(2-OH) was replaced by 12:0, **B<sub>3</sub>** differed from **B<sub>1</sub>** since one 14:0(3-OH) was replaced by one 12:0(3-OH), and **B<sub>4</sub>** differed from **B<sub>3</sub>** by the replacement of 12:0(2-OH) with 12:0. The presence of one 12:0(2-OH), as identified in chemical analysis, was confirmed by the difference of 16 u between different couples of a pseudomolecular ions, like **B<sub>1</sub>** – **B<sub>2</sub>** or **B<sub>3</sub>** – **B<sub>4</sub>**. This difference indicated the replacement of the 12:0(2-OH) unit by one 12:0, a substitution that is only possible for a secondary fatty acid and not for a primary which is always hydroxylated at C-3. The species from **B<sub>5</sub>** to **B<sub>7</sub>** had the same lipid composition of shown for **B<sub>1</sub>**, **B<sub>2</sub>**, **B<sub>4</sub>**, respectively, except that one phosphate was missing.

A similar pattern similar was identified in almost all the other peak clusters, although some peaks were missing probably due to their low abundance. Considering **B<sub>1</sub>** as reference, the homolog species in the other clusters were identified as follows (figure and table 5.2.1): **A<sub>1</sub>** contained one additional 12:0, **C<sub>1</sub>** was missing one 12:0(3-OH), **D<sub>1</sub>** lacked one 12:0(3-OH) and one 12:0 whereas **E<sub>1</sub>** conserved the two units of 14:0(3-OH) and that of 12:0(2-OH). The occurrence in every cluster of the 12:0(2-OH) was indicated by the presence of peaks differing for 16 u, as discussed above. Therefore, considering the **B<sub>1</sub>** composition, the location of the four primary fatty acids was straightforward: the two amide-linked 14:0(3-OH) units were amide-linked, whereas the other two 3-hydroxyl-bearing fatty acids were ester-bound substituents at *O*-3 of each glucosamine residue (figure 5.2.2).

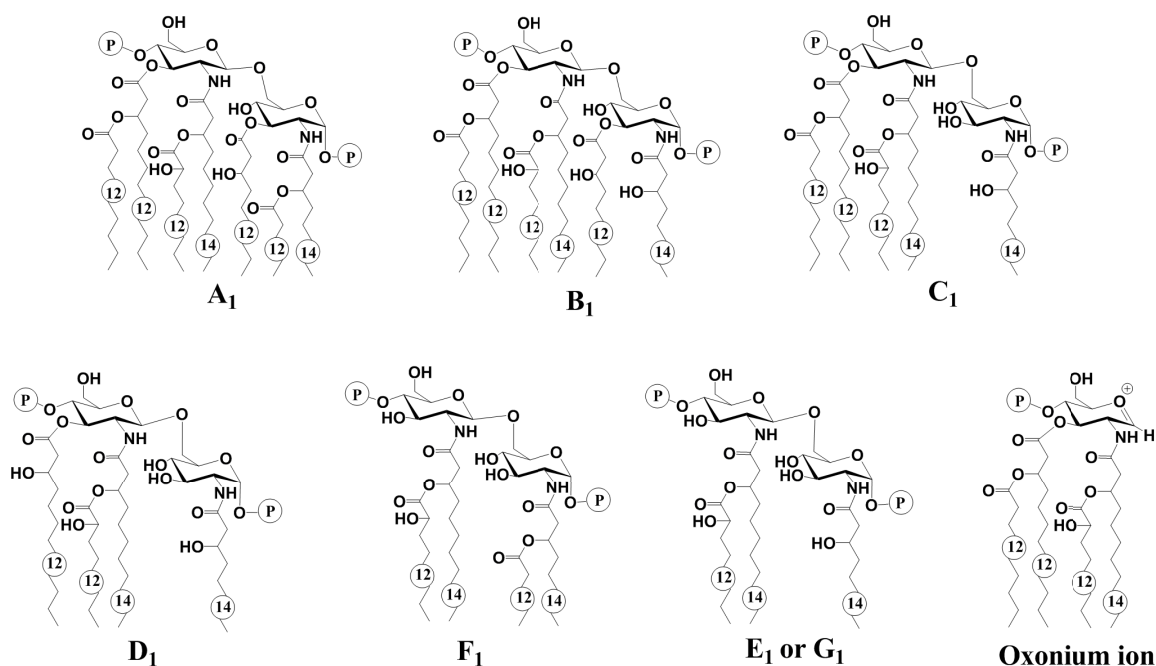


Figure 5.2.2: Structures of the Lipid A from *A. baumannii* strain SMAL, species from **A<sub>1</sub>** to **E<sub>1</sub>** were detected in the intact Lipid A spectrum and molecules **F<sub>1</sub>** and **G<sub>1</sub>** were obtained from ammonia-treated Lipid A. **A<sub>1</sub>**, **B<sub>1</sub>** and **C<sub>1</sub>** yielded the same oxonium ion

The location of the two secondary fatty acids was inferred analysing the infrared multi-photon dissociation (IRMPD) MS/MS data recorded in positive mode or the molecular ions complexed with triethylamine (Kondakova and Lindner, 2005). Under such conditions, [**B<sub>1</sub>** + TEA] at  $m/z = 1830.4$  u produced an abundant oxonium fragment ion at  $m/z = 1046.8$  u (structure in figure 5.2.2), representative of the non-reducing glucosamine moiety of the Lipid A with its substituents, one phosphate, one 14:0(3-OH), one 12:0(2-OH), one 12:0(3-OH) and one 12:0. On the basis of this information, the two secondary fatty acids identified in **B<sub>1</sub>**, were located on the non-reducing glucosamine moiety, and their exact position was inferred analysing the ammonia treated LA (see below). The same oxonium ion was observed for **A<sub>1</sub>** and **C<sub>1</sub>** species.

The exact position of the ester-linked fatty acids was inferred by analysis of the ammonia-treated LA (Silipo *et al.*, 2002). Accordingly, analysis of the negative ESI spectrum (figure 5.2.3) of the ammonia-treated Lipid A identified the secondary fatty acids on the corresponding primary amide-linked residues: it contained three different clusters, named **F**, **G** and **H**, related to tetra-, tri- and di-acylated species, respectively (table 5.2.2).

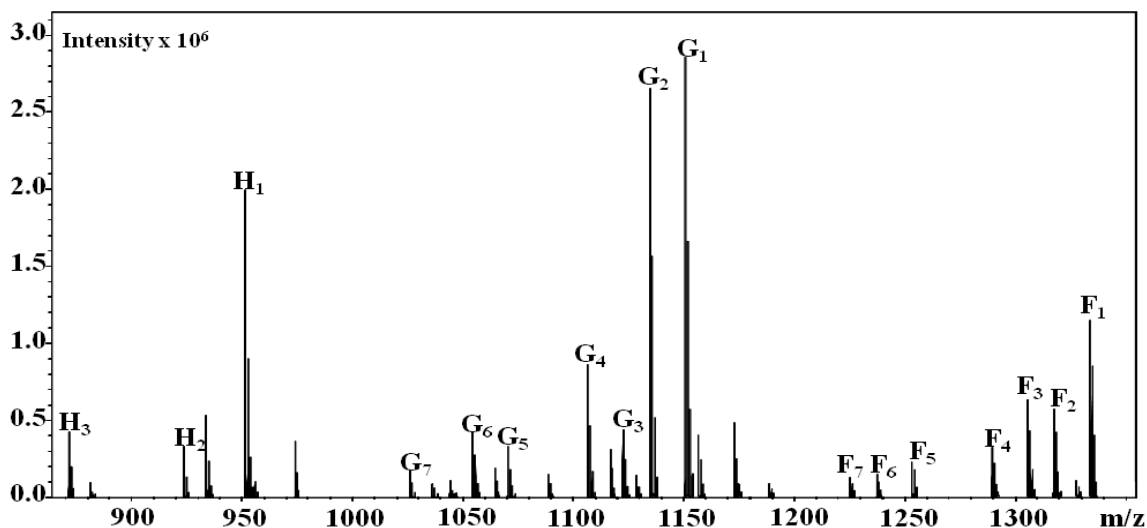


Figure 5.2.3: Pseudomolecular peaks identified by ESI-FT-ICR MS (structures in figure 5.2.2) of ammonia-treated Lipid A from *A. baumannii* strain SMAL.

The more informative clusters were **F** and **G**, whereas the diacylated species, **H**<sub>1-3</sub>, were identified as side-products of the chemical treatment: namely from the ammonia removal of the secondary fatty acid located on the amide-linked acyl residue of both **F** and **G** clusters.

The composition of the predominant species, **G**<sub>1</sub> (figure 5.2.3, table 5.2.2), disclosed the occurrence of two 14:0(3-OH), one 12:0(2-OH), and two phosphates. The distribution pattern within each cluster was similar to that of the native Lipid A, i.e., the substitution of 12:0(2-OH) with 12:0, the replacement of one 14:0(3-OH) by one 12:0(3-OH), and the lack of one phosphate unit. Information from **G**<sub>1</sub> ion were combined with the indication contained in the oxonium ion (1046.8 u, structure in figure 5.2.2) descending from **B**<sub>1</sub> peak of the native Lipid A: actually, according to the oxonium ion composition, the hexa-acylated **B**<sub>1</sub> species possessed two secondary fatty acids on the non-reducing glucosamine, one 12:0(2-OH) and one 12:0. The finding that only the 12:0(2-OH) unit was left after ammonia treatment led to position this fatty acid on the amide linked 14:0(3-OH), whereas the other, 12:0, lost during the chemical treatment, was considered ester bound on the 12:0(3-OH) unit. On the basis of the above consideration, the location of the secondary fatty acids composing the penta-, tetra- and tri-acylated species in the native Lipid A, was determined (figure 5.2.2). Finally, cluster **F** mass distribution indicated the occurrence of tetra-acylated Lipids A with a fatty acid composition different from that described for the tetra-acylated Lipids A in the native sample (cluster **D**).

Ion ( <i>m/z</i> )	Rel. Int. (%)	Species	n-Acyl	Proposed fatty acid/phosphate composition
1332.8	40.9	<b>F<sub>1</sub></b>	4	2 x 14:0(3-OH), 12:0(2-OH), 12:0, 2 x P
1316.8	20.1	<b>F<sub>2</sub></b>	4	2 x 14:0(3-OH), 2 x 12:0, 2 x P
1304.8	22.0	<b>F<sub>3</sub></b>	4	14:0(3-OH), 12:0(3-OH), 12:0(2-OH), 12:0, 2 x P
1288.8	11.6	<b>F<sub>4</sub></b>	4	14:0(3-OH), 12:0(3-OH), 2 x 12:0, 2 x P
1252.8	11.6	<b>F<sub>5</sub></b>	4	2 x 14:0(3-OH), 12:0(2-OH), 12:0, P
1236.8	5.1	<b>F<sub>6</sub></b>	4	2 x 14:0(3-OH), 2 x 12:0, P
1224.8	4.6	<b>F<sub>7</sub></b>	4	14:0(3-OH), 12:0(3-OH), 12:0(2-OH), 12:0, P
1150.6	100	<b>G<sub>1</sub></b>	3	2 x 14:0(3-OH), 12:0(2-OH), 2 x P
1134.6	95.8	<b>G<sub>2</sub></b>	3	2 x 14:0(3-OH), 12:0, 2 x P
1122.6	15.6	<b>G<sub>3</sub></b>	3	14:0(3-OH), 12:0(3-OH), 12:0(2-OH), 2 x P
1106.6	30.1	<b>G<sub>4</sub></b>	3	14:0(3-OH), 12:0(3-OH), 12:0, 2 x P
1070.6	11.6	<b>G<sub>5</sub></b>	3	2 x 14:0(3-OH), 12:0(2-OH), P
1054.7	14.8	<b>G<sub>6</sub></b>	3	2 x 14:0(3-OH), 12:0, P
1026.6	6.2	<b>G<sub>7</sub></b>	3	14:0(3-OH), 12:0(3-OH), 12:0, P
952.5	69.8	<b>H<sub>1</sub></b>	2	2 x 14:0(3-OH), 2 x P
934.5	18.5	<b>H<sub>2</sub></b>	2	14:0(3-OH), 12:0(3-OH), 2 x P
872.5	14.9	<b>H<sub>3</sub></b>	2	2 x 14:0(3-OH), P

Table 5.2.2: Molecular species of ammonia-treated Lipid A from *A. baumannii* strain SMAL identified by ESI-FT-ICR MS (spectrum in figure 5.2.3, structures in figure 5.2.2). The two glucosamine units have been omitted.

This discrepancy was only apparent and witnessed the effectiveness of the ammonia treatment; actually, lipid composition of cluster **F** was not related to that of the cluster **D**, but reflected the distribution of the ester bound acyls on the primary amide linked fatty acids of the originally hepta-acylated Lipid A family (cluster **A**). The above information led to assign the structure of the hepta-acylated species; actually, **F<sub>1</sub>** composition reflected the presence of two 14:0(3-OH), one 12:0(2-OH), one 12:0 and two phosphates, therefore when compared to **G<sub>1</sub>**, **F<sub>1</sub>** contained one additional 12:0 unit. Consequently, the only position compatible with the chemical treatment adopted and still available on the disaccharide backbone, was the 14:0(3-OH) unit on the GlcN-I residue yielding to both **F<sub>1</sub>** and **A<sub>1</sub>** structures reported in figure 5.2.2.

### 5.3 Structural variation of Lipid A under different growth conditions

The influence of the environment on the bacterial Lipid A structure of *A. baumannii* strain SMAL was tested growing cells in FBS (Fetal Bovine Serum) medium at 37°C, since this condition is closer, to that experienced from the bacterium during the infection process in humans. Growth in Luria Broth (LB) at the same temperature was performed as control experiment (section 8.3).

Lipid A from FBS growth was analysed via MALDI-TOF (figure 5.3.1) because it did not produce any result with ESI MS. The failure to produce data on ESI MS might be related to the low purity grade of the sample, since the extraction procedure employed (hot phenol-water) did not remove efficiently the components of the complex medium used.

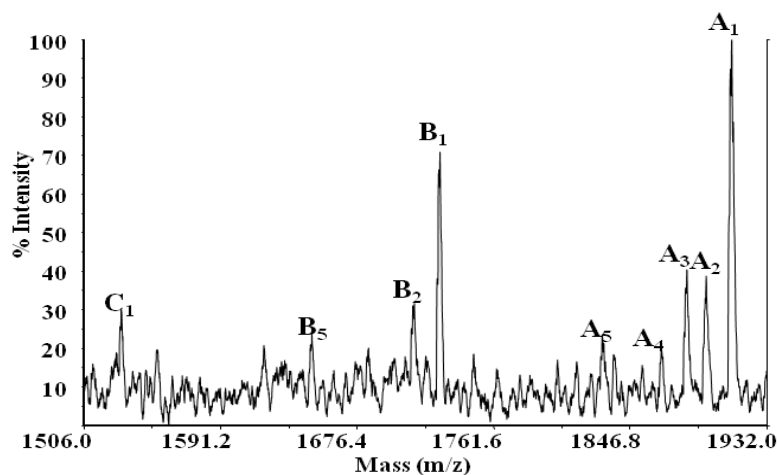


Figure 5.3.1: Linear ion negative MALDI-TOF spectrum of Lipid A from *A. baumannii* strain SMAL grown in FBS at 37 °C. Peaks labels are referred to the species indicated in table 5.2.1

Since the instrument used (MALDI or ESI) could modify the proportion between the pseudomolecular ions, MALDI of the intact Lipid A was recorded and it was found comparable to the ESI spectrum of the same sample (figure 5.3.2).

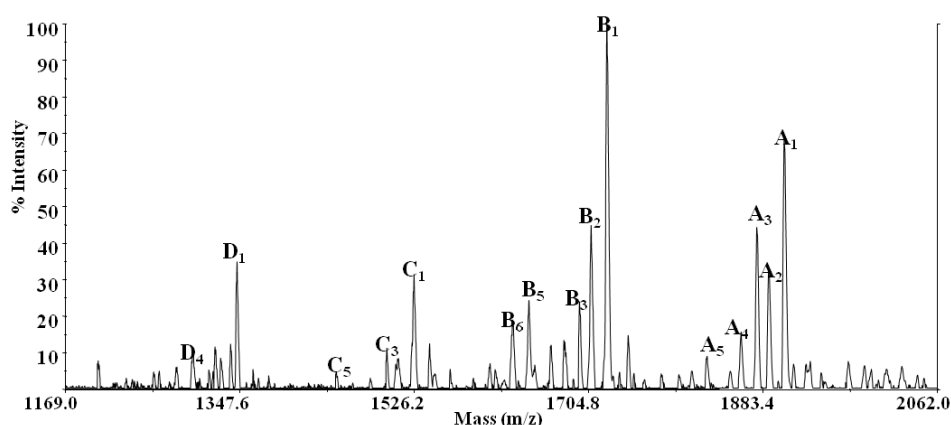


Figure 5.3.2: Linear ion negative MALDI-TOF spectrum of intact Lipid A from *A. baumannii* strain SMAL grown in LB at 28 °C. The proportions among species are comparable to that found in ESI spectrum (figure 5.2.1). Peaks labels are referred to the species indicated in table 5.2.1

The ion negative MALDI-TOF spectrum of Lipid A from FBS at 37°C (figure 5.3.1) identified two main clusters **A<sub>1</sub>** and **B<sub>1</sub>**, related to hepta- and hexa-acylated species, respectively. The composition of each cluster was analogous to that reported for the Lipid A from LB at 28 °C (figure 5.2.1, table 5.2.1), but the proportion among the hepta- and the hexa-acylated species was reversed, being the hepta-acylated species the most abundant.

In order to determine which growth parameter, medium and/or temperature, induced this effect, Lipid A obtained from the cultivation in LB at 37°C, was analysed through ESI MS and the spectrum (figure 5.3.3) showed the occurrence of hexa- and hepta-acylated species in proportions similar to those found for the Lipid A obtained from LB at 28°C (figure 5.2.1).

These results suggest that the acylation pattern changes with growth conditions, and that the higher amounts of the hepta-acylated Lipid A is not related to growth temperature but to the different environment created from the growth medium.

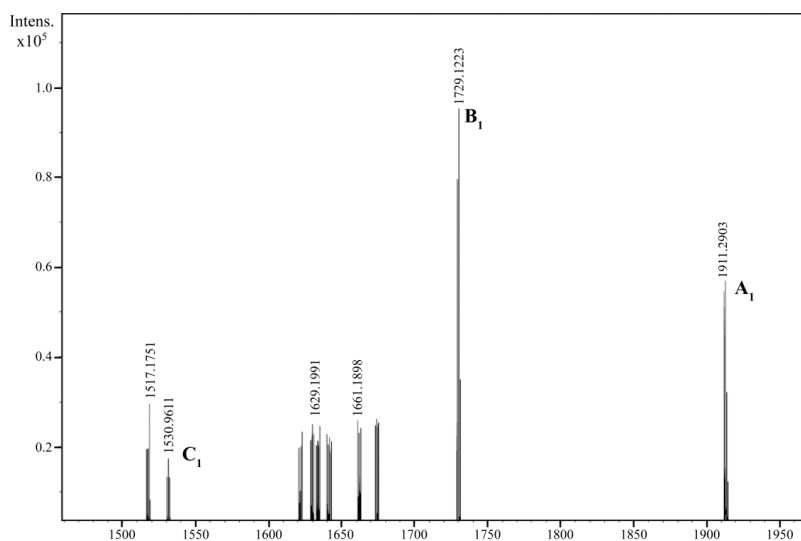


Figure 5.3.3: Pseudomolecular peaks of Lipid A from *A. baumannii* strain SMAL grown in LB at 37°C measured by ESI-FT-ICR MS as control experiment. Peaks labels are referred to the species indicated in table 5.2.1

#### 5.4 Spectroscopic characterization of Core oligosaccharide from the growth in Luria Broth at 28 °C

The complete structure of Core oligosaccharide **1** (figure 5.4.1) was deduced by combining the NMR spectroscopic data of the products isolated by alkaline degradation and acid hydrolysis (section 9.7). The first approach provided the structure of the incomplete Core oligosaccharide **2** (figure 5.4.1) caused by the lost of unit(s) during the alkaline treatment. This information was recovered by analyzing the product **3** obtained by mild acid hydrolysis (figure 5.4.1).

The truncated Core oligosaccharide (Figure 5.4.1, **2**) comprising the lipid A sugar backbone and a 2-amino-2-deoxyuronic acid derivative possessing a double bond conjugated to the carboxy group ( $\Delta$ HexNA), which results from  $\beta$ -elimination of the 4-substituted GlcNAc.

The  $^1\text{H}$  NMR spectrum of **2** (Figure 5.4.2 a) contains eight anomeric signals and three sets of diastereotopic methylene signals due to the presence of three Kdo residues. A detailed analysis of both the homo- and heteronuclear NMR spectra of the product **2** led to the complete assignment of its proton and carbon chemical shifts (table 5.4.1), which revealed its structure. Because the substituent at *O*-4 of  $\Delta$ HexNA was lost during the alkaline treatment of the LPS, the product obtained from mild acid hydrolysis (figure 5.4.1, **3**) was analyzed by NMR spectroscopy, which revealed an additional monosaccharide residue, unit **I** (Figure 5.4.2 b, table 5.4.2), but lacked the lipid A moiety (residues **A** and **E**) and the two Kdo units (**Kb** and **Kc**) as expected.

Combining the information from both **2** and **3**, the complete structure of the core oligosaccharide was determined as oligosaccharide **1** (figure 5.4.1). Surprisingly, this structure is equivalent to that previously described for *A. baumannii* strain ATCC 19606 (Vinogradov *et al.*, 2002).

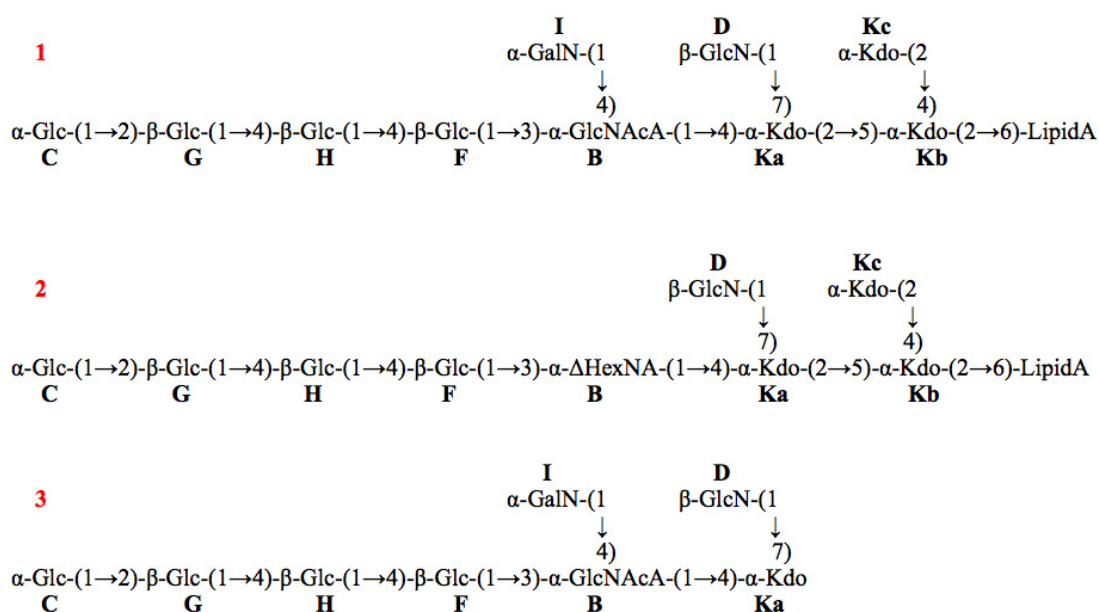


Figure 5.4.1: **1**: Complete structure of the Core oligosaccharide of LOS produced by *A. baumannii* strain SMAL. All sugars are D configured and in pyranose form. **2**: Oligosaccharide structure isolated after alkaline hydrolysis of LOS.  $\Delta$ HexNA is an hex-4-en-2-aminuronic residue that results from the  $\beta$ -elimination. **3**: Oligosaccharide structure obtained from LOS after mild acid hydrolysis. The structure of Lipid A family is reported in figure 5.2.2

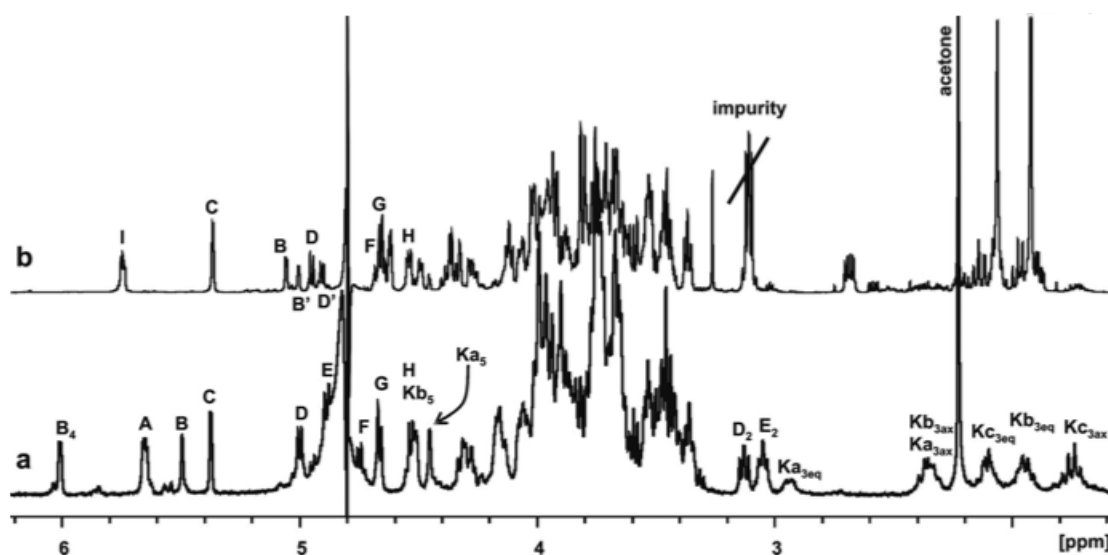


Figure 5.4.2: **a**: (500 MHz, 296 K,  $D_2O$ )  $^1H$  NMR spectrum of oligosaccharide **2** derived from the alkaline degradation of *A. baumannii* LOS (table 5.4.1). **b**: (600 MHz, 300 K,  $D_2O$ ) of oligosaccharide **3** derived from LOS after mild hydrolysis (table 5.4.2). Residue **A** and **E** are non reducing and reducing glucosamine units of Lipid A, respectively. The residues close to the free reducing end of the oligosaccharide give rise to different signals in the spectrum, as **B** and **B'**, **D** and **D'**, because their magnetic environment is affected by the different ring forms of the reducing Kdo residue. In both spectra, signals are labelled according to figure 5.4.1.

	<b>1</b>	<b>2</b>	<b>3ax</b>	<b>3eq</b>	<b>4</b>	<b>5</b>	<b>6</b>	<b>6'</b>	<b>7</b>	<b>8</b>	<b>8'</b>
<b>A</b>	5.66	3.41	3.89	-	3.65	4.16	4.29	3.77	-	-	-
<b>6)-<math>\alpha</math>-GlcN1P</b>	<i>91.9</i>	<i>55.9</i>	<i>70.8</i>	-	<i>70.8</i>	<i>73.7</i>	<i>70.8</i>	-	-	-	-
<b>B</b>	5.49	3.75	4.67	-	6.01	-	-	-	-	-	-
<b>3)-<math>\Delta</math>-HexAN</b>	<i>98.6</i>	<i>51.9</i>	<i>72.4</i>	-	<i>105.0</i>	<i>146.3</i>	<i>168.8</i>	-	-	-	-
<b>C</b>	5.37	3.54	3.75	-	3.45	4.07	3.80	3.80	-	-	-
<b><i>t</i>-<math>\alpha</math>-Glc</b>	<i>98.7</i>	<i>72.4</i>	<i>73.9</i>	-	<i>70.9</i>	<i>72.9</i>	<i>61.6</i>	-	-	-	-
<b>D</b>	5.00	3.13	3.68	-	3.48	3.55	3.75	3.94	-	-	-
<b><i>t</i>-<math>\beta</math>-GlcN</b>	<i>98.7</i>	<i>57.1</i>	<i>73.5</i>	-	<i>71.2</i>	<i>77.1</i>	<i>61.9</i>	-	-	-	-
<b>E</b>	4.89	3.05	3.85	-	3.73	3.75	3.71	3.45	-	-	-
<b>6)-<math>\beta</math>-GlcN4P</b>	<i>100.9</i>	<i>56.9</i>	<i>73.5</i>	-	<i>75.2</i>	<i>75.2</i>	<i>63.7</i>	-	-	-	-
<b>F</b>	4.75	3.36	3.67	-	3.68	3.66	4.00	3.83	-	-	-
<b>4)-<math>\beta</math>-Glc</b>	<i>102.7</i>	<i>74.0</i>	<i>75.2</i>	-	<i>79.5</i>	<i>76.2</i>	<i>61.1</i>	-	-	-	-
<b>G</b>	4.66	3.52	3.59	-	3.44	3.46	3.74	3.92	-	-	-
<b>2)-<math>\beta</math>-Glc</b>	<i>102.6</i>	<i>77.1</i>	<i>75.7</i>	-	<i>70.1</i>	<i>77.1</i>	<i>61.8</i>	-	-	-	-
<b>H</b>	4.53	3.36	3.67	-	3.78	3.63	3.99	3.87	-	-	-
<b>4)-<math>\beta</math>-Glc</b>	<i>103.6</i>	<i>74.3</i>	<i>74.9</i>	-	<i>79.9</i>	<i>76.2</i>	<i>61.2</i>	-	-	-	-
<b>Ka</b>	-	-	2.94	2.33	4.88	4.45	4.32	4.17	3.96	3.96	-
<b>4,7)-<math>\alpha</math>-Kdo</b>	<i>176.0</i>	<i>101.8</i>	<i>35.6</i>	-	<i>72.4</i>	<i>63.7</i>	<i>71.4</i>	<i>77.6</i>	<i>60.9</i>	-	-
<b>Kb</b>	-	-	1.94	2.37	3.98	4.51	3.71	3.89	3.66	3.89	-
<b>4,5)-<math>\alpha</math>-Kdo</b>	<i>176.1</i>	<i>100.8</i>	<i>35.6</i>	-	<i>73.8</i>	<i>70.4</i>	<i>73.8</i>	<i>70.8</i>	<i>65.0</i>	-	-
<b>Kc</b>	-	-	2.11	1.74	4.05	3.99	3.74	3.99	3.74	3.95	-
<b><i>t</i>-<math>\alpha</math>-Kdo</b>	<i>176.0</i>	<i>103.4</i>	<i>35.6</i>	-	<i>67.0</i>	<i>68.1</i>	<i>73.2</i>	<i>72.2</i>	<i>64.1</i>	-	-

Table 5.4.1:  $^1\text{H}$  (regular) and  $^{13}\text{C}$  (italic) chemical shifts at 500 MHz, 296 K in  $\text{D}_2\text{O}$ , measured for oligosaccharide **2** obtained after alkaline hydrolysis (figure 5.4.2 a).  $\Delta\text{HexAN}$  (residue **B**) results from  $\beta$ -elimination of the 4-substituted GlcNA. All sugars are D configured and in pyranose form

	1	2	3	3'	4	5	6	6'	7	8/8'
<b>B</b>	5.06	4.27	4.34	3.98	4.11	-	-	-	-	-
<b>3,4)-<math>\alpha</math>-GlcNAcA</b>	<i>95.9</i>	<i>54.3</i>	<i>78.2</i>	<i>75.3</i>	<i>74.4</i>	<i>176.1</i>	-	-	-	-
<b>B'</b>	5.00	4.26	4.38	3.98	4.11	-	-	-	-	-
<b>3,4)-<math>\alpha</math>-GlcNAcA</b>	<i>97.2</i>	<i>54.3</i>	<i>78.0</i>	<i>75.3</i>	<i>74.4</i>	<i>176.1</i>	-	-	-	-
<b>C</b>	5.37	3.52	3.75	3.45	4.06	3.80	3.75	-	-	-
<b><i>t</i>-<math>\alpha</math>-Glc</b>	<i>98.6</i>	<i>72.6</i>	<i>74.0</i>	<i>70.7</i>	<i>72.9</i>	<i>61.4</i>	-	-	-	-
<b>D</b>	4.95	3.12	3.68	3.47?	3.53?	3.93*	-	-	-	-
<b><i>t</i>-<math>\beta</math>-GlcN</b>	<i>99.2</i>	<i>57.1</i>	<i>73.5</i>	<i>71.2</i>	<i>77.5</i>	<i>61.8*</i>	-	-	-	-
<b>D'</b>	4.90	3.09	3.66	3.43	3.47	3.93*	-	-	-	-
<b><i>t</i>-<math>\beta</math>-GlcN</b>	<i>98.9</i>	<i>57.2</i>	<i>73.5</i>	<i>70.7</i>	<i>77.3</i>	<i>61.8*</i>	-	-	-	-
<b>F</b>	4.67	3.36	3.62	3.57	3.74	3.95*	-	-	-	-
<b>4)-<math>\beta</math>-Glc</b>	<i>104.2</i>	<i>73.8</i>	<i>75.2</i>	<i>76.1</i>	<i>74.0</i>	<i>61.8*</i>	-	-	-	-
<b>G</b>	4.66	3.51	3.59	3.46	3.75	3.92	3.70	-	-	-
<b>2)-<math>\beta</math>-Glc</b>	<i>102.7</i>	<i>77.3</i>	<i>75.5</i>	<i>70.8</i>	<i>74.0</i>	<i>61.9</i>	-	-	-	-
<b>H</b>	4.54	3.35	3.66	3.76	3.66	4.00	3.87	-	-	-
<b>4)-<math>\beta</math>-Glc</b>	<i>103.6</i>	<i>74.4</i>	<i>76.2</i>	<i>79.4</i>	<i>75.0</i>	<i>61.8</i>	-	-	-	-
<b>I</b>	5.74	3.54	4.00	4.02	3.96	3.70	3.90	-	-	-
<b><i>t</i>-<math>\alpha</math>-GalN</b>	<i>96.6</i>	<i>52.2</i>	<i>67.5</i>	<i>68.9</i>	<i>72.3</i>	<i>61.7</i>	-	-	-	-
<b>Kap</b>	-	-	1.95	2.16	4.13	4.32	3.92	4.12	~3.80	-
<b>4,7)-<math>\alpha</math>-Kdop</b>	<i>178.8</i>	<i>97.5</i>	<i>34.0</i>	<i>72.1</i>	<i>64.0</i>	<i>71.2</i>	<i>77.8</i>	<i>61.5</i>	-	-
<b>Kaf</b>	-	-	2.21	2.67	4.48	4.62	3.66	3.97	-	-
<b>4,7)-<math>\alpha</math>-Kdof</b>	<i>178.7</i>	<i>106.2</i>	<i>44.3</i>	<i>79.9</i>	<i>85.4</i>	<i>71.0</i>	<i>80.1</i>	-	-	-

\*Overlapped signals

Table 5.4.2:  $^1\text{H}$  (regular) and  $^{13}\text{C}$  (italic) chemical shifts at 600 MHz, 300 K in  $\text{D}_2\text{O}$ , measured for oligosaccharide **3** obtained after acid hydrolysis (figure 5.4.2 b). Residues **A** and **E** (non reducing and reducing GlcN units of Lipid A) and **Kb** and **Kc** (two Kdo units) are missing, but residue **I** is present. All sugars are D configured and in pyranose form

## 5.5 Conclusions

The complete sequence of the Core oligosaccharide of LOS of *Acinetobacter baumannii* strain SMAL was achieved through the combined use of chemical and spectroscopic procedures. The backbone is formed of 12 sugar residues, which are organized as a highly branched inner core moiety and is equivalent to one of the structures reported for *A. baumannii* ATCC 19606 (Vinogradov *et al.*, 2002). This region contains a motif that could be present within the *A. baumannii* LPS (Vinogradov *et al.*, 2002; Vinogradov *et al.*, 1998); however, it is also present in the Core region of LPS from *A. radioresistens* (Leone *et al.*, 2007).

In contrast to the Core region of LPS from *A. baumannii* ATCC 19606, the galactosamine linked to GlcNAcA is not *N*-acetylated, and the Core oligosaccharide is not truncated. These features might reflect the adaptation of the bacterium to the host environment, in particular, the cationic amino sugars decrease the net negative charge of the Core region and thus might shield the bacterial membrane from the effect of host defense agents, like the cationic antimicrobial peptides.

The structure of the Lipid A family was disclosed through mass spectrometry analyses and it varies both with the growing medium composition and the temperature. Analysis of the intact and ammonia-treated Lipid A, showed a heterogeneous blend of molecules, differing for both degree and type of acylation pattern (figure 5.2.2). In particular, when the bacterium was grown in LB at 28°C (or 37°C) it produced a complex family of glycolipids, containing the diphosphorylated glucosamine disaccharide backbone variously substituted, ranging from tri- to hepta-acylated molecules. Within each cluster, the different species either were due to the non-stoichiometric replacement of (*S*)-12:0(2-OH) with 12:0 or one (*R*)-14:0(3-OH) with (*R*)-12:0(3-OH), or to the lack of one phosphate unit. At this regard, it must be noted that concerning the genus *Acinetobacter*, (*S*)-12:0(2-OH) was reported so far only for the LPS of *A. radioresistant* (Leone *et al.*, 2007) where it was present in small amounts. The hexa-acylated lipid A displays those features usually considered important for an agonistic endotoxin, as that of *E. coli*, namely six fatty acids with a chain length of fourteen and/or twelve carbons, distributed in an asymmetric fashion on the glucosamine disaccharide backbone (Alexander and Rietschel, 2001). Another feature emerging from the present study is the modulation of the Lipid A family composition upon the growth medium used. The growth of *A. baumannii* in FBS at 37°C, promoted the biosynthesis of hepta-acylated Lipid A, a species usually considered as a weak immunostimulant of TLR4-MD2, and also able to confer antibiotic resistance to the bacterium. FBS medium was chosen as a mimic of the host environment, the results obtained open the way to new experiments finalized to the analyse the modulation of the Lipid A structure in response to other, and possibly more host-like, stimuli. In summary, *A. baumannii* strain SMAL, was able to modulate its lipid A structures in response to the growth medium, passing from a mixture with putative agonistic activity to one for which less inflammatory properties are expected. This data contribute to a better understanding of the virulence of this emerging successful pathogen.

## CHAPTER VI

### IDENTIFICATION AND STRUCTURAL DETERMINATION OF THE CAPSULAR POLYSACCHARIDES FROM TWO CLINICAL ISOLATES OF *Acinetobacter baumannii*, STRAINS SMAL AND MG1

Lipopolysaccharides from many *Acinetobacter* species have been described, and the occurrence of both R- (Fregolino *et al.*, 2010; Vinogradov *et al.*, 2002 ) and S-forms of LPS was disclosed (Haeseley *et al.*, 1998; Vinogradov *et al.*, 2001). More than 10 surface polysaccharides were isolated from different *A. baumannii* strains (Pantophlet, 2008), but in most cases it is not clear if they originate from CPSs or OPSs. To date, only two CPSs from *Acinetobacter* species were defined, and belonged to *A. calcoaceticus* BD4 (Kaplan *et al.*, 1985) and to *A. lwoffii* F78 (Hanuszkiewicz *et al.*, 2008). The structure of capsular polysaccharides by two clinical isolates of *A. baumannii* strains SMAL and MG1 was elucidated. Hot phenol/water extractions of the dry biomasses, followed by enzymatic digestions and repeated ultracentrifugations led to the isolation of capsular material: these polysaccharides were negative to Western Blot analysis with anti-lipid A antibodies, and their structures were established on the basis of NMR spectroscopy and GC-MS analyses. The *A. baumannii* MG1 CPS consisted of a linear aminopolysaccharide with acyl substitution heterogeneity at the N-4 amino group of the bacillosamine residue; NMR analysis disclosed the occurrence of 3-hydroxy-butyrric acid on 19% of the bacillosamine residue, as shown in figure 6.3.3. The repeating unit of the CPS produced by strain SMAL comprised a pentasaccharide backbone, as depicted in figure 6.4.2-2, which was previously described as the O-antigen of another *Acinetobacter baumannii* species (strain ATCC 17961) (MacLean *et al.*, 2009) while here it occurs as a capsule. Together with the peculiarity of the structures found for these two *A. baumannii* strains, these data are of importance to put on molecular basis serological tools. In addition to this, these results highlight that care must be taken in the development of these diagnostic devices, because similar if not identical polysaccharides might be constituents of the lipopolysaccharides O-antigen or of the bacterial envelope capsule, as here reported for *A. baumannii* SMAL.

#### **6.1 Isolation and chemical analyses of ultracentrifuge supernatants and sediment**

Freeze-dried cells of *A. baumannii* MG1 and SMAL were treated with aqueous 90% phenol-chloroform-light petroleum (PCP) to extract R-form LPS, and the remaining pellets were successively extracted according to the hot phenol/water method. The water phases were further purified, i.e. nucleic acid and protein contaminants were removed by enzymatic digestion and the resulting solutions were dialyzed and subjected to several cycles of ultracentrifugation (UC) (section 8.3). Sugar analysis of the UC sediments gave the same compositions as identified for the LOSs from the two *A.*

*baumannii* strains, namely D-Glc, D-GalN, D-GlcN, and 3-deoxy-D-manno-oct-2-ulosonic acid (Kdo). The monosaccharide composition of the UC supernatant from *A. baumannii* MG1 comprised L-GalNA, D-QuiN4N (bacillosamine), and D-GlcN. The absolute configuration of QuiN4N was assigned using the same sugar obtained from the CPS produced by *A. lwoffii* F78 (Hanuszkiewicz *et al.*, 2008) as standard, and similarly the GalNA butylglycoside was compared to the analogue derivative obtained from the LPS of *Halomonas pantelleriensis* (Corsaro *et al.*, 2006). Furthermore, after weak methanolysis and acetylation, GC-MS analysis showed the presence of QuinN4N substituted at N-4 by (S)-3-hydroxybutyric acid. The substituted position was assigned on the basis of the retention time and mass spectrum analogies with the same residue identified in the CPS of *A. lwoffii* F78. The sugar composition of the UC supernatant from *A. baumannii* SMAL revealed the presence of D-Gal, D-Glc, D-GlcN, D-GalN, and 2,3-diacetoamido-2,3-dideoxy-glucuronic acid (DAGA).

### 6.2 Electrophoretic and Western blot analysis of ultracentrifuge supernatant and sediment

The sediments and supernatants from UC were analyzed by SDS-PAGE. The gel was first fixed with Alcian blue then with silver nitrate, and disclosed the occurrence of LOS molecules in the sediment (figure 6.2.1), whereas the supernatants contained high molecular mass material which was sensible to Alcian blue (figure 6.2.2, lines 1-4) (section 9.2). Here, the presence of LOS was negligible and was detected only after having overloaded the gel (figure 6.2.2, lines 5 and 6).



Figure 6.2.1: SDS-PAGE (stacking gel 5%, separating gel 15 %), stained with Alcian blue and silver nitrate procedure of UC sediments; 1: *A. b.* SMAL (2 µg); 2: *A. b.* MG1 (2 µg); 3: *E. coli* O16 LPS (2 µg)

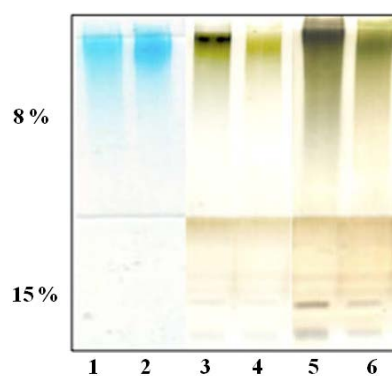


Figure 6.2.2: SDS-PAGE (Stacking gel 5%, separating gel 8 and 15 %) of the UC supernatants; lines 1 and 2 are stained only with Alcian blue; lines 3-6 are silver stained applying Alcian blue as fixative first. 1: *A. b.* SMAL (1 µg); 2: *A. b.* MG1 (1 µg); 3 and 5: *A. b.* SMAL (1 and 3 µg); 4 and 6: *A. b.* MG1 (1 and 3 µg).

In order to exclude that the isolated polysaccharides might originate from LPS, the CPS preparation was subjected to Western blot analysis developed after mild acid hydrolysis of the membrane with the monoclonal antibody (mAb) A6 (Kuhn *et al.*, 1992), which specifically recognizes the free bisphosphorylated diglucosamine backbone of lipid A (section 9.2).

This antibody had been used earlier for the identification of non-stainable S-form LPS in various *Acinetobacter* strains and LOS in *A. lwoffii* F78 (Hanuszkiewicz *et al.*, 2008). The CPS isolated from *A. baumannii* MG1 and SMAL did not bind mAb A6 (figure 6.2.3, lines 2 and 3). Only when applied in high amounts (figure 6.2.3., lines 4 and 5), a very faint smear appeared at the bottom of the membrane, with a migration similar to that observed for the purified LOS (figure 6.2.3, lines 6 and 7), confirming its occurrence in trace amounts. The lack of reaction of mAb A6 with the material in the upper part of the gel pointed at the presence of a CPS in both, *A. baumannii* MG1 and SMAL.

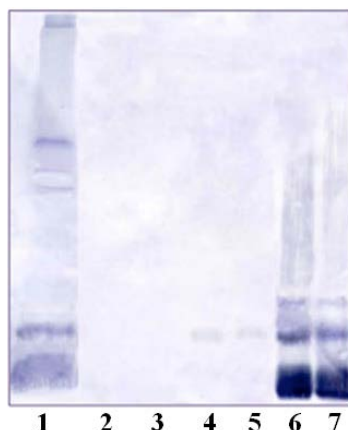


Figure 6.2.3: Western blot of the UC supernatants (lines 2-5) and sediments (lines 6-7) from *A. baumannii* SMAL and MG1, detected with mAb A6. **1**: LPS *E. coli* O16 (8  $\mu$ g); **2** and **4**: UC supernatant of *A. baumannii* SMAL (5 and 25  $\mu$ g); **3** and **5**: UC supernatant of *A. baumannii* MG1 (5 and 25  $\mu$ g); **6** and **7**: UC sediments from *A. baumannii* SMAL and MG1, respectively (3  $\mu$ g each)

### 6.3 Spectroscopic characterization of the CPS from *A. baumannii* strain MG1

In order to establish the structure of the repeating unit of the CPS of *A. baumannii* MG1, the UC supernatant was analyzed.

The  $^1\text{H}$  NMR spectrum (figure 6.3.1) contained several diagnostic signals: three anomeric ones (5.30-4.50 ppm), and those of four *N*-acetyl methyl protons (approx. 2.00 ppm) and two methyl signals (approx. 1.2 ppm). Of the latter, the most intense signal originated from H-6 of the bacillosamine, and the other one was related to 3-hydroxybutyric acid (HBA) present in non-stoichiometric amounts. The sugar residues were labelled with a letter (**A-C**) in order of their decreasing anomeric chemical shifts, and **D** corresponded to HBA. By analysis of the 2D NMR spectra of the polysaccharide all proton and carbon chemical shifts could be assigned (table 6.3.1).

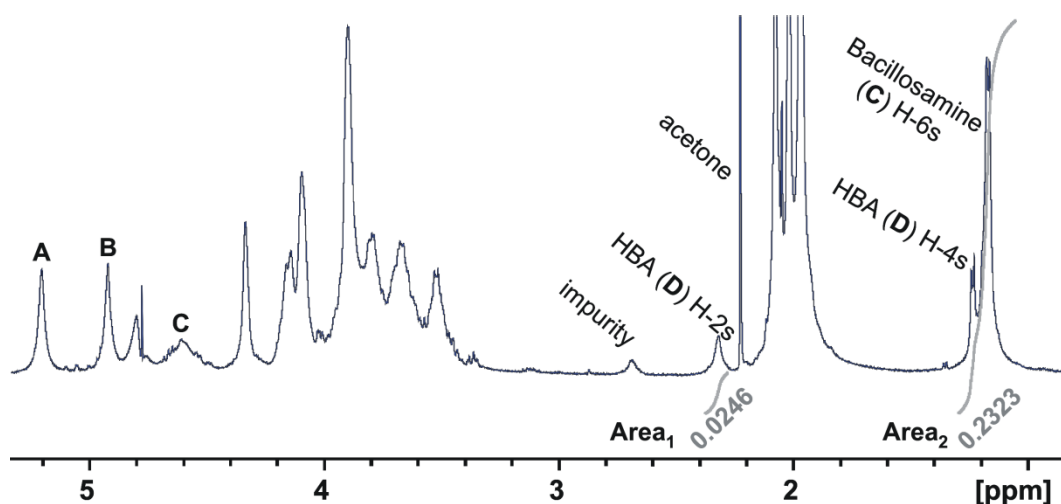


Figure 6.3.1: (500 MHz, 298 K,  $D_2O$ )  $^1H$  NMR spectrum of the repeating unit of the CPS from *A. baumannii* MG1 (table 6.3.1).  $Area_1$  represents the integration of the methylene protons from HBA (residue **D**,  $Area_1$ );  $Area_2$  accounts for all the methyl signals and comprehends H-4s from HBA (**D** residue) and H-6s from bacillosamine (**C** residue) regardless the type of *N*-substitution at C-4 of this last unit (HBA or acetyl). Comparison of  $Area_1$  and  $Area_2$  according to formula 1, suggested a substitution degree with HBA at N-4 of the bacillosamine residue of 19%.

	1	2	3	4	5	6-6'
<b>A</b>	5.21	4.16	3.91	4.34	4.10	-
<b>4)-<math>\alpha</math>-L-GalpNAcA</b>	98.5	50.4	68.1	79.7	72.7	175.1
<b>B</b>	4.93	3.91	3.90	3.67	4.09	3.72-3.63
<b>4)-<math>\alpha</math>-D-GlcpNAc</b>	99.5	54.6	70.4	79.7	71.6	60.7
<b>C</b>	4.60	3.80	3.87	3.80	3.52	1.17
<b>3)-<math>\beta</math>-D-QuipNAc4NR*</b>	101.8	57.9	76.8	57.9	72.5	17.6
<b>D</b>	-	2.33 x 2	4.19	1.24	-	-
<b>HBA</b>	175.3	46.2	66.0	23.8	-	-

\* R is Acetyl (81%) or HBA (19%)

Table 6.3.1:  $^1H$  (regular) and  $^{13}C$  (italic) chemical shifts (298 K,  $D_2O$ , in ppm) of the repeating unit of the CPS from *A. baumannii* MG1 (proton spectrum in figure 6.3.1)

Residue **A** was classified as a *O*-4 substituted  $\alpha$ -GalpNAcA. The *galacto* stereochemistry was identified by the weak scalar correlations in both the COSY and TOCSY spectra of H-4 to its vicinal protons (H-3 and H-5), the  $\alpha$ -configuration was established on the basis of the chemical shift (5.21 ppm) and on the broad singlet shape of the H-1 signal.

The chemical shifts of the ring carbons identified one nitrogen-bearing carbon, namely C-2 (50.4 ppm), which was *N*-acetylated as proven by the H-2 deshielded chemical shift and by the presence of *N*-acetyl signals in the proton spectrum. The C-4 signal appeared in the low field region of the HSQC spectrum (79.7 ppm) proving glycosylation at this position, and H-5 displayed a long-range correlation with a carbon at 175.1 ppm, confirming the uronic acid feature of this residue. Similar considerations identified **B** as a *O*-4 substituted 2-acetamido-2-deoxy- $\alpha$ -glucopyranose. With regard to unit **C** (bacillosamine), the multiplicity of the anomeric proton could not be assigned since it appeared as a very broad singlet at 4.60 ppm. Therefore, the  $\beta$ -configuration was suggested from both the  $^1\text{H}$  and  $^{13}\text{C}$  anomeric chemical shifts and confirmed by the NOE contacts (figure 6.3.2) of H-1 to both, H-3 and H-5, due to the axial orientation of these three protons. The examination of the carbon chemical shifts of this residue identified two nitrogen bearing carbons, i.e. C-2 and C-4 (both at 57.9 ppm), and C-3 which was glycosylated (76.8 ppm). Using the same approach, the HBA residue was completely assigned and, based on the GC-MS data, placed at the amino group at C-4 of residue **C**.

Information regarding the substitution degree at *N*-4 of **C** was deduced from the integration of two groups of signals in the high field region of the proton spectrum (figure 6.3.1), namely the broad peak at 2.33 ppm, which accounted for the two methylene protons of HBA (Area<sub>1</sub>), and the two methyl groups (Area<sub>2</sub>) at 1.24 (H-4 protons of HBA) and 1.17 ppm (H-6 protons of **C**).

At this regard, methyl signal at 1.17 ppm comprehended the methyl protons from all the bacillosamine residues present in the polymer, regardless their acylation state on the nitrogen at C-4, that could be either acetylated or substituted with the HBA unit. This methyl signal could not be integrated directly, but its contribute to Area<sub>2</sub> was deduced as follows: both Area<sub>1</sub> and Area<sub>2</sub> were normalized with respect to the number of protons they represented (two and three, respectively), so that (Area<sub>2</sub>)/3 represented the number of HBA residues plus those of bacillosamine, while (Area<sub>1</sub>)/2 reflected the total number of HBA moieties. In this way, the bacillosamine amount was deduced subtracting Area<sub>1</sub> from Area<sub>2</sub>, this difference together with Area<sub>1</sub>, was elaborated according to formula 1, disclosing an overall substitution degree with HBA at C-4 of this unit equal to 19%.

$$\% \text{ HBA} = \frac{(\text{Area}_1)/2}{(\text{Area}_2)/3 - (\text{Area}_1)/2} \times 100$$

*Formula 1*

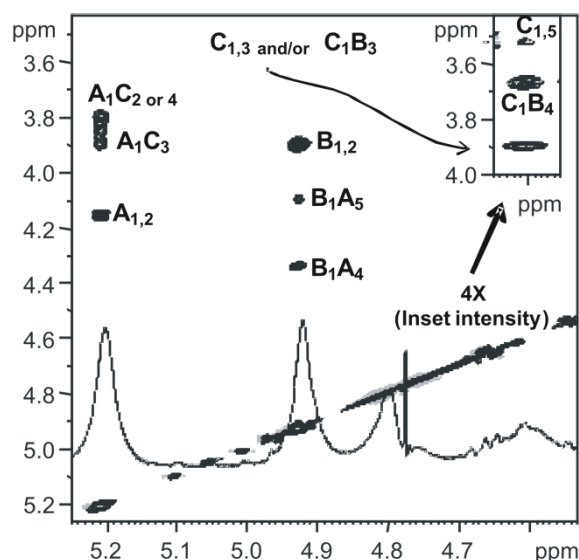


Figure 6.3.2: The anomeric area of the NOESY spectrum (500 MHz, 298 K,  $D_2O$ ) of the CPS from *A. baumannii* MG1 (table 6.3.1). The inset shows the NOE contacts identified for residue **C**. The broad anomeric signal of **C** induced the same pattern in the NOE densities, which appeared large and flattened on the baseline; these signals were recognized by amplifying the area of interest, as indicated in the inset. The intra-residue NOE  $C_{1,3}$  maybe overestimated due to the coincidence of the signals from H-3 of **C** with H-3 of **B** (table 6.3.1).

The analysis of the NOESY spectrum (figure 6.3.2) showed a spatial proximity between H-1 of **A** and H-3 of **C**, H-1 of **B** and H-4 of **A**, and H-1 of **C** and H-4 of **B**, and thus, disclosed the sequence between the three residues as reported in figure 6.3.3



Figure 6.3.3: Structure of the repeating unit of the CPS from *A. baumannii* MG1. R is HBA (19%) or acetyl. Residues are labelled according to the NMR assignment in table 6.3.1

Finally, CPS proton and HSQC spectra were recorded in 10 mM deuterated HCl (data not shown). Under this condition a large low field shift was found for H-5 and (less) H-1 signals of the GalpNAcA residue suggesting that the carboxylic group of this residue was in the free acid form. The structure of the of CPS (figure 6.3.3) was further confirmed by the NMR analysis of the di- and trisaccharide obtained after solvolysis with triflic acid and purification of the crude water extract (section 9.8).  $^1\text{H-NMR}$  of the trisaccharide is showed in figure 6.3.4 and all proton and carbon chemical shifts were assigned using 2D NMR (table 6.3.2).

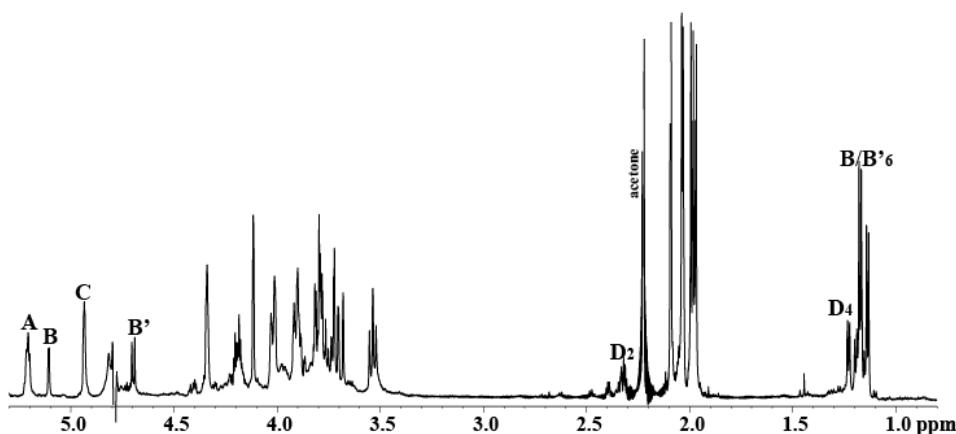


Figure 6.3.4: (600 MHz, 288 K,  $D_2O$ )  $^1H$  NMR spectrum of the trisaccharide of the CPS from *A. baumannii* strain MG1 obtained after solvolysis with triflic acid. The bacillosamine is present as reducing unit (**B** is  $\alpha$ , **B'** is  $\beta$  configured, table 6.3.2)

	1	2	3	4	5	6-6'
<b>A</b>	5.2	4.19	3.89	4.33	4.1	-
<b>4)-<math>\alpha</math>-L-GalpNAcA</b>	<i>98.6</i>	<i>50.3</i>	<i>67.8</i>	<i>71</i>	<i>73.2</i>	<i>175.1</i>
<b>B</b>	5.10	4.01	3.99	3.78	3.96	1.14
<b>3)-<math>\alpha</math>-D-QuinpNAc4NR*</b>	<i>92.1</i>	<i>54.3</i>	<i>74.8</i>	<i>58.3</i>	<i>68</i>	<i>17.9</i>
<b>C</b>	4.93	3.89	3.77	3.54	4.01	3.80-3.70
<b><i>t</i>-<math>\alpha</math>-D-GlcpNAc</b>	<i>100.2</i>	<i>54.9</i>	<i>72.2</i>	<i>70.6</i>	<i>73.5</i>	<i>61.2</i>
<b>B'</b>	4.68	3.74	3.83	3.78	3.53	1.17
<b>3)-<math>\beta</math>-D-QuinpNAc4NR*</b>	<i>95.8</i>	<i>57.1</i>	<i>76.8</i>	<i>58.2</i>	<i>72.4</i>	<i>17.9</i>
<b>E</b>	-	2.32	4.19	1.23	-	-
<b>S-3-HBA</b>	<i>174.8</i>	<i>46.4</i>	<i>65.9</i>	<i>23.9</i>	-	-

\* R is Acetyl or HBA

Table 6.3.2:  $^1H$  (regular) and  $^{13}C$  (italic) chemical shifts (288 K,  $D_2O$ , in ppm) of the trisaccharide of the CPS from *A. baumannii* MG (proton spectrum in figure 6.3.4)

#### 6.4 Spectroscopic characterization of the CPS from *A. baumannii* Strain SMAL

The proton NMR spectrum of the CPS produced by strain SMAL showed five anomeric signals and a crowded carbinolic area, together with the occurrence of four *N*-acetyl methyl signals. The analysis of the 2D NMR spectra was impaired by the high number of signals, many of which overlapped, and from their broad shape which resulted in poor quality spectra. These problems were circumvented by studying the deacetylated CPS and recording the sample under alkaline conditions (proton spectrum in figure 6.4.1), due to which the amino-geminal protons were shifted to high field.

The five anomeric signals were labelled **A-E** in decreasing order of their chemical shifts, and the attribution of the 2D homo- and heteronuclear spectra (table 6.4.1) followed the strategy described above for the MG1 CPS and characterized the structure of the repeating unit (figure 6.4.2-1).

Residue **A** was identified as  $\alpha$ -Galp branched at *O*-3, *O*-4 and *O*-6. The  $\alpha$ -configuration was established from both, anomeric proton and carbon chemical shifts. The analysis of the proton and carbon signals identified **B** as terminal 2,3-diamino-dideoxy- $\beta$ -glucopyranosuronic acid (DAGA), as indicated by the trans diaxial disposition of all the ring protons together with the occurrence of two nitrogen-bearing carbons (*C*-2 and *C*-3, 56.5 and 57.8 ppm, respectively), and from the  $^1\text{H}$ ,  $^{13}\text{C}$  long-range correlation between H-5 and *C*-6 at 175.9 ppm.

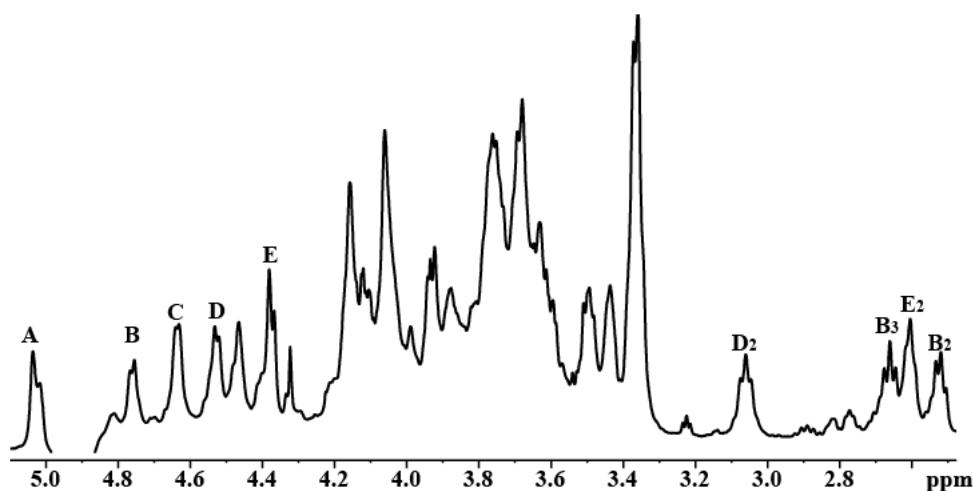


Figure 6.4.1: (600 MHz, 291 K, 30 mM NaOD in  $\text{D}_2\text{O}$ )  $^1\text{H}$  NMR spectrum of the CPS from *A. baumannii* SMAL. Signals are labelled according to the NMR attribution in table 6.4.1

Residue **C** was identified as  $\beta$ -Glc<sub>p</sub>, substituted at position 6, due to the low-field displacement of the corresponding carbon signal in comparison to the standard value (61.8 ppm) (Bock and Pedersen, 1983) Monosaccharides **D** and **E** were recognized as  $\beta$ -galacto and  $\beta$ -gluco configured, respectively. The complete carbon chemical shift attribution identified **D** as an *O*-3 substituted  $\beta$ -Gal<sub>p</sub>N residue, while **E** was a terminal  $\beta$ -Glc<sub>p</sub>N. The sequence of the monosaccharides was determined from NOE connectivities between H-1 of **A** and H-6 of **C**, H-1 of **B** and H-4 of **A**, H-1 of **C** and H-3 of **D**, H-1 of **D** and H-3 of **A**, H-1 of **E** and H-6 of **A** (figure 6.4.3), which was confirmed by the observed *inter*-residual HMBC correlations.



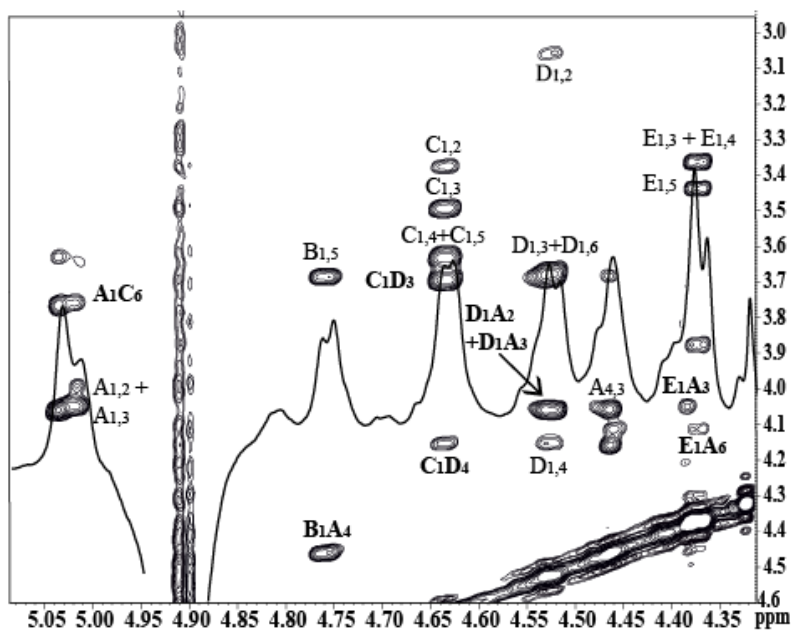


Figure 6.4.3: (600 MHz, 291 K, 30 mM NaOD in  $D_2O$ ) Attribution of the anomeric region of NOESY spectrum of the CPS from *A. baumannii* SMAL. Inter- and intra-residue contacts are labelled (table 6.4.1).

On the basis of the above information and considering that the alkaline treatment removed the pre-existing acetyl groups, the structure of the repeating unit of the *O*-deacylated CPS produced from *A. baumannii* SMAL was as shown in figure 6.4.2- 2. It was further confirmed by the analysis of the oligosaccharide (figures 6.4.4, table 6.4.2) obtained after periodate degradation of the purified CPS (section 9.8).

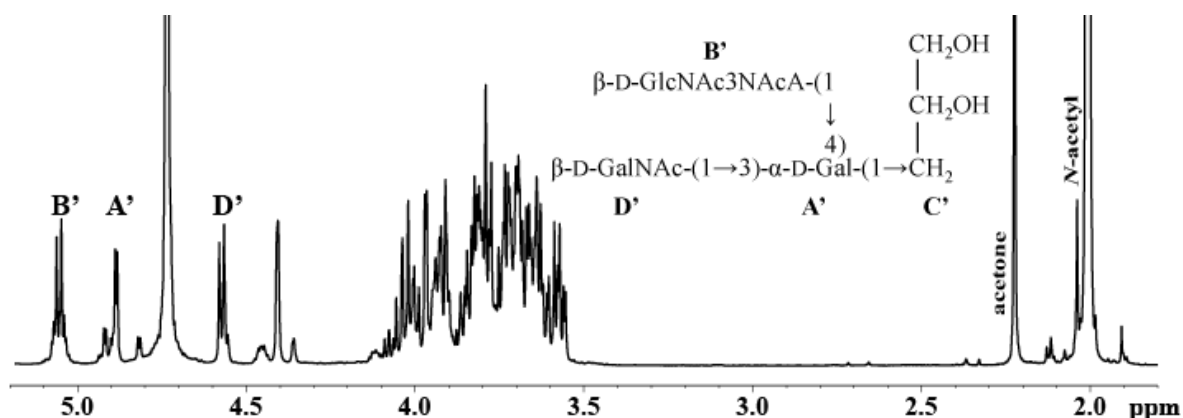


Figure 6.4.4: (600 MHz, 305 K,  $D_2O$ )  $^1H$  NMR spectrum and structure of the periodate degradation product from *A. baumannii* SMAL. All monosaccharides are in pyranose form, signals and residues labelling reflects the NMR assignment in table 6.4.2

	<b>1</b>	<b>2</b>	<b>3</b>	<b>4</b>	<b>5</b>	<b>6-6'</b>
<b>A'</b>	4.89	3.71	3.92	4.40	3.90	3.79-3.64
<b>3,4,6)-<math>\alpha</math>-D-Galp</b>	<i>99.6</i>	<i>68.5</i>	<i>70.9</i>	<i>76.5</i>	<i>71.1</i>	<i>61.3</i>
<b>B'</b>	5.05	3.81	4.04	5.59	3.79	-
<b><i>t</i>-<math>\beta</math>-DAGA</b>	<i>102.1</i>	<i>54.7</i>	<i>55.7</i>	<i>71.4</i>	<i>77.4</i>	<i>176.9</i>
<b>C'</b>	-	-	-	3.63-3.67	3.94	3.56-3.73
<b>Glycerol</b>	-	-	-	63.6	71.5	69.7
<b>D'</b>	4.57	4.00	3.72	3.97	3.69	3.83-3.69
<b>3)-<math>\alpha</math>-D-GalpNAc</b>	<i>105.1</i>	<i>53.9</i>	<i>72.2</i>	<i>68.9</i>	<i>76.1</i>	<i>62.2</i>

Table 6.4.2:  $^1\text{H}$  (regular) and  $^{13}\text{C}$  (italic) chemical shifts (305 K, in ppm,  $\text{D}_2\text{O}$ ) of the periodate degradation product from *A. baumannii* SMAL CPS. Labels are in analogy to those used for the parent polysaccharide, similarly glycerol numbering reflects that of the protons in the parent Glcp C

## 6.5 Conclusions

The carbohydrate material produced from two *A. baumannii* clinical isolates, MG1 and SMAL, was studied with the purpose to establish their location in the cell envelope together with their structures. Western blot analysis classified these materials as CPSs and the extensive use of NMR spectroscopy determined the carbohydrate sequence of each repeating unit. With regard to *A. baumannii* MG1, the repeating unit of the capsular structure is constituted from three different amino sugars (figure 6.3.3) and is quite similar to the *O*-antigen of the LPS from another strain of *A. baumannii* (figure 6.5.1) (Vinogradov *et al.*, 2003)



Figure 6.5.1. Structure of the *O*-antigen of the LPS from *A. baumannii* strain 24.

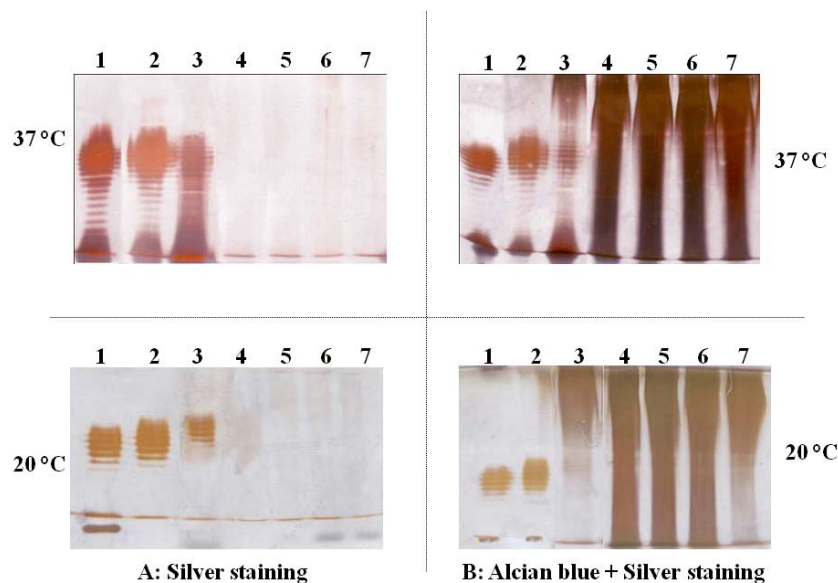
Indeed, both polymers possess a  $\beta$ -bacillosamine residue acylated non-stoichiometrically with HBA at *N*-4, but they differ in the absolute configuration of the GalpNA residue and the acetylation at *O*-6 of the GlcpN unit, which is absent in the MG1 CPS. As far as *A. baumannii* SMAL is concerned, its CPS is constituted of a pentasaccharide repeating unit (figure 6.4.2-2), rich in amino sugars, as was often found in CPS or *O*-antigens from this bacterial species. The structure of this polysaccharide is not new, and it was recently reported for the *O*-antigen of another *A. baumannii* strain, ATCC 17961 (MacLean *et al.*, 2009). The structures of the CPSs from *A. baumannii* MG1 and SMAL may contribute to the establishment of a serotyping scheme for this bacterium.



	<b>1</b>	<b>2</b>	<b>3</b>	<b>4</b>	<b>5</b>	<b>6-6'</b>
<b>A</b>	5.27	4.06	4.07	3.99	3.92	1.22
<b>2)-<math>\alpha</math>-D-Rhap4NAc</b>	<i>102.1</i>	<i>79.2</i>	<i>69.2</i>	<i>54.3</i>	<i>69.4</i>	<i>18.0</i>
<b>B</b>	5.13	4.32	4.12	4.27	4.10	3.77
<b>3)-<math>\alpha</math>-D-GalpNAc</b>	<i>101.5</i>	<i>50.2</i>	<i>78.1</i>	<i>69.7</i>	<i>72.4</i>	<i>62.4</i>
<b>C</b>	4.97	3.88	3.88	3.88	4.39	1.17
<b>3)-<math>\alpha</math>-L-Fucp</b>	<i>100.4</i>	<i>68.3</i>	<i>79.6</i>	<i>72.9</i>	<i>68.2</i>	<i>16.4</i>
<b>D</b>	4.59	3.31	3.60	3.54	3.55	3.95-3.86
<b>4)-<math>\beta</math>-D-Glcp</b>	<i>105.1</i>	<i>74.6</i>	<i>75.5</i>	<i>77.7</i>	<i>76.2</i>	<i>60.9</i>

Table 7.1.1:  $^1\text{H}$  (regular) and  $^{13}\text{C}$  (italic) chemical shifts at 300 K in  $\text{D}_2\text{O}$  measured for the O-chain from *E. coli* O157:H (proton spectrum in figure 7.1.1).

Water extracts at 20°C and 37 °C were purified by enzymatic treatments, dialysis and repeated ultracentrifugations (section 8.4). UC sediments and supernatants were screened by SDS-PAGE stained with silver nitrate only (figure 7.1.2 gels **A**) and with Alcian blue fixative prior the silver nitrate (figure 7.1.2 gels **B**). The UC sediments stained with silver (figure 7.1.2 gels **A**, lines 3) showed a migration pattern equal to the phenolic LPS (figure 7.1.2 gels **A**, lines 2); other materials was revealed by double staining and appeared as a smear in the high molecular weight region (figure 7.1.2 gels **B**, lines 3). UC supernatants resulted totally negative to the presence of LPS or others species with the silver staining (figure 7.1.2 gels **A**, lines 4-7), but very positive to the double staining (figure 7.1.2 gels **B**, lines 4-7). The presence of L-Gal in the chemical analyses and the positivity to the Sulfate test (Silvestri *et al.*, 1982) suggested the occurrence of agarose in the samples. Its presence, originating from the growth on solid medium, explained the positivity to Alcian blue stain able to fix on the gel this polymer. Sugars compositional analyses showed in first two UC supernatants the presence of D-Fuc4NAc (4-acetamido-4,6-dideoxy-D-galactose), D-GlcNAc (*N*-acetyl-D-glucosamine), D-ManNAcA (*N*-acetyl-D-mannosaminuronic acid) characteristics of the *Enterobacterial common antigen* repeating unit. Further analyses were focused on the purification and isolation of this polysaccharide.



7.1.2: SDS-PAGE (stacking gel 5%, separating gel 12 %) of UC sediments and supernatants from water extracts of *E. coli* O157:H<sup>-</sup> grown at 37 °C and 20°C . Gels **A** are stained with silver nitrate, **B** with Alcian blue first and then silver nitrate. **1**: LPS of *E. coli* O55:B5 as standard; **2**: LPS from phenol phases of *E. coli* O157:H<sup>-</sup>; **3**: UC sediments from water phases of *E. coli* O157:H<sup>-</sup>; **4-7**: UC supernatants from water extracts of *E. coli* O157:H<sup>-</sup>. Sample were loaded in quantity of 6µg.

## 7.2 Purification and immunodetection analysis of LPS in water extracts

In order to remove the contamination, UC sediment from water extract at 20 °C was chromatographed on Q-Sepharose resin with a NaCl gradient (section 9.9, table 7.2.1). The fractions were monitored using the phenol-H<sub>2</sub>SO<sub>4</sub> test (table and figure 7.2.1; section 9.5).

Fraction	A <sub>490</sub>	NaCl (M)	Fraction	A <sub>490</sub>	NaCl (M)
1	0.05	0.01	12	0.06	0.4
2	0.88	0.01	13	0.02	0.7
3	0.69	0.01	14	0.11	0.7
4	0.21	0.01	15	0.07	0.7
5	0.11	0.2	16	0.07	0.7
6	0.18	0.2	17	0.09	1
7	0.37	0.2	18	0.04	1
8	0.07	0.2	19	0.05	1
9	0.04	0.4	20	0.09	1
10	0.18	0.4	21	0.11	1
11	0.07	0.4	22	0.02	1

Table 7.2.1: Q-Sepharose fractions of the UC sediment from water extract of *E. coli* O157:H<sup>-</sup> grown at 20 °C. They were eluted with NaCl gradient and monitored through the phenol-H<sub>2</sub>SO<sub>4</sub> test

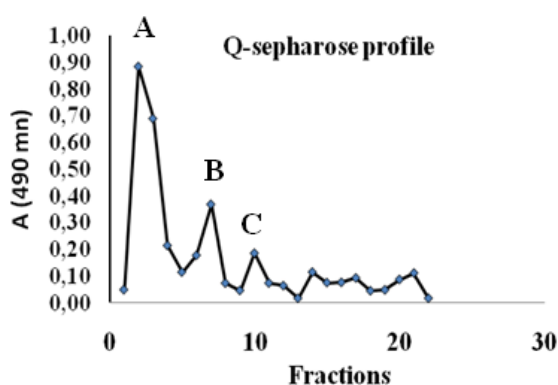


Figure 7.2.1: Profile of the *Q*-sepharose chromatography (table 7.2.1)



On the basis of chromatographic profile (figure 7.2.1), new fractions were obtained: **A** (fractions 1-4), **B** (fractions 5-8) and **C** (fractions 9-13). The SDS-PAGE of the fractions **A**, **B**, **C** (figure 7.2.2) revealed a more abundant presence of LPS with a minor amount of high molecular weight bands (related to the presence of agarose), in the fractions eluted with low ionic strength.

Figure 7.2.2: SDS-PAGE (stacking gel 5 %, separating gel 12 %) of **A**, **B**, **C** fractions obtained from *Q*-Sepharose chromatography. **R**: LPS of *E. coli* O55:B5 as standard; **1**: **A** (fractions 1-4); **2**: **B** (fractions 5-8); **3**: **C** (fractions 9-13). Sample were loaded in quantity of 4  $\mu$ g.

Chemical analyses confirmed this evidence because of the reduction of the galactose amount in the fraction **A** respect to the UC-sediment (figures 7.2.3 and 7.2.5).

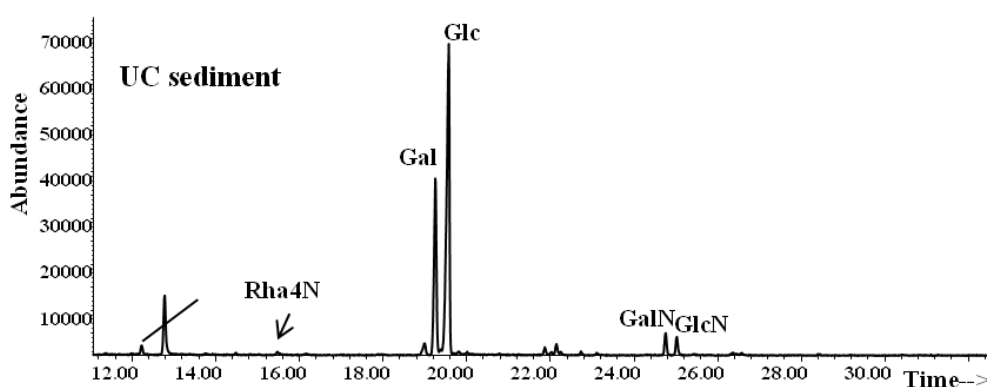


Figure 7.2.3: GC-MS chromatogram of the acetylated *O*-methyl glycosides relative to the UC sediment from water extract of *E. coli* O157:H<sup>-</sup> grown at 20 °C.

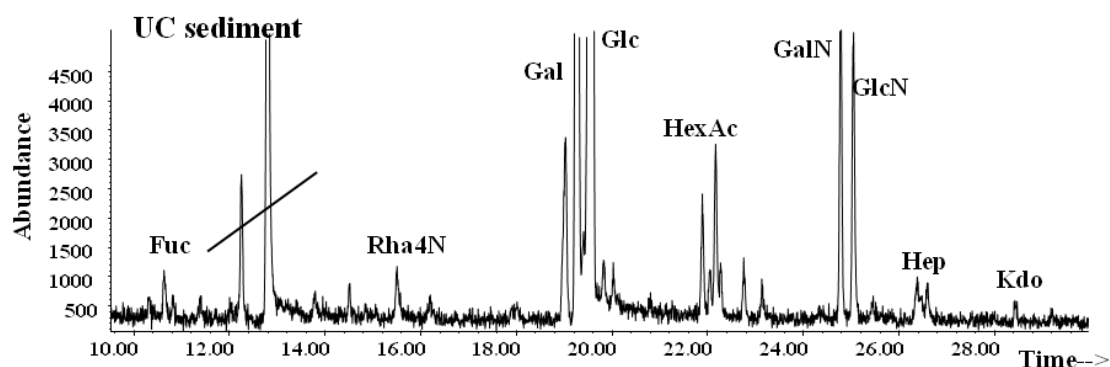


Figure 7.2.4: Zoom of the GC-MS chromatogram of the acetylated *O*-methyl glycosides relative to the UC sediment from water extract of *E. coli* O157:H grown at 20 °C. Characteristics sugars of the LPS of *E. coli* O157 are appreciable.

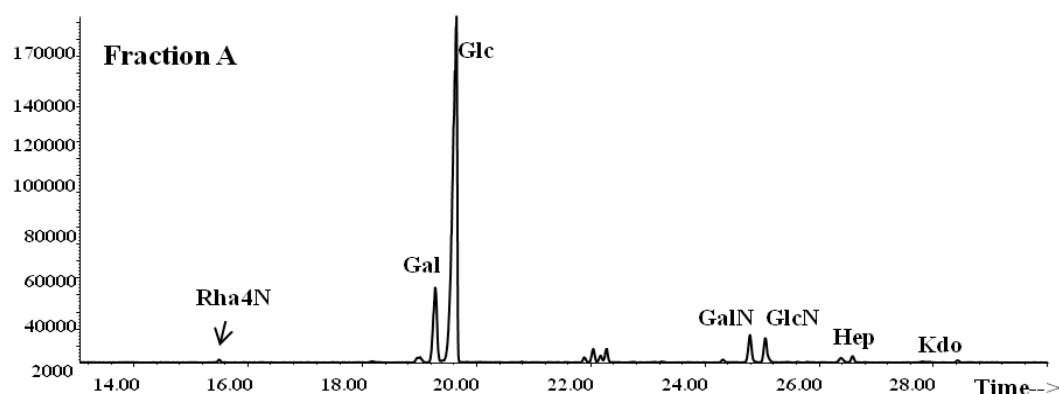


Figure 7.2.5: GC-MS chromatogram of the acetylated *O*-methyl glycosides relative to the fraction A from *Q*-Sephadex purification

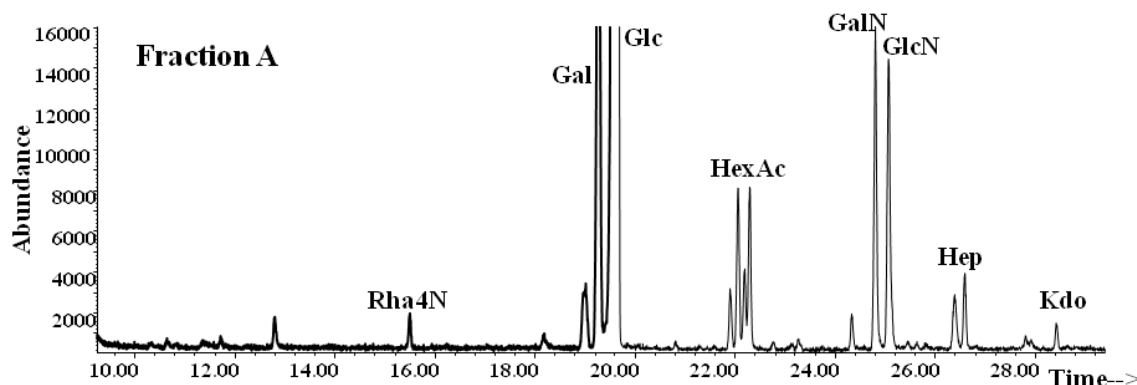


Figure 7.2.6: Zoom of the GC-MS chromatogram of the acetylated *O*-methyl glycosides relative to the fraction A from *Q*-Sephadex purification. The relative abundances of the sugars are increased respect to those found in UC-sediment analysis (figure 7.2.4); the Fucose (Fuc) resulted absent.

Finally, the fraction A obtained from *Q*-Sephadex containing the LPS of *E. coli* grown at 20 °C, was subjected to a Western Blot analysis with a polyclonal antibody for the LPS of *E. coli* O157 (figure 7.2.7 A and SDS-PAGE B, lines 1, section 9.2). Not purified LPS from water extract at 37 °C was also analyzed (figure 7.2.7 A and B, lines 3) and both LPSs were recognized by antibody as the phenolic LPS (figure 7.2.7 A, line 4).

These data, together with that obtained by chemical and spectroscopic analyses, suggested the analogy of the structure among the LPSs extracted from the water and phenol phases. In conclusion, the water-LPS is not subject to structural variability caused by phase variation but it is a result of a non complete repartition of the LPS in the phenol phase.

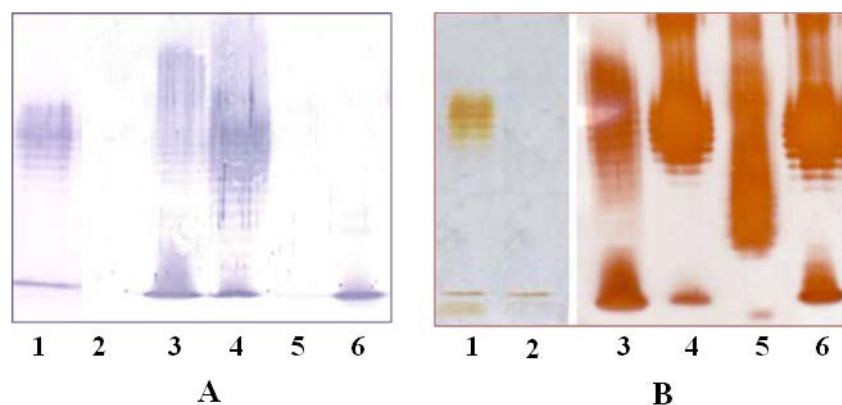


Figure 7.2.7: **A:** Western blot with primary Ab for LPS of *E. coli* O157. **B:** SDS-PAGE (5% stacking gel, 12 % separating gel) stained with silver nitrate. **1:** Fraction A of *Q*-Sepharose containing the LPS of *E. coli* O157:H<sup>-</sup> grown at 20 °C; **2:** First UC supernatant containing ECA<sub>CYC</sub> and ECB<sub>CYC</sub> from water extract at 20 °C; **3:** LPS of *E. coli* O157:H<sup>-</sup> from water extract at 37 °C; **4:** LPS of *E. coli* O157:H<sup>-</sup> from phenol extract at 37 °C; **5:** LPS of *Rhizobium rhizogenes* as negative check; **6:** LPS of *E. coli* O55:B5. Samples were loaded in quantity of 6µg.

### 7.3 Characterization of the two cyclic forms of the Enterobacterial common antigen

The first UC supernatant from water extract at 20 °C was purified by an enzymatic hydrolysis with  $\beta$ -agarase, dialysis and different gel permeation chromatographies (section 9.9). In particular GPC Biogel-P100 allowed the separation of the two cyclic forms of *Enterobacterial common antigen* (ECA) that were completely characterized by mono and bidimensional NMR. Proton NMR showed, for both polysaccharides, the occurrence of the three anomeric signals (A-C, or A'-C') corresponding to the trisaccharide repeating unit of the *Enterobacterial common antigen* (figure 7.3.1). The form indicated with ECA<sub>CYC</sub> corresponded to that characterized elsewhere (Erbel *et al.*, 2003), the other form indicated with ECB<sub>CYC</sub> presented only small variations of chemical shifts with respect to ECA<sub>CYC</sub> (table 7.3.1 and 7.3.2). The absence of reducing sugars signals and the high solubility in water of the samples was a further confirmation of the presence of ECA<sub>CYC</sub> and excluded the other possible forms of ECA like ECA<sub>PG</sub> and ECA<sub>LPS</sub>.



ECB <sub>CYC</sub>								
A'	5.19	3.77	4.00	4.31	4.23	1.06	2.07	-
3)- $\alpha$ -D-Fucp4NAc	<i>101.4</i>	<i>68.4</i>	<i>74.9</i>	<i>51.7</i>	<i>67.3</i>	<i>16.6</i>	<i>23.2</i>	<i>175.8</i>
B'	4.95	3.96	3.79	3.75	3.97	3.83-3.75	2.03	-
4)- $\alpha$ -D-GlcpNAc	<i>95.7</i>	<i>54.3</i>	<i>70.5</i>	<i>78.3</i>	<i>71.6</i>	<i>61.2</i>	<i>23.3</i>	<i>175.3</i>
C'	4.80	4.51	4.07	3.77	3.80	-	2.07	-
4)- $\beta$ -D-ManpNAcA	<i>99.6</i>	<i>54.4</i>	<i>73.5</i>	<i>78.4</i>	<i>78.5</i>	<i>175.2</i>	<i>23.2</i>	<i>176.6</i>

Table 7.3.2: <sup>1</sup>H (regular) and <sup>13</sup>C (italic) chemical shifts at 303 K in D<sub>2</sub>O (600  $\mu$ l), measured for ECB<sub>CYC</sub> (figure 7.3.1)

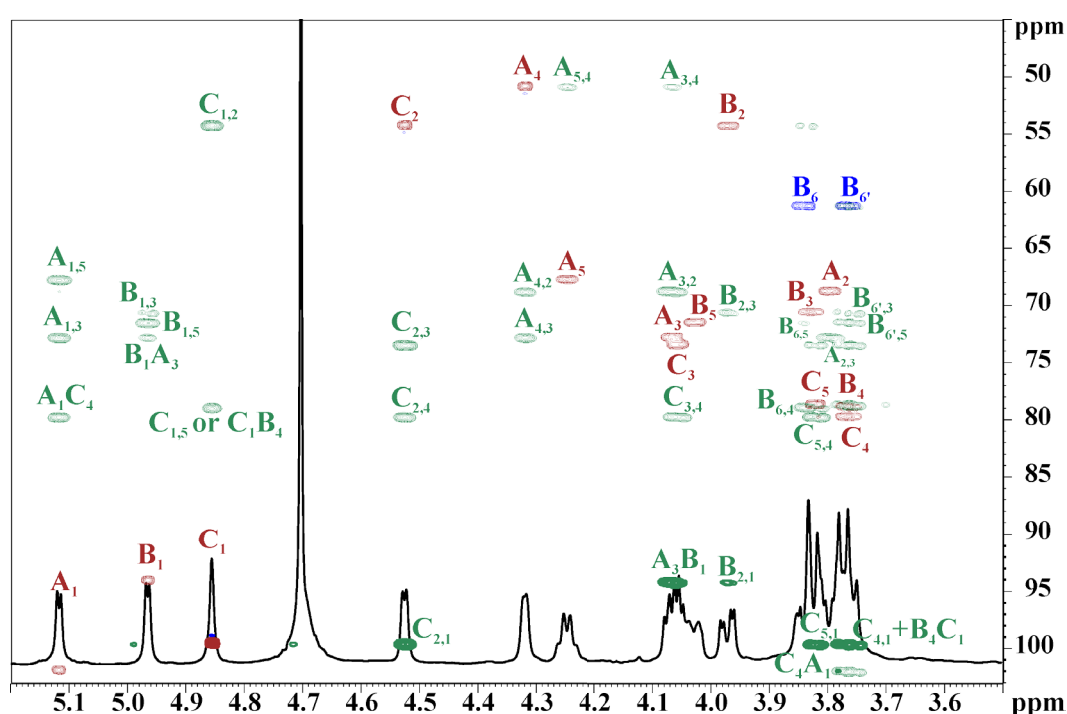


Figure 7.3.2: (600 MHz, 303K, D<sub>2</sub>O), Attributions of the HSQC (red and blue) and HMBC (green) spectra of ECB<sub>CYC</sub> (table 7.3.1)

The ring dimension of these molecules was determined through MALDI-TOF experiments (figures 7.3.3 and 7.3.4). The mass of the ECB<sub>CYC</sub> (m/z 2428.43) (figure 7.3.3) corresponded to a tetrameric molecule, while ECB<sub>CYC</sub> (m/z 3035.69) (figure 7.3.4) differed from the ECB<sub>CYC</sub> only for the addition of one repeating unit (m/z 607.26), therefore it is the pentameric form.

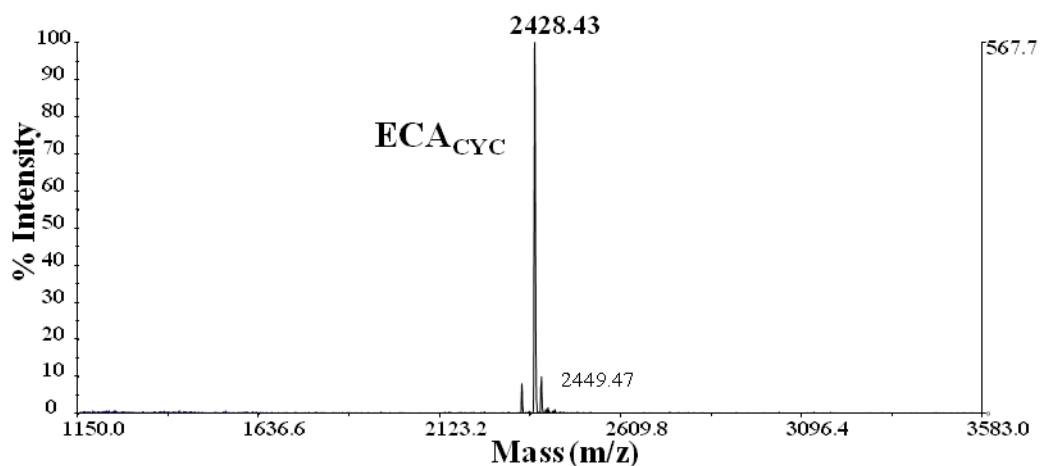


Figure 7.3.3: Ion negative MALDI-TOF spectrum of  $ECA_{CYC}$

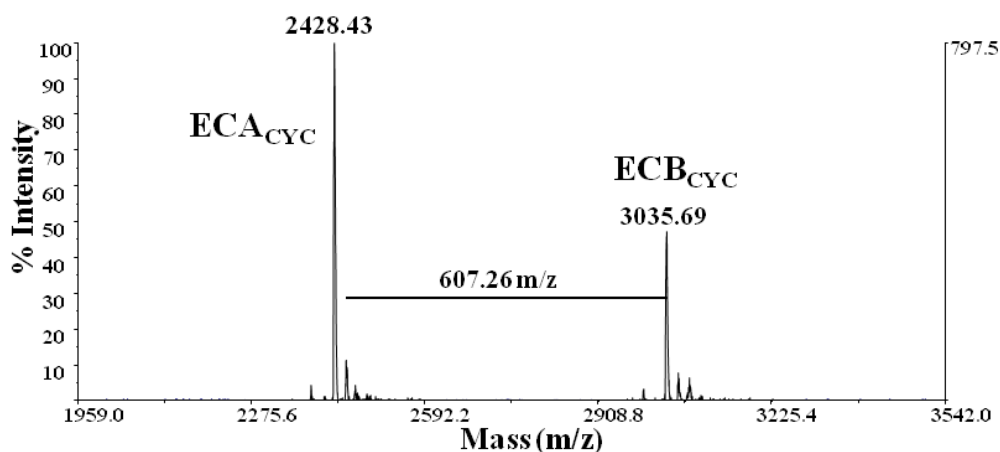


Figure 7.3.4: Ion negative MALDI-TOF spectrum of the mixture of  $ECA_{CYC}$  and  $ECB_{CYC}$

#### 7.4 Conclusions

These studies conducted on the LPS in the water cellular extracts of the pathogenic *E. coli* O157:H<sup>-</sup> proved that it is not involved in the phase variation, since no structural difference was found respect to phenolic LPS. The chemical identity of the LPSs in the water phase of cellular extracts was demonstrated by chemical analyses and through an immunodetection analysis with an antibody raised from the LPS of *E. coli* O157. Furthermore, the investigation of water extracts led to the identification, purification and characterization of two cyclic forms of the *Enterobacterial common antigen*. Literature data report the production of  $ECA_{CYC}$  from different *Enterobacteriaceae*, in particular that of *E. coli* K12 is constituted by 4 repeating units and each molecule contains from 0 to 4 *O*-acetyl groups (Erbel *et al.*, 2003; Kajimura *et al.*, 2005).

The presence of the tetrameric  $ECA_{CYC}$  for a pathogenic strain of *E. coli* and together with the pentameric form,  $ECB_{CYC}$ , represents a new datum. Further studies will be focused on the study of biological functions of these molecules and eventually on their implication as a virulence factor .

## PART III: MATERIALS AND METHODS

### CHAPTER VIII

#### ISOLATIONS OF LIPOPOLYSACCHARIDES AND CAPSULAR POLYSACCHARIDES

##### *8.1 Rhizobium radiobacter RV3*

*Rhizobium radiobacter* Rv3 strain DSM 30207 was grown in liquid shake culture in Nutrient Broth (NB, Fluka, cod. 03856, 24 l) medium at 27 °C for 40 h (early stationary phase). Cells were collected by centrifugation (3500 g, 4 °C, 15 min), washed sequentially with ethanol, acetone and diethyl ether and finally freeze-dried (yield 0.3 g/l). Isolation of LOS was performed on dry cells by aqueous 90 % phenol-chloroform-light petroleum (PCP) (2 : 8 : 5 v/v/v) extraction (Galanos *et al.*, 1969). After removal of the light solvents under vacuum, LOS was precipitated from the phenol with water, washed with aqueous 80 % phenol and acetone, finally the solid was suspended in water and lyophilized (2%  $w_{\text{LOS}}/w_{\text{cells}}$ ). The remaining cell pellet was extracted according to the hot phenol-water protocol (Westphal and Jann, 1965): cells were treated with 30 ml of water and an equal volume of 90 % phenol, solution was incubated at 68 °C for 20 minutes. Phenol-water phases separation was performed by spinning at 4 °C. Dialysis (cut-off 10000 Da) was used for phenol removal from the extractions phases which were finally freeze-dried. LOS was recovered only in water extract (7.4 %  $w_{\text{LOS}}/w_{\text{cells}}$ ) together with high quantity of cyclic  $\beta$ -glucans and for this reason not further considered.

##### *8.2 Cupriavidus necator DSM 13513*

Cells of *Cupriavidus necator* DSM 13513 were cultivated in Nutrient Broth (8 l) medium at 26 °C, collected by centrifugation (9800 g, 4 °C, 15 min), washed with distilled water and extracted according water-phenol protocol (section 8.1) and LPS was found in water extract only (160 mg). This latter (50 mg) was purified from protein and nucleic contaminants by enzymatic treatment and ultracentrifugation. It was solved in the digestion buffer (100 mM TRIS, 50 mM NaCl, 10 mM MgCl<sub>2</sub>, buffer at pH 7.5) at a concentration of 5 mg ml<sup>-1</sup>, and treated with DNase (Sigma, cod. DN25) at 37 °C overnight, successively Proteinase K (Sigma, cod. P5147) was added and the solution left at 56 °C for 4 h. The sample, after dialysis (cut-off 10000 Da), was ultracentrifugated (440000 g, 4 °C, 16 h) and LPS was recovered both in the supernatant (7 mg) and sediment (15 mg), but this last was used for further analyses.

### 8.3 *Acinetobacter baumannii* clinical isolates SMAL and MG1

*Acinetobacter baumannii* SMAL and MG1 strains were multidrug-resistant (MDR) clinical isolates representative of a clonal lineage causing nosocomial infections, including sepsis, in different Italian settings and recovered since 2002. The isolates were identified by using the Vitek 2® automated instrument ID system (BioMérieux, Marcy l'Etoile, France), and sequencing of blaOXA-51-like gene (Turton *et al.*, 2006) species identification was also confirmed by using gyrB PCR method previously described (Higgins *et al.*, 2007). Genomic relatedness among *A. baumannii* isolates was investigated by pulsed-field gel electrophoresis (PFGE) (Endimiani *et al.*, 2007).

Strains SMAL and MG1 were grown in liquid shake culture in Luria Broth (LB, Sigma, cod. 3022, 24 l) medium at 28 °C and cells were collected by centrifugation (9800 g, 4 °C, 20 min), washed sequentially with distilled water, ethanol, acetone, ethyl ether, suspended in water and freeze-dried (yield 0.3 g/l for both strain). Isolation of LOS was performed on dry cells by PCP extraction (section 8.1) (strain SMAL yield 0.8 %  $w_{\text{LOS}}/w_{\text{cells}}$ ; strain MG1 yield 0.7 %  $w_{\text{LOS}}/w_{\text{cells}}$ ). The remaining cell pellet was extracted according to the hot phenol-water protocol (section 8.1) and in both cases preliminary chemical and electrophoretic analysis revealed the presence of polysaccharide material in the water phases (strain SMAL yield 22 %  $w/w_{\text{cells}}$ , strain MG1 yield 20 %  $w/w_{\text{cells}}$ ), hence phenol phases were not investigated.

CPSs were purified from nucleic acid, proteins and LOS by enzymatic treatment (section 8.2) (DNAse, Roche Germany 04716728001; Proteinase K, Roche Germany 03115836001) and repeated ultracentrifugations. After dialysis and freeze-drying, enzyme-treated water phase (30 mg for each strain) was solved in distilled water and ultracentrifugated (105 000 g, 4 °C for 12 h). The LOS-containing sediment was suspended in water and ultracentrifugated again in the same conditions. This sediment was lyophilized and used for further analysis (strain SMAL yield 9 mg, strain MG1 13 mg). The CPS-containing supernatants were pooled and ultracentrifugated (500 000 g, 4 °C, 48 h), the supernatant, namely the purified CPS, was freeze-dried and finally used for the chemical analyses (strain SMAL yield 18 mg, strain MG1 yield 15 mg). Furthermore, *A. baumannii* strain SMAL was cultivated in 50 ml of LB and 50 ml of FBS (Fetal Bovine Serum, EuroClone, cod. ECS0180D) at 37 °C. In order to verify the variation of Lipid A structure, dry cells were extracted according to the hot phenol-water method and LOS was recovered in the water layer, after dialysis and freeze drying. Yields were similar to that reported above.

#### **8.4 *Escherichia coli* O157:H**

Cells were cultivated on solid Nutrient-Agar at 37 °C and 20 °C and extracted according to the phenol-water protocol (section 8.1). Water extracts were treated with DNase, Proteinase K (section 8.2), dialysed and freeze-dried (96 mg for 37 °C and 171 mg for 20 °C). LPSs were further purified by four ultracentrifugation steps (440 000 g, 4 °C, 16h), resuspending in distilled water the UC sediments obtained each time. Finally, the UC sediments were freeze-dried (7 mg for 37 °C and 15 mg for 20 °C).

## CHAPTER IX

### GENERAL AND ANALYTICAL METHODS

#### *9.1 Electrophoretic and chemical analyses*

Discontinuous SDS-PAGE (Sodium Dodecyl Sulphate Polyacrylamide Electrophoresis) (Laemmli, 1970) of samples were performed on Mini Protean III Bio-Rad system run at 150 constant voltage. Gels were realized as reported: 5 % stacking gel, 12 % separating gel for LOS of *R. radiobacter*, LPS of *E. coli* O157: H<sup>-</sup>, LPS of *C. necator* and 8% for neoglycoprotein analysis. Gels were stained according to the silver stain procedure for Lipopolysaccharide (Kittelberger and Hilbink, 1993), with coomassie procedure for proteins (Zehr *et al.*, 1989) and Alcian blue fixative for negative charged polysaccharides (Min *et al.*, 1986).

Total fatty acid content and monosaccharide composition were determined by treating the LPS (1 mg) with methanolic HCl 1 M at 80 °C for 16 h. The solution was extracted three times with an equal volume of *n*-hexane, the top layers (*n*-hexane) were combined and dried. Fatty acids methyl esters (FAME) were analyzed directly by GC-MS. The bottom layer (methanol) was dried and the *O*-methyl glycosides were acetylated with dry pyridine (100 µl) and Ac<sub>2</sub>O (50 µl) at 80 °C for 20 min. The mixture of acetylated *O*-methyl glycosides was analysed by GC-MS.

The absolute configuration was determined by GC-MS analysis of the chiral 2-octyl (Leontein *et al.*, 1978) or 2-butyl (Gerwig *et al.*, 1978) derivatives. The ester-linked fatty acids were selectively released from LPS by base-catalysed hydrolysis (0.5 M NaOH, 37 °C, 2 h). The solution was acidified to pH 4.0 by addition of 1 M HCl drops and extracted twice with an equal volume of CHCl<sub>3</sub>. Fatty acids were recovered in the organic layer, esterified with diazomethane and analysed by GC-MS.

Glycosyl-linkage analysis of LPS was performed derivatizing monosaccharides as partially methylated alditol acetates (PMAA) and analysed by GC-MS (Ciucanu and Kerek, 1984) 1-2 mg of sample were solubilized in dry DMSO (1 ml) and then powdered NaOH (100 mg) was added to promote the sugars deprotonation (3 h, 25 °C). Solution was treated with 200 µl of iodomethane (from 0°C to 25 °C, 16 h) and per-*O*-methylated lipopolysaccharide was extracted by adding water and chloroform to the reaction mixture. The organic layer was washed with 50 ml of water, dried under vacuum, dissolved in 2 M TFA. After 1 h at 120 °C, it was dried and acid traces were removed by isopropanol washing and drying. Partially methylated monosaccharides were converted in alditols by reduction with NaBD<sub>4</sub> in ethanol (1 h, 25 °C), followed by borates treatment with methanol and AcOH. Methylated alditols were finally acetylated (150 µl of Py, 150 µl of Ac<sub>2</sub>O, 80 °C, 30 min.) and salts removed with water-chloroform extraction.

All GC-MS analyses were performed with an Hewelett–Packard 5890 instrument, equipped with a SPB-5 capillary column (Supelco, 30 m x i.d. flow rate, 0.8 ml/min, He as a carrier gas). EI mass spectra were recorded with an ionization energy of 70 eV and an ionizing current of 0.2 mA. The temperature program used for the analyses was the following: 150 °C for 5 min, 150→280 °C at 3 °C/min, 300 °C for 5 min.

Exceptions regarded:

Monosaccharides and fatty acids of LOS from *A. baumannii* strain SMAL: 150 °C for 3 min, 150→300 °C at 10 °C/min, 300 °C for 18 min.

Monosaccharides of CPSs from *A. baumannii* strains SMAL and MG1: 150 °C for 5 min, 150→300 °C at 10 °C/min, 300 °C for 12 min.

## 9.2 Immunodetection analyses

The ultracentrifuge sediments and supernatants of *A. baumannii* water extract were subjected to SDS-PAGE and Western Blot using an antilipid A monoclonal antibody (mAb) A6 (Kuhn *et al.*, 1992). SDS-PAGE was performed with 5 % stacking gel; separating gel composition was optimized for the type of molecule screened, and it was 15 % for LOS or, in the case of CPS molecules, it was polymerized using two different acrylamide percentages: 8 % (top half) and 15 % (bottom half). LPSs of *E. coli* O157:H<sup>-</sup> were analysed with 12 % separating gel and Western Blot using a non commercial polyclonal antibody for LPS of *E. coli* O157.

Western blot analysis was accomplished on Biorad Trans Blot Cell System and a PVDF membrane (pore size 0.45 µm). The membrane blotting was performed in Trans-Buffer (Tris 2,4 g/l, glycine 11,5 g/l, 15 % methanol) for 16 h, at 10 °C, 26 V for *Acinetobacter baumannii* samples and for 2 h at 4 °C, 100 V for LPS of *E. coli*. The membrane was incubated with 1 % AcOH (100 °C, 2 h) to cleave the Kdo glycosidic linkage; this step is necessary because the primary antibody A6 is specific for the Lipid A in its free form, namely without the core region.

Western blot detection of samples was performed as follows: membrane was washed with Tris-Tween buffer (3 x 30 min; Tris 1.21 g/l, Tween 20 0.5 ml/l, pH 8.0); blocked for 1 h in Tris-Tween buffer with evaporated defatted milk (5 %); incubated for 16 h with the primary antibody A6 or in that for LPS of *E. coli* O157 (dilution 1:200) in dilution buffer (Na<sub>2</sub>HPO<sub>4</sub> 1.78 g/l, NaCl 8.77 g/l, Tween 20 0.5 ml/l, pH 7.4) and 2 % of evaporated defatted milk. Membrane was then washed with Tris-Tween buffer (3 x 15 min) and *Acinetobacter baumannii* samples were incubated for 2 h with secondary antibody alkaline phosphatase (AP) conjugated goat anti-mouse IgG (Jackson ImmunoResearch, cod 115-055-003, 1:1000) while *E. coli* O157:H<sup>-</sup> samples with goat anti-rabbit AP-IgG (Sigma, cod. A3687) antibody.

Finally, membrane was rinsed with Tris-Tween buffer (2 x 15 min) first and with PBS after; membrane was then wash with AP-buffer (10 min; 0.1 M NaHCO<sub>3</sub>, 1 mM MgCl<sub>2</sub> · 6 H<sub>2</sub>O, pH 9.0) and treated with a solution containing AP-buffer, NBT (Biomol, cod. 06428, 50 mg/ml in 70 % DMF) and BCIP (Biomol, cod. 02291, 50 mg ml<sup>-1</sup> in DMF) in ratio 2:1 v/v respectively or in alternative with the premixed NBT-BCIP solution (Sigma, cod. B6404) until color development.

### **9.3 Isolation of oligosaccharides from LOS of *Rhizobium radiobacter* RV3**

The de-*O*-acylation of LOS (60 mg) was performed dissolving the sample in anhydrous hydrazine (25 mg ml<sup>-1</sup>), stirred at 37°C for 30 min, cooled, poured into ice-cold acetone (15 ml), and allowed to precipitate. The precipitate was centrifuged (6000 g, 30 min), washed twice with ice-cold acetone, dried, and then dissolved in water and lyophilized (50 mg). The sample was de-*N*-acylated with 4 M KOH (10 mg ml<sup>-1</sup>) for 16 h at 120 °C (Gargiulo *et al.*, 2008), and after neutralization it was desalted by gel permeation chromatography on Sephadex G-10 (Pharmacia, 1.5 × 50 cm, eluent water, flow 0.5 ml min<sup>-1</sup>) column. The resulting oligosaccharide fraction (9 mg) eluted in the void volume and was further purified by HPAEC on a CarboPack PA-100 column (9 x 250 mm) eluted with a linear gradient of 30-37% of 1 M sodium acetate in 0.1 M NaOH at 2.0 ml min<sup>-1</sup> over 100 min. In this condition **OS1** and **OS2** retention time was 41 and 62 min., respectively. Finally, **OS1** and **OS2** were desalted as mentioned above, yielding to 1.2 and 0.7 mg, respectively.

### **9.4 Preparation of the carbohydrate component of the neoglycoprotein**

LOS (100 mg) was de-*O*-acylated as described in the section 9.3 and dephosphorilated with 48 % aqueous HF (20 mg ml<sup>-1</sup>) for 48 h at 4 °C. Solution was diluted and HF removed by dialysis (cut-off 3500 Da). De-*O*-acylated and dephosphorilated mixture of oligosaccharides were reduced by treatment with NaBH<sub>4</sub> (20 mg) overnight at 4 °C. The reducing agent was destroyed with few drops of glacial AcOH, salts were removed by dialysis (cut-off 3500 Da) and finally sample was freeze-dried (60 mg). Complete delipidation was afforded with 4 M KOH treatment (section 9.3), yielding to the complete deacylated, dephosphorylated and reduced oligosaccharide mixture (**OS**, 40 mg).

### **9.5 Synthesis and characterization of OS-BSA conjugate**

The oligosaccharides (section 9.4) were conjugated to the protein carrier, commercial BSA, using glutaraldehyde as linker by the formation of Schiff bases with BSA lysines residues and with free amino groups of the oligosaccharides (Holst *et al.*, 1991).

BSA (10 mg, Sigma, cod. A7906) was activated with glutaraldehyde (5% final concentration; Sigma, cod. 40855) in Argon saturated buffer (2 ml, Na<sub>2</sub>CO<sub>3</sub> 50 mM pH 9.2).

The reaction was left under stirring overnight at 25 °C in the dark. Formation of the Schiff base between BSA lysines and glutaraldehyde was monitored with the TNBS test (Habeeb, 1966) (section 3.3). Known volumes of BSA-glutaraldehyde and BSA standard solution (1 mg ml<sup>-1</sup>), used for calibration, were diluted with Na<sub>2</sub>CO<sub>3</sub> 50 mM pH 9.2 buffer to a volume of 300 µl. The solutions were treated with 300 µl of 0.1% 2,4,6-trinitrobenzenesulphonic acid (TNBS) or picrylsulfonic acid (Sigma, cod. P2297), mixed and incubated at 40 °C for 2 h. Then, 300 µl of 10 % SDS were added to solubilise the protein, and finally 150 µl of 1 M HCl were added, before the UV<sub>440</sub> measures.

BSA-linker adduct was extensively dialyzed at 4°C, in the dark, versus degassed Na<sub>2</sub>CO<sub>3</sub> 50 mM buffer at pH 9.2; finally **OS** (4 mg) was added and the solution was stirred overnight at 25 °C. Schiff bases cross-linking glutaraldehyde with **OS** and BSA were then reduced adding NaBH<sub>4</sub> (50 mg, 6h, r.t.), the excess of the reducing agent was destroyed upon addition of few drops of glacial AcOH and the solution was dialysed and directly desalted on Biogel P-2 (Bio-Rad, 1.5 x 116 cm, eluent NH<sub>4</sub>HCO<sub>3</sub> 50 mM, flow 0.2 ml min<sup>-1</sup>). **OS-BSA** conjugate was further chromatographed on Sephacryl HR-100 (GE-Healthcare, 1.5 x 116 cm, eluent NH<sub>4</sub>HCO<sub>3</sub> 50 mM, flow 0.25 ml min<sup>-1</sup>). The eluates were monitored with an in-line refraction index detector (Knauer, K-2310). The conjugate was eluted in proximity of void volume as a broad peak, whereas unreacted **OS** was highly retained from the gel and recovered after almost one column volume. On the basis of the chromatographic profile, fractions proximal to the void volume were pooled in three groups, **OS-BSA<sub>A</sub>**, **OS-BSA<sub>B</sub>** and **OS-BSA<sub>C</sub>** (2, 7, and 2 mg, respectively), and analyzed on SDS-PAGE, using BSA as reference. Molecular weight of the three conjugates was evaluated via gel permeation chromatography on TSK G5000PW<sub>XL</sub>, run on Agilent 1100 system, using NH<sub>4</sub>HCO<sub>3</sub> 50 mM at 1.0 ml min<sup>-1</sup> and monitoring the eluate with the UV detector at 210 nm ; calibration curve was calculated using commercial protein standards (section 3.3). The quantity of the carbohydrate component of the glycoconjugate were determined through the phenol-H<sub>2</sub>SO<sub>4</sub> test (Dubois *et al.*, 1956) and the quantitative GC-MS estimation (section 3.3) on **OS-BSA<sub>B</sub>**, the most abundant fraction. Accordingly to the first method, precise volumes of the **OS-BSA<sub>B</sub>** sample and of the **OS** standard solution (1.9 mg ml<sup>-1</sup>) were diluted with water until a final volume of 200 µl and equal volumes of a 5% phenol solution were added. Finally, 1 ml of concentrate H<sub>2</sub>SO<sub>4</sub> was added to the solutions and, after vigorous mixing, carbohydrate containing samples appeared orange-yellow and the UV measures were performed at 490 nm. With regard to the GC-MS quantification, mannose monosaccharide (calibration standard) and **OS-BSA<sub>B</sub>** were converted in acetylated *O*-methyl glycosides and analyzed according to the procedure and parameters described in the section 9.1.

### 9.6 Isolation of the 4-deoxy- $\beta$ -D-arabinohexose

LPS was hydrolyzed with AcOH 1% (100 °C, 2 h), the precipitate (Lipid A) was collected for centrifugation (9800 g, 4 °C, 15 min) and the supernatant (30 mg) was fractionated on Biogel-P2 (Biorad, 1.5 x 98 cm, eluent  $\text{NH}_4\text{HCO}_3$  50 mM, flow 0.2 ml min<sup>-1</sup>). On the basis of <sup>1</sup>H-NMR, the fraction (6 mg) eluted in the void volume of the column was the *O*-antigen still derivatized with the 4dAraHex. Therefore, the *O*-antigen, was hydrolyzed with TFA 10 mM (10 mg ml<sup>-1</sup>) at 100 °C for 3 h. The reaction was monitored by TLC ( $\text{CHCl}_3$ :  $\text{CH}_3\text{OH}$ :  $\text{H}_2\text{O}$  14:6:1, L-Rha as reference). After neutralization with  $\text{NH}_4\text{HCO}_3$ , the solution was chromatographed on Biogel-P2 (Biorad, 1 x 47 cm, eluent water, flow rate 0.1 ml min<sup>-1</sup>) and fractions were combined on the basis of TLC (isopropanol: water 8:2, L-Rha as reference) migration. Monosaccharide isolated was directly used spectroscopic studies.

### 9.7 Isolation of oligosaccharides from LOS of *A. baumannii* strain SMAL

LOS (20 mg) obtained from PCP extraction was totally deesterified by hydrazinolysis and deamidated by strong alkaline hydrolysis as described in the section 9.3. Oligosaccharides were desalted on a Sephadex G-10 column (GE-Healthcare, 96.5 x 1.5 cm, eluent water, flow 0.2 ml min<sup>-1</sup>) and purified by HPLC (Agilent 1100) on a TOSOH TSK3000 PW<sub>XL</sub> size exclusion column (87.6 mm x 30 cm, 7 $\mu$ m; TOSOH precolumn 6.00 mm x 4 cm) eluted with water at 0.8 ml min<sup>-1</sup> (**OS**<sub>2</sub> product, 3 mg). Another LOS portion (15 mg) was hydrolysed with AcOH 1% (100 °C, 2h); the precipitate (Lipid A, 5 mg) was collected for centrifugation (9800 g, 4 °C, 15 min) and washed with water. The supernatants were combined, freeze-dried and chromatographed on TSKHW-40 size exclusion column. The **OS**<sub>3</sub> (8 mg) was the first product eluted and was used directly for NMR studies.

### 9.8 Chemical treatments on CPSs from *A. baumannii* strains SMAL and MG1

Deacetylation of SMAL CPS was performed treating the purified water extract (10 mg) according to the strong alkaline hydrolysis protocol (section 9.3). The sample was desalted by size exclusion chromatography on Biogel-P2 (Biorad, 1.5 x 120 cm, eluent  $\text{NH}_4\text{HCO}_3$  50 mM, flow 0.2 ml min<sup>-1</sup>) where it was recovered in the void volume of the column (4 mg).

Smith degradation (Defaye and Wong, 1986) was accomplished on the UC purified CPS (15 mg) of *A. baumannii* SMAL. The sample was solved in 1 ml of water and treated with an equal volume of 0.1 M  $\text{NaIO}_4$  for 72 h at 4 °C. Sample was reduced ( $\text{NaBH}_4$ , 10 mg), neutralized with AcOH and dialyzed (cut-off 3500 Da). Finally, it was hydrolyzed (1 % AcOH, 2 h, 100 °C), centrifugated and the supernatant was purified on Biogel P2 (as above).

Solvolysis procedure with triflic acid (0.5 ml, -20 °C for 3 h) was performed on the water extract of *A. baumannii* MG1 (20 mg) under anhydrous conditions. The solution was neutralized with NH<sub>4</sub>OH 28% (Perepelov *et al.*, 2000) and was fractionated on Biogel P2 (as above). The product was further purified on by HPLC (Agilent 1100) on a RP-C8 (Supelco Supelcosil, 15 mm x 4.6 cm) column, eluted with water at 0.8 ml min<sup>-1</sup> in isocratic condition monitoring the eluate with the RI and UV detector at 210 nm.

### **9.9 LPS purification and isolation of the Enterobacterial common antigen from *E. coli* O157:H**

UC sediment of the water extract (10 mg) at 20 °C, were partially delipidated with NaOH 10 mM at 37 °C for 2 h. After neutralization the solution was chromatographed on Q-Sepharose Fast flow (GE-Healthcare, 1 x 3.5 cm, 0.2 ml min<sup>-1</sup>) ion exchange column, eluted with a NaCl gradient (10 mM, 200 mM, 400 mM, 700 mM, 1 M). The fractions were monitored using phenol-H<sub>2</sub>SO<sub>4</sub> test (section 9.5) and combined accordingly. Chemical and electrophoretic screening of the pooled fractions revealed that the LPS was eluted with NaCl 10 mM and 200 mM (3 mg and 2 mg, respectively).

The first UC supernatant of the water extract at 20 °C (100 mg) was hydrolyzed with β-agarase (Sigma, cod. A6306) in a 50 mM potassium buffer pH 6.0 at 43 °C. The hydrolysis was monitored with the Nelson-Somogyi reducing sugar test (Somogyi, 1952), using Gal (1 mg ml<sup>-1</sup>) for calibration. The sample, after agarase treatment, was dialysed, freeze-dried (60 mg) and fractionated on size exclusion column Sephacryl HR-100 (GE-Healthcare, 1.5 x 100 cm, eluent NH<sub>4</sub>HCO<sub>3</sub> 50 mM, flow 0.2 ml min<sup>-1</sup>). The fraction containing ECA<sub>CYC</sub> (15 mg) was retained from the gel and recovered after about one column volume. This fraction was further chromatographed on Biogel-P30 (Biorad, 1.5 x 74 cm, eluent NH<sub>4</sub>HCO<sub>3</sub> 50 mM, flow 0.2 ml min<sup>-1</sup>) and ECA<sub>CYC</sub> was recovered in the void volume of the column. The last fractionation was performed on Biogel P-100 (Biorad, 1.5 x 74 cm, eluent NH<sub>4</sub>HCO<sub>3</sub> 50 mM). The proton NMR of the single fractions allowed to isolate pure ECA<sub>CYC</sub> (2 mg) and ECB<sub>CYC</sub> (1 mg).

The O-antigen used for spectroscopic analyses was obtained from the LPS after acid hydrolysis as described in the section 9.7.

## CHAPTER X

### MASS SPECTROMETRY

#### *10.1 Preparations of Lipid As*

Free lipid A was obtained by hydrolysis of LPS with 1% acetic acid at 100 °C for 2 h. After centrifugation (9800 g, 4 °C, 20 min), Lipid A was collected as a precipitate, washed two or three times with water and finally freeze-dried. 1-5 mg of *Acinetobacter baumannii* SMAL LOS returned 0.3 -1 mg of Lipid A. The purified Lipid A. from *Cupriavidus necator* was obtained first washing crude water extract (50 mg) with 15 ml of a CHCl<sub>3</sub>: CH<sub>3</sub>OH: H<sub>2</sub>O (16: 8: 1 v/v/v) mixture for phospholipids removal. Then, the dry water extract was further purified by ultracentrifugation (440000g, 4°C, 16 h) and UC solid (40 mg) was treated with AcOH 6 %. However, the sample was not completely soluble in the acid solution, so it was centrifugated and the clear supernatant was treated for 3 h at 100 °C. The Lipid A was collected by centrifugation and freeze dried (0.8 mg).

The selective ester-bound acyloxyacyl deacylation was promoted by NH<sub>4</sub>OH 28 % treatment (200 µl, 25 °C, 16 h) directly on Lipid A (0.2-0.6 mg) of *Cupriavidus necator* and *Acinetobacter baumannii* strain SMAL at 28 °C (Silipo *et al.*, 2002). Furthermore, Lipid A (0.2 mg) of *Cupriavidus necator* was dephosphorylated by treatment with 100 µl of HF 48 % at 25 °C for 4 h.

#### *10.2 Electrospray Ionization Fourier-Transform Ion Cyclotron Resonance Mass Spectrometry*

ESI-FT-ICR-MS analysis was performed in negative and positive ion mode using a hybrid Apex Qe FT-ICR-MS (Bruker Daltonics, Billerica, MA, USA), equipped with a 7 T superconducting magnet and the Apollo dual ion source. The instrument was controlled by Bruker's ApexControl software, version 2.0.0.36, and data was recorded in broadband mode with 512 k data sampling rate. Mass scale was calibrated externally, using compounds of known structure. For the negative ion mode samples (~ 10 ng·µl<sup>-1</sup>) were dissolved in a 50:50:0.001 (v/v/v) mixture of 2-propanol, water, and triethylamine (pH ~ 8.5). For the positive ion mode a 30:10:0.4 (v/v/v) mixture of water, acetonitril, and acetic acid (pH ~ 3) was used. The samples were sprayed at a flow rate of 2 µl·min<sup>-1</sup>. Capillary entrance voltage was set to 3.8 kV, and drying gas temperature to 150°C. The spectra, which showed several charge states for each component, were charge deconvoluted, using the DataAnalysis Software (Bruker Daltonics) and mass numbers given refer to monoisotopic molecular masses. For unspecific fragmentation the voltage in the external collision cell was increased from 3V to 30V. Infrared multi-photon dissociation (IRMPD) of isolated parent ions was performed with a 25 W, 10.6 µm CO<sub>2</sub> laser (Synrad, USA).

The unfocused laser beam was directed through the centre of the trap. Duration of laser irradiation was adapted to generate optimal fragmentation and varied between 10 - 80 ms. Fragment ions were detected after a delay of 0.5 ms. Details on the structural characterization of LPS by FT ICR-MS are given elsewhere (Kondakova and Lindner, 2005).

### ***10.3 MALDI-TOF mass spectrometry***

The analyses were conducted using a Applied BioSystems (Framingham, MA) Voyager STR instrument equipped with delayed extraction technology. The matrix solution was prepared by dissolving 2,5-dihydroxybenzoic acid in TFA 0.1 M : CH<sub>3</sub>CN (30:70 by volume) at a concentration of 20 mg ml<sup>-1</sup>. Freeze-dried Lipid As were dissolved in CHCl<sub>3</sub>:CH<sub>3</sub>OH:H<sub>2</sub>O (2:3:1 by volume), while the ECA<sub>CYC</sub> and ECB<sub>CYC</sub> in water. The sample matrix solution mixture (1:1 v/v, 1 µl) was deposited into a stainless steel gold-plate 100 sample MALDI probe tip and dried at 25 °C. Ions formed by a pulsed UV laser beam (nitrogen laser, λ= 337 nm) were accelerated through 25 KV. Mass spectra were recorded in negative linear ion mode, using a delay time of 150 ms, grid voltage of 0.5% and 1000 shots/spectrum and laser intensity of about 2000.

## CHAPTER XI

### NMR SPECTROSCOPY

#### *11.1 Oligosaccharides from Rhizobium radiobacter Rv3*

NMR experiments were carried out on a Bruker DRX-600 spectrometer equipped with a CryoProbe operating at 303 K. Chemical shift of spectra recorded in D<sub>2</sub>O are expressed in  $\delta$  relative to internal acetone (<sup>1</sup>H at 2.225 ppm, <sup>13</sup>C at 31.45 ppm). Two-dimensional spectra (DQ-COSY, TOCSY, TROESY, gHSQC, gHMBC and gHSQCTOCSY) were measured using standard Bruker software. For the homonuclear experiment, 512 FIDs of 2048 complex data points were collected, with 40 scans per FID, mixing times of 120 ms for TOCSY and gHSQCTOCSY, and 250 ms for TROESY spectra acquisition. The spectral width was set to 10 ppm and the frequency carrier was placed at the residual HOD peak. For the HSQC spectrum, 512 FIDs of 2048 complex points were acquired with 50 scans per FID, the GARP sequence was used for <sup>13</sup>C decoupling during acquisition. gHSQCTOCSY and gHMBC were not measured for **OS2** due to the low amount of compound available. Data processing was performed with standard Bruker Topspin 3 program, the spectra were assigned using the computer program Pronto (Kjaer *et al.*, 1994).

#### *11.2 O-Chain from Cupriavidus necator*

Spectra of LPS were recorded at 303 K in D<sub>2</sub>O con a Bruker DRX-600 spectrometer equipped with a CryoProbe and were calibrated on internal acetone. Two dimensional homonuclear spectra (DQ-COSY, TOCSY, NOESY) were recorded with 1024 FIDs of 2048 data points and 16 scans per FID. For heteronuclear HSQC and HMBC spectra, 512 FIDs of 2048 complex points were acquired with 24 and 240 scans per FID, respectively. Spectra of 4-deossi- $\beta$ -D-arabinohexose were recorded at 298 K. For Two-dimensional experiments (DQ-COSY, TOCSY, TROESY, HSQC), 512 FIDs of 2048 complex data points were collected with 8 scans per FID for COSY and 24 for the others. Data were transformed, processed and analysed with Bruker Topspin 2.1 software.

#### *11.3 Oligosaccharides from Acinetobacter baumannii SMAL and MG1*

<sup>1</sup>H and <sup>1</sup>H-<sup>13</sup>C NMR experiments on **OS2** were carried out with a Varian Inova 500 spectrometer form Consortium INCA (L488/92, Cluster 11) equipped with a reverse probe operating at 296 K. The spectra of **OS3** were recorded at 300 K with a Bruker DRX-600 spectrometer equipped with a cryogenic probe. All spectra were calibrated with respect to internal acetone. For all homonuclear experiments were measured with data sets of 2048 x 512 points, 32 scans were acquired, and mixing

times of 200 and 120 ms were employed for ROESY and TOCSY experiments, respectively. Each data matrix was zero-filled in both dimensions to give a matrix of 4096 x 2048 points and was resolution-enhanced in both 391 dimensions by a shifted sine-bell function before Fourier transformation. The HSQC experiment was performed by using a data set of 2048 x 512 points, whereas for the HMBC experiment a data set of 2048 x 256 points was used. For each  $t_1$  value, 64 scans were acquired, and the HMBC sequence was optimized for a 6 Hz long- 396 range coupling constant. All NMR spectra were acquired and transformed by using the Topspin 3.0a program and studied with Pronto software.

#### ***11.4 Capsular polysaccharides from Acinetobacter baumannii SMAL and MG1***

*A. baumannii* MG1 homo- and heteronuclear spectra were recorded using Varian Inova 500 MHz spectrometer equipped with a inverse z-gradient probe (Consortium INCA, L488/92, Cluster 11) operating at 298 K. With regard to *A. baumannii* SMAL, spectra were acquired on a Bruker 600 MHz equipped with a CryoProbe, operating at 291 K for the fully deacetylated capsule, or at 305 K for the periodate degraded product. Chemical shifts are expressed in ppm relative to internal acetone ( $^1\text{H}$  at 2.225 ppm,  $^{13}\text{C}$  at 31.45 ppm). Two-dimensional spectra (DQ-COSY, TOCSY, NOESY, gHSQC and gHMBC) were measured using the standard Varian or Bruker software.

For the homonuclear experiment, 512 FIDs of 2048 complex data points were collected, with 40 scans per FID, a mixing time of 120 or 200 ms was applied for the TOCSY and NOESY spectra, respectively. For the HSQC and HMBC spectra, 256 FIDs of 2048 complex points were acquired with 50 scans per FID. Processing of the Varian and Bruker data and analysis was performed with Bruker TopSpin 2.1 program.

#### ***11.5 O-Chain and the Enterobacterial common antigen from E. coli O157: H***

The two forms of the *Enterobacterial common antigen* (ECA and ECB) were analysed at 308 K in  $\text{D}_2\text{O}$  on a Bruker DRX-600 spectrometer equipped with a CryoProbe; *O*-Chain from phenolic LPS at 300 K (calibrated on internal acetone). ECA and ECB two-dimensional experiments 512 FIDs of 2048 complex data points were collected; DQ-COSY with 24 scans, NOESY and TOCSY 32 scans, HSQC 40 scans, HMBC 64 scans and HSQCTOCSY 110 scans per FID. COSY, NOESY, TOCSY and HSQC relative to the *O*-Chain were recorded with 40, 48, 40, 140 scans per FID. Processing and analyses of spectra were performed with Bruker Topspin 2.1 software.

## PART IV: STRUCTURAL CHARACTERIZATION OF MENB OMVs MEMBRANE CONSTITUENTS

This part of the thesis regards a project developed in collaboration with the Novartis Vaccines Diagnostic of Siena and it is reported as accepted by a clearance process.

### 1: Introduction

#### 1.1 *Neisseria meningitidis* and the new vaccine approach against group B based on Outer Membrane Vesicles (OMVs)

*Neisseria meningitidis* is an encapsulated diplococcal Gram-negative bacterium. Commonly it colonizes the mucosal membranes of the human nasopharynx but when it enters in the bloodstream can cause meningitis and sepsis. Most infection cases are acquired by person-to-person contact through aerosol droplets or contacts with respiratory secretions from asymptomatic carriers. *Neisseria* has been isolated only in humans because cannot get iron other than from human sources (transferrin and lactoferrin). Meningococcal meningitis remains a worldwide problem and occurs in both endemic and epidemic forms.

12 distinct *N. meningitidis* serogroups have been defined on the basis of the immunochemistry of their CPSs (table 1); groups A, B, C, W135 and Y are the foremost responsible of severe meningitis and septicemia especially in infants and young children.

Serogroups	Structure of CPS repeating unit
A	6)- $\alpha$ -D-ManpNAc(3OAc)-(1 $\rightarrow$ PO <sub>4</sub> $\rightarrow$
B	8)- $\alpha$ -D-Neup5NAc-(2 $\rightarrow$
C	9)- $\alpha$ -D-Neup5NAc(7/8OAc)-(2 $\rightarrow$
H	4)- $\alpha$ -D-Galp-(1 $\rightarrow$ 2)-glycerol-PO <sub>4</sub> -(1 $\rightarrow$
I	4)- $\alpha$ -L-GulpNAcA-(1 $\rightarrow$ 3)- $\beta$ -D-ManpNAcA(4OAc)-(1 $\rightarrow$
K	3)- $\beta$ -D-ManpNAcA-(1 $\rightarrow$ 4)- $\beta$ -D-ManpNAcA(4OAc)-(1 $\rightarrow$
L	3)- $\beta$ -D-GlcpNAc-(1 $\rightarrow$ 3)- $\alpha$ -D-GlcpNAc-(1 $\rightarrow$ 3)- $\beta$ -D-GlcpNAc-PO <sub>4</sub> -(1 $\rightarrow$
X	4)- $\alpha$ -D-GlcpNAc-PO <sub>4</sub> -(1 $\rightarrow$
Y	6)- $\alpha$ -D-Glcp-(1 $\rightarrow$ 4)- $\alpha$ -D-NeupAc-(2 $\rightarrow$
W135	6)- $\alpha$ -D-Galp-(1 $\rightarrow$ 4)- $\alpha$ -D-NeupAc-(2 $\rightarrow$
Z	4)- $\alpha$ -D-GalpNAc-(1 $\rightarrow$ 1)-glycerol-(3 $\rightarrow$ PO <sub>4</sub> -(1 $\rightarrow$
29E	7)- $\beta$ -D-Kdo-(2 $\rightarrow$ 3)- $\alpha$ -D-GalpNAc-(1 $\rightarrow$

Table 1: *Neisseria meningitidis* serogroups classification on the base of CPSs structures

Group A is characterized by its propensity to cause large-scale epidemics in developing countries, as Africa and Asia (Wang *et al.*, 1992). Meningococcus B (MenB) is the most important cause of endemic meningitis in industrialized countries, accounting for 30%–40% of cases in North America and for up to 80% in certain European countries, and most of the remaining cases are caused by group C. MenB is especially diffused in Norway, Netherlands, Germany and Denmark, while increasing proportions of group C strains have been reported from Slovak and Czech Republics, Greece, Republic of Ireland, Spain (Berron *et al.*, 1998), Canada and the United Kingdom (Ramsay *et al.*, 1997). Group B also can cause severe persistent epidemics, such as that occurred in Latin American countries or in Norway and New Zealand (Martin *et al.*, 1998). Approximately 10%-15% of the disease in the United States is caused by groups Y and W135, however since 2000 group W135 has caused outbreaks in Saudi Arabia, Burkina Faso, making complex the epidemiological situation in this region (Mayer *et al.*, 2002).

Groups A, C, Y and W135 infections are prevented by vaccines based on high molecular weight CPS. Groups A and C were licensed in 1976 in the USA and Europe, tetravalent ACYW135 in USA in 1982 (Brandt *et al.*, 1978; Vodopija *et al.*, 1983) These vaccines unfortunately failed in induce an immunological memory and were poorly effective in young children and infants. Consequently, efficacious CPS-protein conjugate vaccines (table 2) have been developed, these are safe, immunogenic in young infants and induce long-term immune memory (Pon and Jennings, 2008).

Commercial Vaccine	Serogroup	Protein Carrier	Producer
Manjugate	C	CRM197 DTd	Chiron (1999)
Menivact	C	CRM197 DTd	Aventis-Pasteur(2002)
Meningitech	C	CRM197 DTd	Wyeth (2002)
NeisVac-C	C	TTd	Baxter Vaccini (2002)
MCV4	Tetravalent ACYW135	TTd	Sanofi-Pasteur (2005)
Pnc9-MenC	9 valent MenC/S.pneumoniae	CRM 197	Wyeth (2000)
MenAfriVac	A	TTd	Serum Institute of India for Meningitis vaccine project (2010)

Table 2: Glycoconjugate commercial vaccines against serogroups A, C, W135, Y.

Group B is the only serogroup whose infection cannot be prevented by CPS-based vaccines. Its CPS is a polymer of  $\alpha$ -(2→8)-N-acetyl-neuraminic acid (polysialic acid) and it is essentially non immunogenic in humans. It is postulated that oligosaccharides of  $\alpha$ -(2→8)- sialic acid units are present on gangliosides of human cell surfaces including the neural cellular adhesion molecule involved in cell-to-cell adhesion, so that the immune system does not produce antibodies against an antigen having similarity to self-structures.

Another possible explanation is that CPS is easily degraded by neuraminidase or the acidic pH promotes the formation of internal esters with resulting loss of antigenicity. An attempt was made to develop a conjugated vaccine using group B capsular PS in which the *N*-acetyl group of the sialic acid residues were replaced with *N*-propionyl group (Sanofi-Pasteur), (Bruge *et al.*, 2004). The vaccine was tested in a Phase I trial on adult volunteers and found to be safe, but the antibodies induced were devoid of functional activity. New vaccine approaches against serogroup B

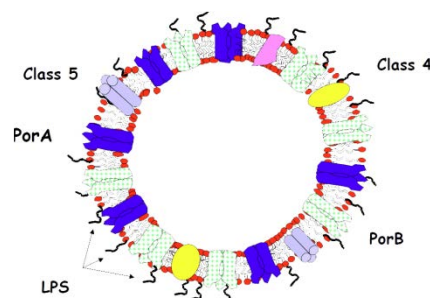


Figure 1: Depiction of OMV

meningococcus have been explored, such as the reverse vaccinology (Rappuoli and Covacci, 2003), and the preparation of Outer-Membrane Vesicles (OMVs) (Fischer *et al.*, 1999). OMVs are small membranous spherical vesicles containing capsular polysaccharide, outer membrane proteins (OMPs) and lipooligosaccharides (LOSs).

The OMV antigen is produced by fermentation of an appropriate *Neisseria meningitidis* strain, followed by concentration and bacterial inactivation, lysis and elaboration of OMV through iterated steps of centrifugation and sonication; OMVs are separated, then characterized according to size and morphology.

A vaccine based on OMVs is already available (MenZB, Novartis), it is effective against homologous strains but it fails against heterologous bacteria because of antigenic variability. One of the outer meningococcal OMPs, PorA, was identified as a major inducer of bactericidal antibodies and is expressed by almost all meningococci. However, there is a large number of PorA proteins with different antigenic specificities so that the elicitation of an immune response against one PorA antigen does not confer protection against strains with heterologous PorA antigens. OMV vaccines are thus strain-specific vaccines that can only be used against clonal disease outbreaks but not for prevention of sporadic disease caused by heterologous strains. PorB and FetA, two other OMPs, may be interesting vaccine candidates and probably only a limited number of combinations of these proteins needs to be used for an effective vaccine (Urwin *et al.*, 2004).

## 2: Results and discussions

### 2.1 Structural characterization of the polysaccharide components on Outer Membrane Vesicles (OMVs) of *Neisseria meningitidis* serogroup B (MenB)

The following discussion regards the analyses performed on the polysaccharide components constituting the MenB OMVs produced by Novartis Vaccines Diagnostic of Siena.

In the frame of this work, different points were defined as targets and analyzed: preliminary spectroscopic analysis on intact OMVs were performed in order to try an identification of the

contribution of LOS and CPS to the sialic acid content on the vesicles. Further analyses were focused on the isolation and structural characterization of LOS. In particular chemical analyses of monosaccharides were accomplished to determine LOS immunotypes of the strain used for vaccine production. Lipid A family were structurally defined through MALDI mass spectrometry. Finally, the content of LOS and CPS outside vesicles was determined, as well. Novartis vaccine lots are named in the text with capital letters, for simplicity.

### 2.1.1 NMR analyses of native capsular polysaccharide and of intact OMVs

Capsular polysaccharide from MenB, a polymer of  $\alpha$ -(2 $\rightarrow$ 8)-*N*-acetyl-sialic acid, was used as reference and it was characterized through mono (figure 2) and bidimensional NMR experiments. The assignment of chemical shifts (table 3) was in agreement with literature data (Bhattacharjee *et al.*, 1975).

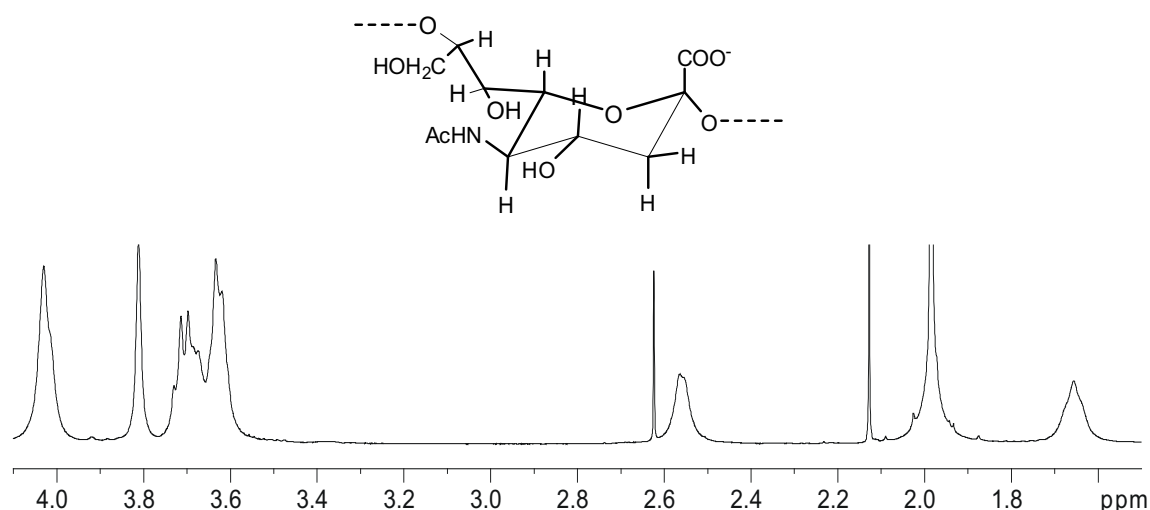


Figure 2:  $^1\text{H}$  NMR spectrum of MenB CPS in  $\text{D}_2\text{O}$ , 600 MHz, 298 K, acetone as internal standard

Nucleus	3-3'	4	5	6	7	8	9-9'	C=O (NHCOCH <sub>3</sub> )
$^1\text{H}$	1.75-2.67	3.72	3.80	3.72	3.91	4.12	3.77-4.12	1.98
$^{13}\text{C}$	41.7	69.6	53.8	74.5	70.7	78.6	62.7	176.3*

Table 3: Chemical shift (ppm) of MenB CPS in  $\text{D}_2\text{O}$ , 600 MHz, 298 K, acetone with internal standard  
\* Determined through  $^1\text{H}$ - $^{13}\text{C}$ -HMBC spectrum.

Spectroscopic analysis on intact vesicles was performed after  $\text{D}_2\text{O}$  exchange through vivaspin system, and  $^1\text{H}$  NMR spectrum (figure 3) showed only signals of soluble components, whereas the insoluble material conferred to the base line an arched shape. In these conditions, neither signals of CPS or LOS were observed; it was concluded that spectroscopic approach did not allow their direct estimation on the vesicle.

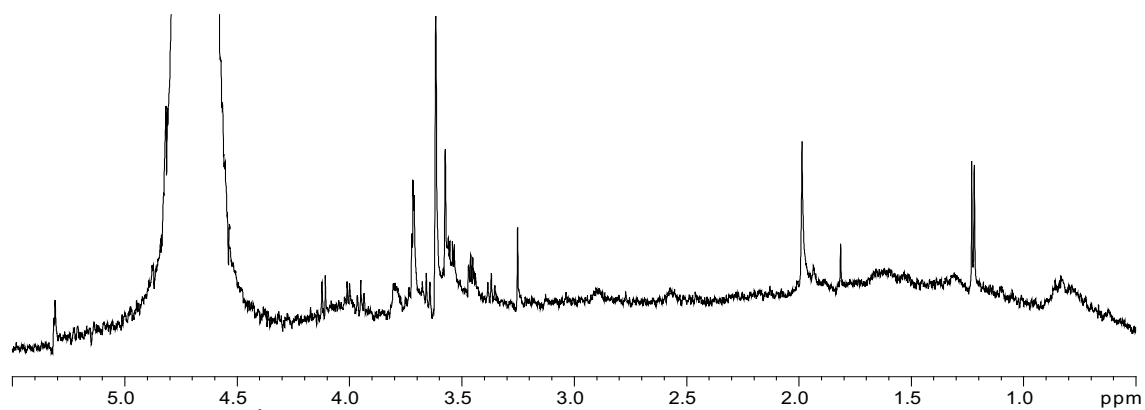


Figure 3:  $^1\text{H}$  NMR spectrum of intact vesicle exchanged with  $\text{D}_2\text{O}$ , 600 MHz, 298 K

### 2.1.2 Electrophoretic and Spectroscopic analyses of LOS and CPS extracted from OMVs

OMVs were treated according to the hot phenol/water method (Westphal *et al.*, 1965). Silver nitrate staining (figure 4, lanes 1 and 2) showed the presence of LOS both in water and in phenol phases, however this latter contained proteins and only minor amount of LOS (figure 4 lane 2'). This behavior of repartition was reproducible for all samples tested, and figure 4 shows the results for sample  $A_3$ . Further analyses were focused on water extracts.

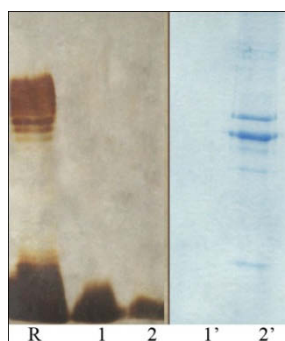


Figure 4: SDS-PAGE of  $A_3$  sample. R: *E. coli* O55:B5 LPS standard (8  $\mu\text{g}$ ); 1 and 1' : water phase (8  $\mu\text{g}$ ) stained respectively with silver and coomassie; 2 and 2' : phenol phase (8  $\mu\text{g}$ ) stained respectively with silver and coomassie.

$^1\text{H}$  NMR analysis of water extracts did not give information on LOS because of the low mobility in solution of this molecule, but it was possible to detect the capsular polysaccharide signals ( $^1\text{H}$  NMR figure 5). Although the spectra contained other dialysis impurities, the CPS signals were recognized in the gHSQC spectrum (figure 6) on the basis of the values reported in table 3.

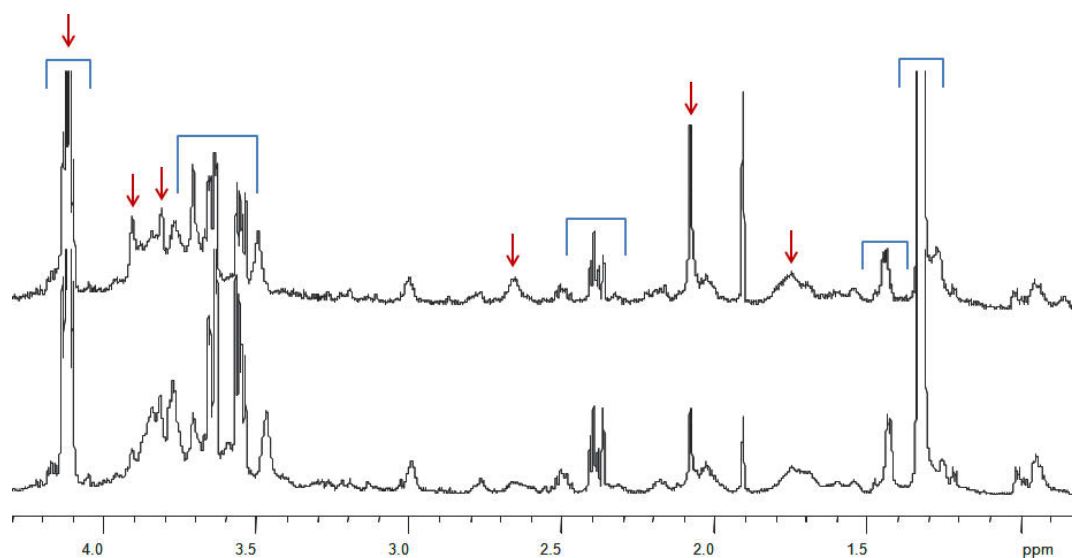


Figure 5:  $^1\text{H}$  NMR of water extracts of  $A_2$  (bottom) and  $A_3$  (top) samples.  $\text{D}_2\text{O}$ , 600 MHz, 298 K, calibrated on *N*-acetyl sialic acid signal (2.08 ppm). Blue semi-squared indicated impurities, red arrows CPS signals.

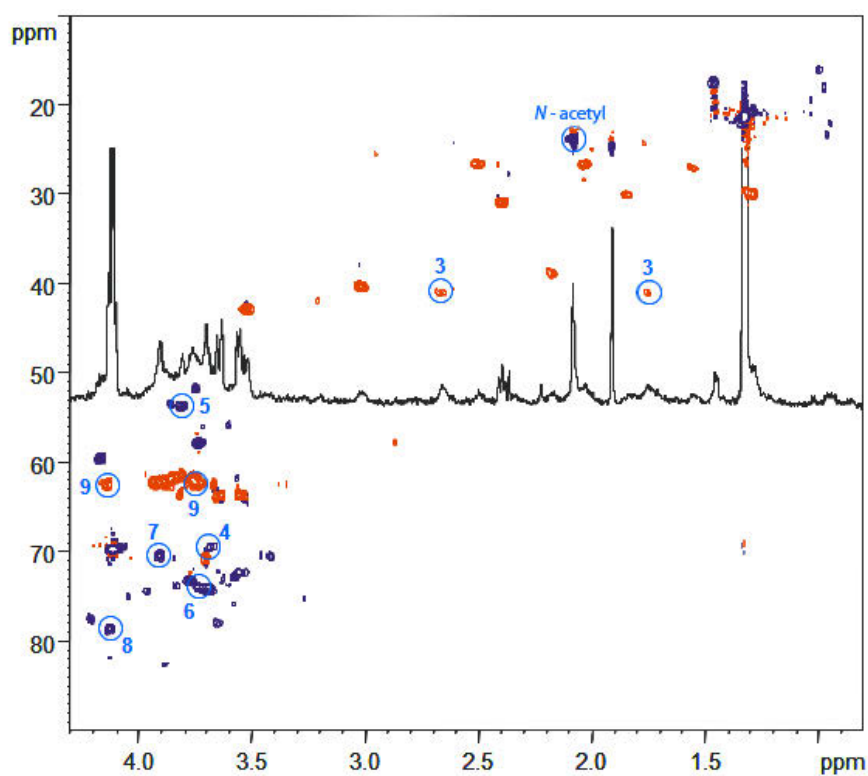


Figure 6:  $^1\text{H}$ - $^{13}\text{C}$ -gHSQC of  $A_3$  water phase,  $\text{D}_2\text{O}$  600 MHz, 298K.. calibrated on *N*-acetyl sialic acid signal (2.08 ppm).  $^{13}\text{C}$  signals were underlined with blue circles.

DOSY experiment on  $A_3$  sample was measured to estimate the mobility in solution of CPS. The mobility of the CPS from OMV was higher (figure 7-a) with respect to that of the intact CPS (figure 7-b) this could be attributable to a depolymerization process promoted by the phenol/water extraction. To prove this hypothesis, intact CPS was submitted to the same extraction and DOSY spectrum was recorded (figure 7-c).

The mobility of the sample was intermediate between that of the intact sample and that extracted from the OMV; this experiment proved that the hot treatment induced a depolymerization of the sample but also that the entity of this depolymerization was different from that observed for the sample extracted from the OMV. In conclusion, the loss of molecular weight of CPS contained in water phase was related only in part to the hot extraction treatment and the contribute from the sonication treatments used for vesicles assembling seems possible.

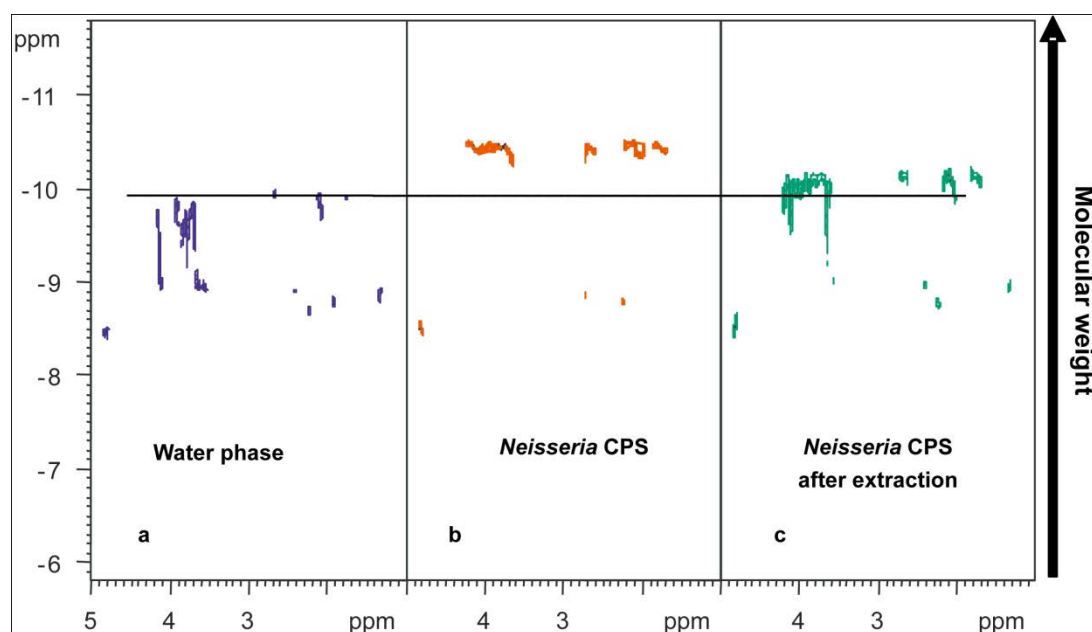


Figure 7: DOSY spectra,  $D_2O$ , 600 MHz, 298 K, acetone as internal standard. a:  $A_3$  water phase, b: intact CPS of MenB, c: CPS of MenB after water/phenol extraction.

### 2.1.3 GC-MS quantification of LOS immunotypes

*Neisseria meningitidis* is classified in immunotypes on the basis of LOSs structures.

Among the 12 LOSs structures only 9 are known in detail and indicated with L, the different immunotypes share a conserved core oligosaccharide (figure 8), and distinct  $R_1$ ,  $R_2$ ,  $R_3$ ,  $R_4$  substituents.

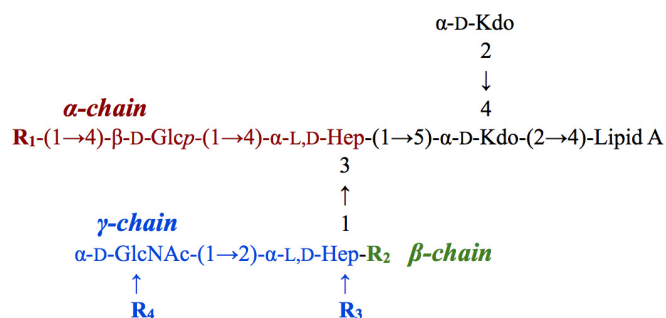


Figure 8: Conserved Core oligosaccharide of *Neisseria meningitidis*

The relationship among the R substituents and the immunotypes classification is showed in table 4.

	<b>R<sub>1</sub></b> <b>(<math>\alpha</math>-chain)</b>	<b>R<sub>2</sub></b> <b>(<math>\beta</math> chain)</b>	<b>R<sub>3</sub></b> <b>(<math>\gamma</math> chain)</b>	<b>R<sub>4</sub></b> <b>(<math>\gamma</math> chain)</b>
<b>L1</b>	<b><math>\alpha</math>-D-Gal-(1→4)-<math>\beta</math>-D-Gal</b>	<b>3-PEA</b>	<b>H</b>	<b>H</b>
<b>sL1</b>	<b><math>\alpha</math>-Neu-(2→6)-<math>\alpha</math>-D-Gal-(1→4)-<math>\beta</math>-D-Gal</b>	<b>3-PEA</b>	<b>H</b>	<b>H</b>
<b>L2</b>	<b><math>\beta</math>-D-Gal-(1→4)-<math>\beta</math>-D-GlcNAc-(1→3)-<math>\beta</math>-D-Gal</b>	<b><math>\alpha</math>-D-Glc</b>	<b>6-7 PEA</b>	<b>Ac 40%</b>
<b>L3</b>	<b><math>\alpha</math>-Neu-(2→3)-<math>\beta</math>-D-Gal-(1→4)-<math>\beta</math>-D-GlcNAc-(1→3)-<math>\beta</math>-D-Gal</b>	<b>3-PEA</b>	<b>H</b>	<b>H</b>
<b>L4</b>	<b><math>\alpha</math>-Neu-(2→3)-<math>\beta</math>-D-Gal-(1→4)-<math>\beta</math>-D-GlcNAc-(1→3)-<math>\beta</math>-D-Gal</b>	<b>H</b>	<b>6-PEA</b>	<b>3-Ac 50%</b>
<b>L5</b>	<b><math>\beta</math>-D-Gal-(1→4)-<math>\beta</math>-D-GlcNAc-(1→3)-<math>\beta</math>-D-Gal</b>	<b><math>\alpha</math>-D-Glc</b>	<b>H</b>	<b>Ac 60%</b>
<b>L6</b>	<b><math>\beta</math>-D-GlcNAc-(1→3)-<math>\beta</math>-D-Gal</b>	<b>H</b>	<b>7-PEA</b>	<b>H</b>
<b>L7</b>	<b><math>\beta</math>-D-Gal-(1→4)-<math>\beta</math>-D-GlcNAc-(1→3)-<math>\beta</math>-D-Gal</b>	<b>3-PEA</b>	<b>H</b>	<b>H</b>
<b>L9</b>	<b><math>\beta</math>-D-Gal-(1→4)-<math>\beta</math>-D-GlcNAc-(1→3)-<math>\beta</math>-D-Gal</b>	<b>6-PEA</b>	<b>H</b>	<b>H</b>

Table 4: *Neisseria meningitidis* immunotypes

$\beta$ -chain (**R<sub>2</sub>**) is an  $\alpha$ -D-Glucose residue diagnostic of L2 and L5 immunotypes or it is a phosphoethanolamine (PEA) in L1, L3, L7 and L8 LOS species.

The structures of L8, L10, L11, L12 are not defined, however L8 has an immunochemical behavior similar to L1. This differs from L3, L7, L9 for the nature of the R<sub>1</sub> substituent in the  $\alpha$ -chain, whereas the difference between L1 and sL1 (sialilated), L3 and L7, L2 and L4 regards the presence of sialic acid. R<sub>3</sub> and R<sub>4</sub> are not relevant for L1, sL1, L3, L7, L9 immunotypes classification.

The occurrence of some substitution patterns resident on the  $\alpha$ -chain allows the individuation of different immunotypes (or combination of them).

Indeed, GC-MS branching point analysis was used to establish the relative ratio of specific immunotypes. Immunotype of the strain of MenB used for OMVs preparations was unknown, so the following discussion started from the assumption that only the most probable immunotypes for group B, L1, sL1, L3, L7 were present, L9 was considered equivalent to L7 because it possesses the same R<sub>1</sub> group.

The speciation of L1, sL1, L3, L7 immunotypes took into account the following characteristic residues located on the  $\alpha$ -chain:

- 4-linked-galactose (4-gal) was representative of L1 and sL1
- 6-linked-galactose (6-gal) was representative of sL1
- 4-linked-2-amino-hexose (4-hexN), considered *gluco*-configured, was representative of L7 and L3

Another important residue was 3-linked-galactose (3-gal): this PMAA derivative is representative of L7 and L3 LOS immunotypes; in this last species, 3-gal is contained twice so that the following formula can be associated to the area of 3-gal: L7 + 2 \* L3.

On the basis of the consideration above, LOS immunotyping of OMV samples was performed considering the area of the PMAA reported in table 5, so that quantification of sL1, L1 and the sum of L3 plus L7 was achieved.

The use of formulas  $3\text{-gal} = (L7 + 2 * L3)$  and  $4\text{-hexN} = (L7 + L3)$  to determine the amount of the single L3 and L7 components, returned for some samples negative values, for this reason these LOS species were not calculated but only their sum (L3 + L7) was considered (see table 5). A possible explanation for the occurrence of negative values could be that the 4-hexN area was computed without any corrective factor, or also that the sample contained other immunotypes different from those considered in our assumption; in fact 4-glcN is also present in the  $\alpha$ -chain of L2, L4, L5; if so, the formulas associated to the 3-gal and 4-hexN areas are not valid and yield to an erroneous result.

Residue	Immunotype	A <sub>3</sub> area	B <sub>2</sub> area	B <sub>4</sub> area	C <sub>3</sub> area	D <sub>1</sub> area
4-gal	L1 + sL1	661172	1167363	374876	1207864	1483381
6-gal	sL1	145310	220656	99677	265378	341871
4-hexN	L7 + L3	149066	319877	147535	197648	196414

Table 5: Areas of diagnostic residues relative to A<sub>3</sub>, B<sub>2</sub>, B<sub>4</sub>, C<sub>3</sub>, D<sub>1</sub> samples

On the basis of these premises, immunotypes composition was estimated for five different samples (table 6, figures 9 - 13)

Immunotype	Calculated as	A <sub>3</sub> area %	B <sub>2</sub> area %	B <sub>4</sub> area %	C <sub>3</sub> area %	D <sub>1</sub> area %
L1	4-gal - 6-gal	63,7	63,7	54,9	66,7	67,4
sL1	6-gal	17,9	14,8	19,9	18,8	20,2
L3 +L7	4-hexN	18,4	21,5	25,3	14,5	32,6

Table 6: Immunotypes quantification

These other derivatives were not considered:

- Neuraminic acid for sL1 and L3 because its detection requires different chemical treatments (carboxyl reduction) and generally it is not quantitative.
- The terminal galactose (*t*-gal) for L7 and L1 because its detector response is different from mono substituted residues.

Intense peaks of *t*-glc and 4-glc were also present, but their abundance was not clear on the basis of the structure of the known immunotyeps. 6-hexN (comparable to 4-hexN) residue could belong to unknown immunotypes structure or to Lipid A.

The presence of 2-hex, 4,6-hex, 2,4-hex, 3,4-gal, residues was unclear, whereas some important residues such as heptoses of Core, and terminal glucosamine were absent. Phosphorylation of these residues can avoid the derivatization process consequently explain of their absence.

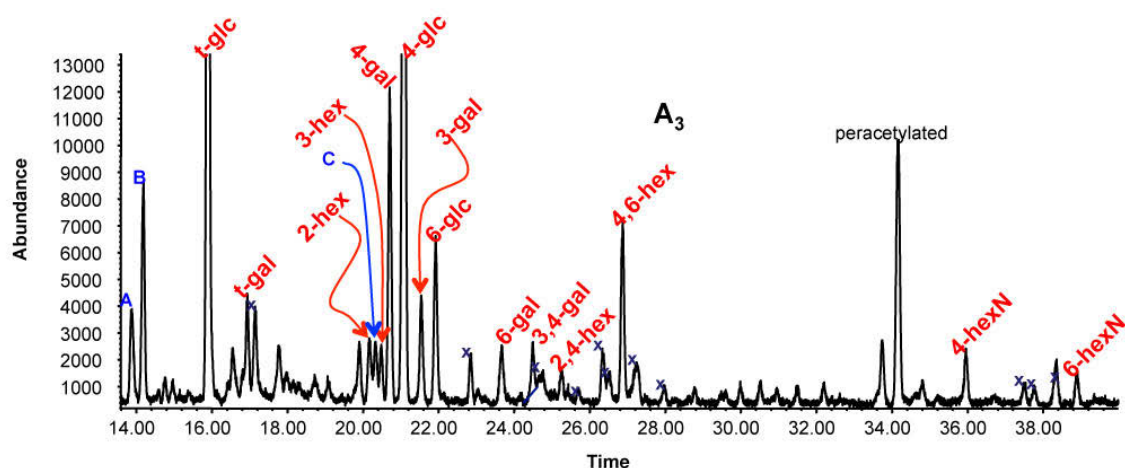


Figure 9:  $A_3$  PMAA chromatogram. A, B, C were complex mixture of glycidic derivatives. A and B: *t*-ketof + 4-pent; C: 6-ketof + undefined derivative. "Hex" indicated an hexose with not attributed configuration.

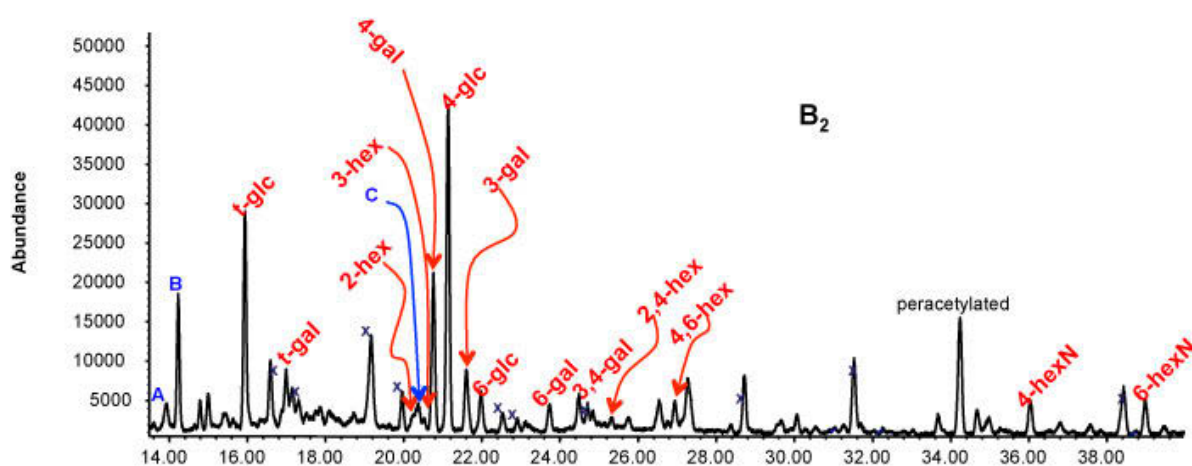


Figure 10: PMAA chromatogram of sample  $B_2$ . A, B, C were complex mixture of glycidic derivatives. A: *t*-ketof + 4-pent, B: 4-pent, C: 6-ketof + undefined derivative. "Hex" indicated an hexose with not attributed configuration.

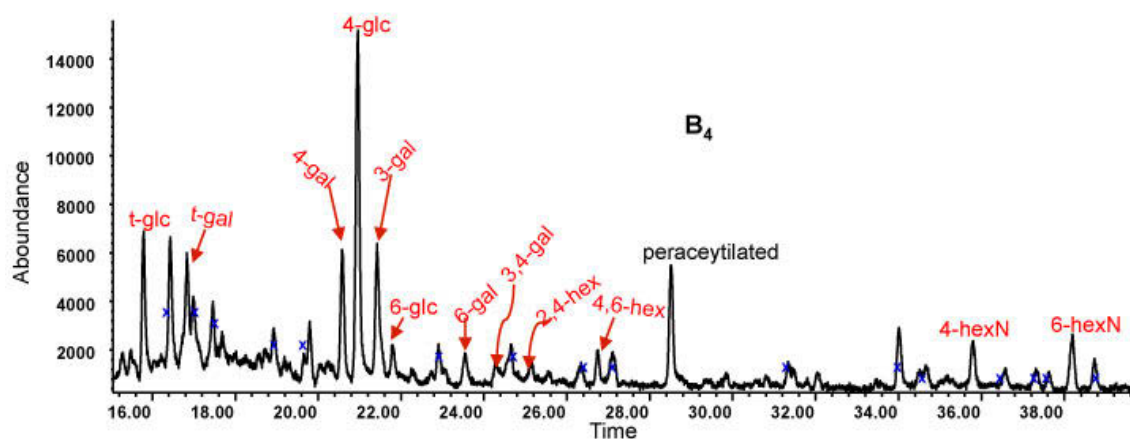


Figure 11: PMAA chromatogram of sample B<sub>4</sub>. "Hex" indicated an hexose with not attributed configuration.

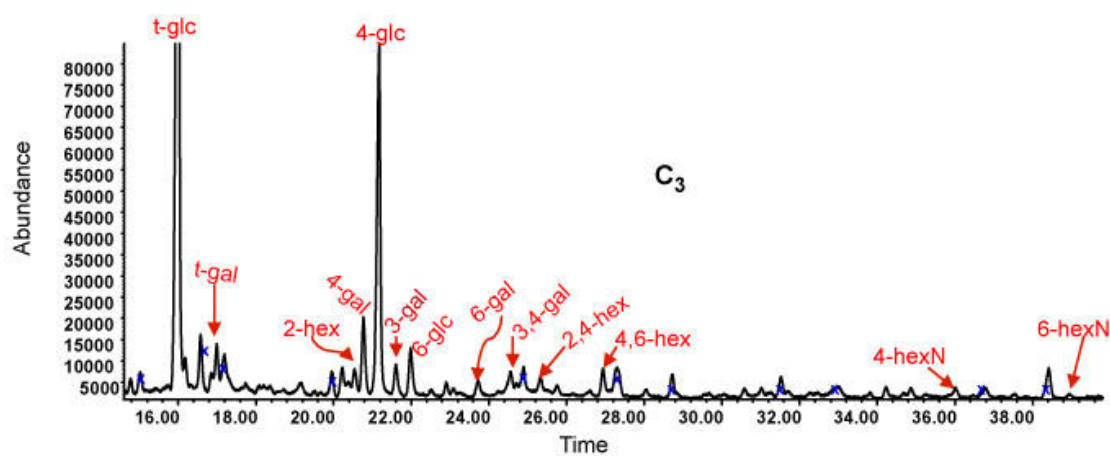


Figure 12: PMAA chromatogram of sample C<sub>3</sub>. "Hex" indicated an hexose with not attributed configuration.

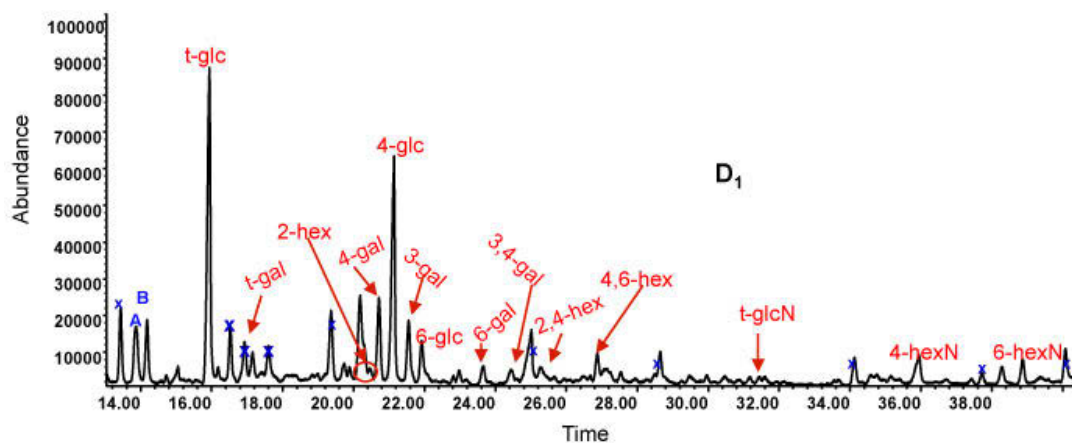


Figure 13: PMAA chromatogram of sample D<sub>1</sub>. A and B: *t*-ketof + 4-pent. "Hex" indicated an hexose with not attributed configuration.

#### 2.1.4 MALDI MS spectrometry characterization of Lipid A

Lipid A was obtained after mild acid hydrolysis of water phase and analyzed by MALDI MS spectrometry.

The ion negative MALDI spectrum (figure 14) recorded on intact Lipid A showed the presence of 5 groups of pseudomolecular ions  $[M-H]^-$  labeled with capital letters **A**, **B**, **C**, **D**, **E** (table 7). Base peak **B** ( $m/z$  1632.38) corresponded to penta-acylated Lipid A with two 3-hydroxytetradecanoic acids (C14:0) 3-OH, one 3-hydroxydodecanoic acid (C12:0) 3-OH, two dodecanoic acids C12:0. It differed from specie **A** for the lacking of one PEA unit on the glucosamine backbone. The less intense peak **C** ( $m/z$  1572.73) was attributed to a tetra-acylated Lipid A with one C12:0 less with respect to **A**. The same composition of fatty acids but one PEA unit was observed for **D**, another tetra-acylated specie **E** was observed which differed from **D** for the substitution of (C12:0) 3-OH with a C12:0.

It is proposed that peaks **A**<sub>1</sub>, **A**<sub>2</sub>, **C**<sub>1</sub> and **C**<sub>2</sub> were originated by fragmentation of **A** and **C**, in particular these peaks were attributed to the loss of  $-CH_2-CH_2-NH_2$  (- 44 u.m.a.) or  $-O-CH_2-CH_2-NH_2$  (- 60 u.m.a.) fragments. Alternatively **A**<sub>1</sub> and **C**<sub>1</sub> might be related to **B** and **E** respectively, by addition of a phosphate.

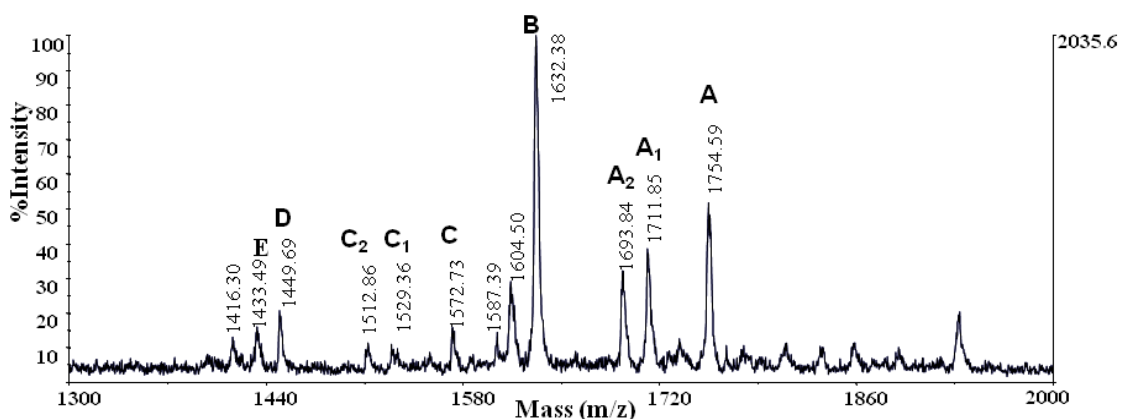


Figure 14: Ion negative MALDI spectrum of intact Lipid A from sample A<sub>3</sub>. (not calibrated)

Species	n. acyl	Composition	Ion (m/z)
A	5	2 x C14:0 3-OH, C12:0 3-OH, 2 x C12:0, 2PEA, 2 x GlcN, 2P	1754.59
A <sub>1</sub>	5	B+80 (P) or A-44	1712.85
A <sub>2</sub>	5	A- 60	1693.84
B	5	2 x C14:0 3-OH, C12:0 3-OH, 2 x C12:0, PEA, 2 x GlcN, 2P	1632.38.
C	4	2 x C14:0 3-OH, C12:0 3-OH, C12:0, 2PEA, 2 x GlcN, 2P	1572.73
C <sub>1</sub>	4	E + 80 or C-44	1529.36
C <sub>2</sub>	4	C-60	1512.86
D	4	2 x C14:0 3-OH, C12:0 3-OH, C12:0, PEA, 2 x GlcN, 2P	1449.69
E	4	2 x C14:0 3-OH, 2 x C12:0, PEA, 2 x GlcN, 2P	1433.49

Table 7: Composition of penta- and tetra-acyl Lipid A of MenB

Oxonium ion (m/z 849,10) observed in the spectrum measured in the positive mode (not showed) was consistent with the presence of three fatty acids, in particular (C14:0) 3-OH, (C12:0) 3-OH and C12:0, on the non-reducing GlcN unit (GlcN II), (figure 15-2).

The location of fatty acids (figure 15-1) was attributed on the basis of literature data (Kulshin *et al.*, 1992; John *et al.*, 2009 ). Lipid A of other samples was investigated (figures 16-20) and the relative abundances of the species individuated in the MALDI spectra are reported in table 8. For simplicity all the values are normalized with respect to the pseudomolecular ion A<sub>1</sub>.

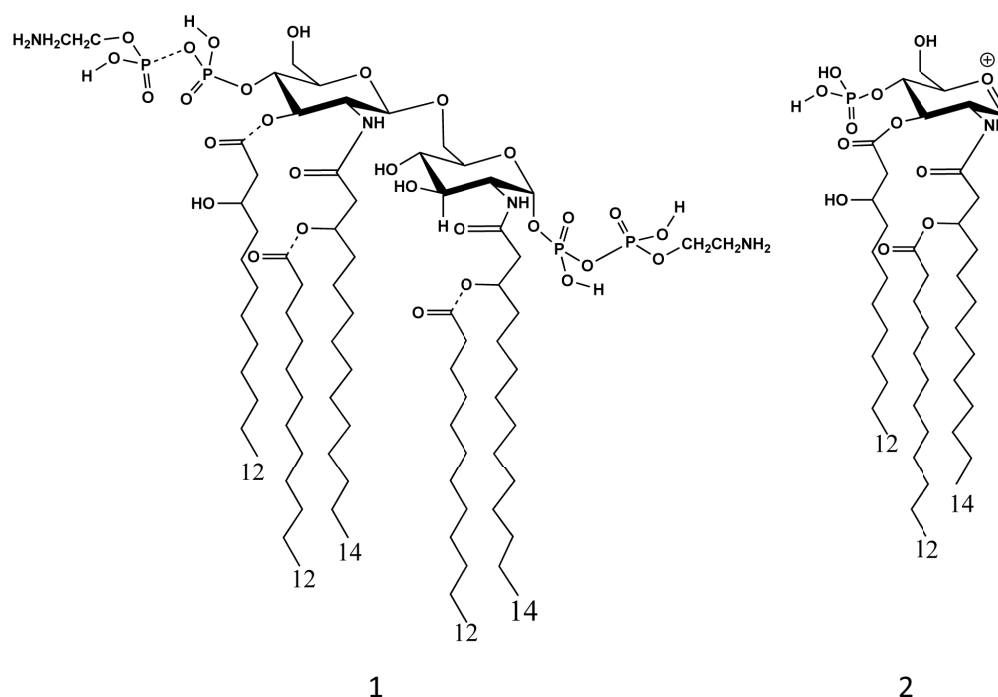


Figure 15: 1: Proposed penta-acyl Lipid A structure. 2: Oxonium ion

Sample	Pseudomolecular ion					
	A	A <sub>1</sub>	B	C	D	E
A <sub>3</sub>	1.25	1	2.5	0.5	0.5	0.37
A <sub>2</sub>	0.5	1	1.67	-	0.25	-
B <sub>3</sub>	-	1	2.32	--	-	0.77
C <sub>4</sub>	0.1	1	0.22	--	0,1	-
D <sub>3</sub>	-	1	1.18	--	0.09	0.21
E <sub>1</sub>	1.38	1	1.53	--	-	-

Table 8: Relative abundances of species identified in MALDI spectra for A<sub>3</sub>, A<sub>2</sub>, B<sub>3</sub>, C<sub>4</sub>, D<sub>3</sub>, E<sub>4</sub> samples

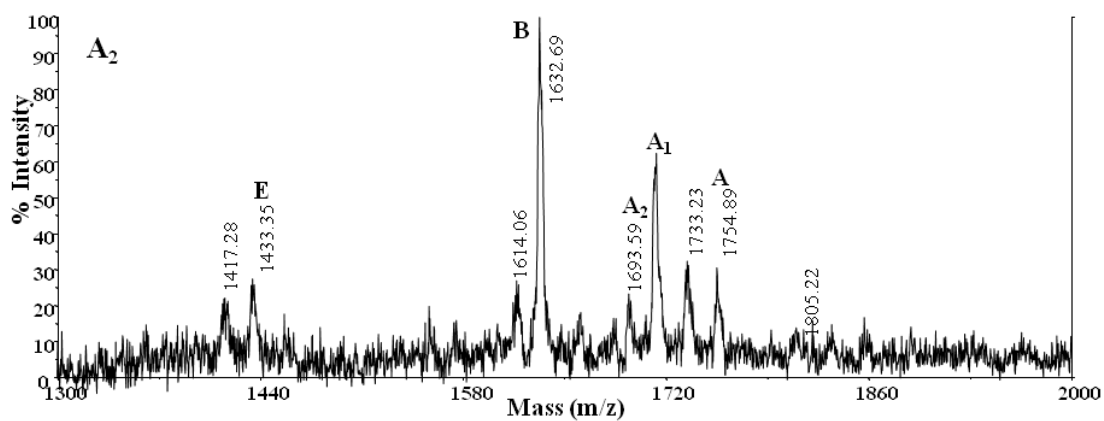


Figure 16: Ion negative MALDI spectrum of Lipid A from sample A<sub>2</sub>. (not calibrated)

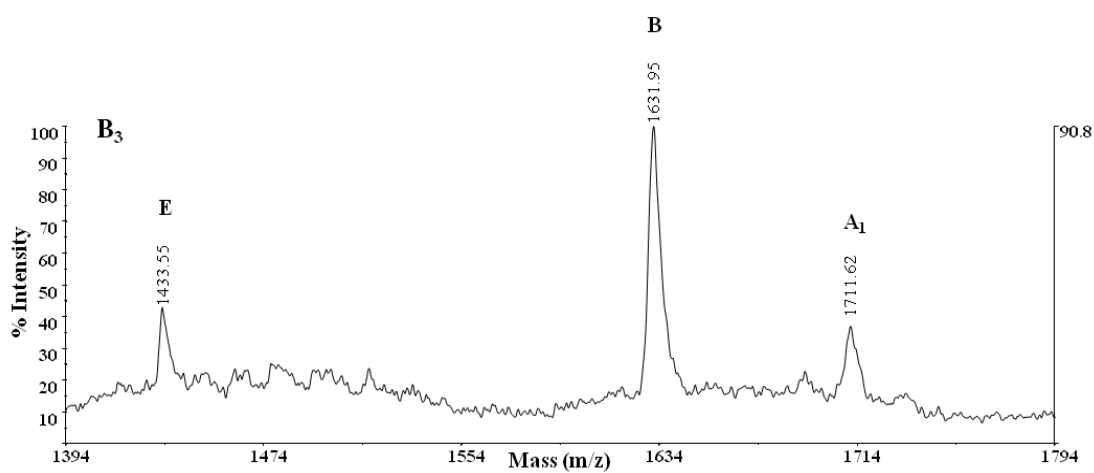


Figure 17: Expansion of ion negative MALDI spectrum of Lipid A from sample B<sub>3</sub>. (not calibrated)

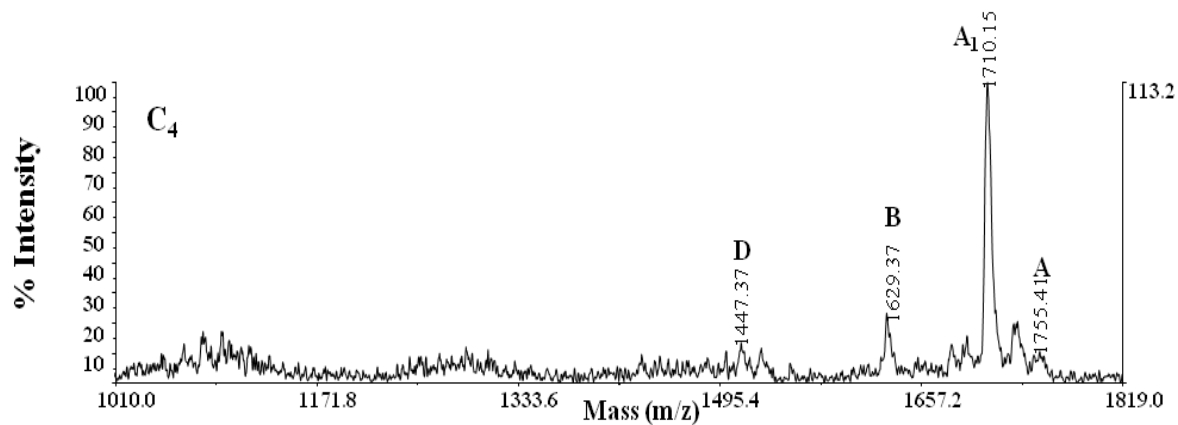


Figure 18: Ion negative MALDI spectrum of Lipid A from sample C<sub>4</sub>. (not calibrated)

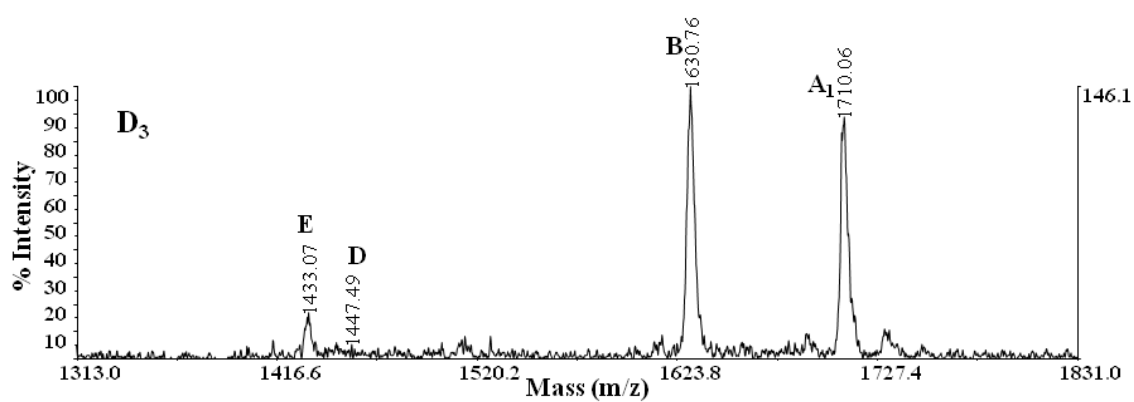


Figure 19: Ion negative MALDI spectrum of Lipid A from sample D<sub>3</sub>. (not calibrated)

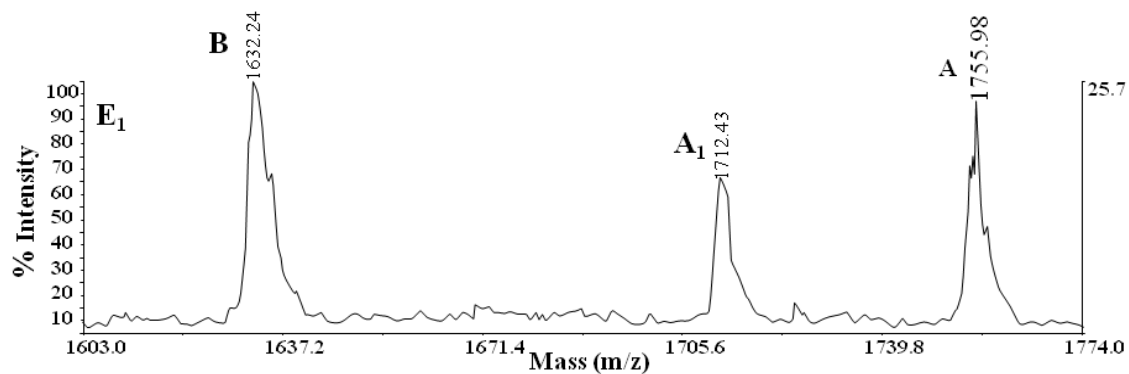


Figure 20: Expansion of ion negative MALDI spectrum of Lipid A from sample E<sub>1</sub>. (not calibrated)

PEA bi-substituted specie (**A**) was present in four of six analyzed samples, PEA mono-substituted species (**B** and **A<sub>1</sub>**) were always present whereas, tetra-acylated (**C**, **D**, **E**) resulted in unimportant amount if not visible at all.

Concluding, the strain analyzed produced predominantly a penta-acyl Lipid A with phosphate groups substituted with PEA units, as well. Structural variations regarded essentially the presence of PEA, phosphate, C12:0 or (C12:0) 3-OH that constituted the non stoichiometric substituents of Lipid A (Van Der Ley *et al.*, 2001).

Future studies could be focalized on the relationship between Lipid A and pyrogenicity caused by bacterium, being Lipid A the immunostimulatory unit of LPS endotoxin.

#### 2.1.5. Chemical and electrophoretic analyses to determine the content of LOS and CPS outside the OMVs

OMVs preparations were filtrated on vivaspin system and the permeates, after dialysis, were extracted with hot water/ phenol mixture. SDS-PAGE analysis of water extracts showed clearly low molecular weight band of LOS only for sample F (figure 21, lane F), whereas phenol extracts (non showed) presented proteins traces.

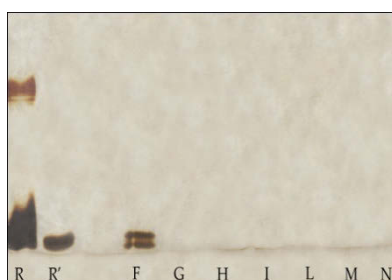


Figure 21: SDS-PAGE with silver stain. R: standard LPS *E.coli* O55:B5 (4 µg); R': LOS MenB (8 µg); samples: F, G, H, I, L, M, N (16 µg)

Further information about the content of CPS and LOS in water extracts were obtained by GC-MS analyses of acetylated *O*-methyl glycosides. Chromatograms showed peaks of 3-deoxy-D-manno-octulosonic acid (Kdo), diagnostic of LPS, and glucosamine (GlcN) only for samples F and G (figures 22, 23). Kdo abundance was very low, and the occurrence of LOS presence cannot be excluded, because in the other samples Kdo amount may be under the analyses revelation limit. This consideration can be applied to the SDS-PAGE as well, in fact in this case sample G was LOS-negative, while chemical analyses proved its presence. Differently from LOS, CPS was contained in all samples as proved by the presence of the diagnostic residue of Neuraminic acid (NeuA) in the chemical analyses (figures 22-27).

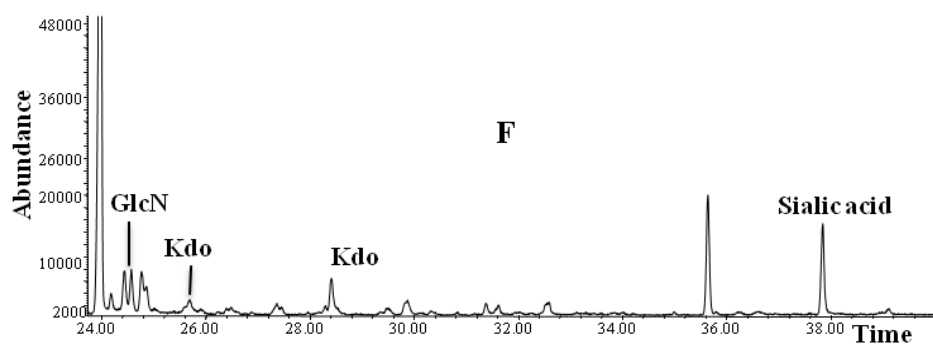


Figure 22: Expansion of GC-MS chromatogram of acetylated *O*-methyl glycosides of *F*

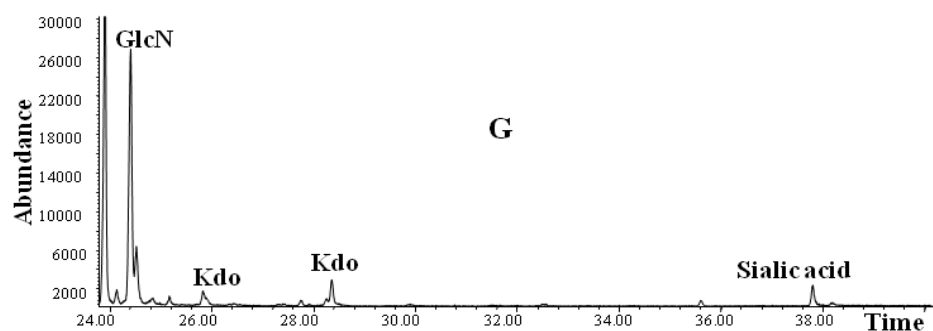


Figure 23: Expansion of GC-MS chromatogram of acetylated *O*-methyl glycosides of sample *G*

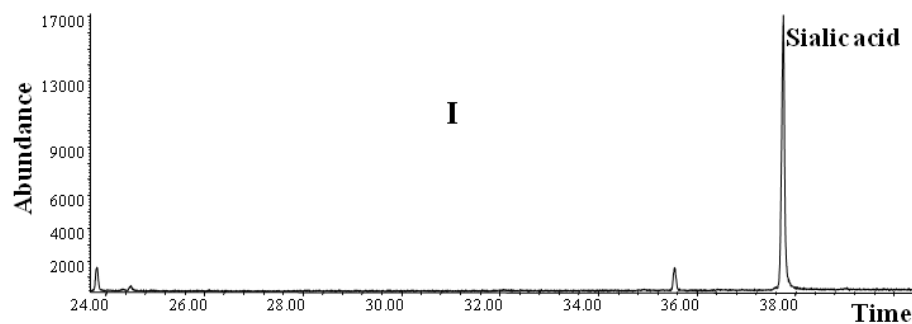


Figure 24: Expansion of GC-MS chromatogram of acetylated *O*-methyl glycoside of sample *I*

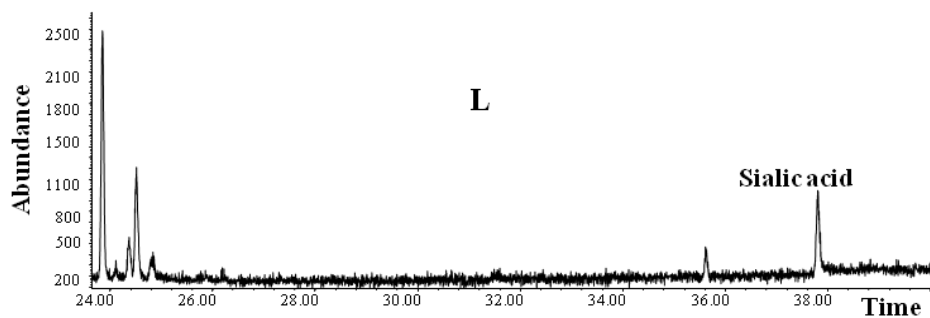


Figure 25: Expansion of GC-MS chromatogram of acetylated *O*-methyl glycosides of *L*

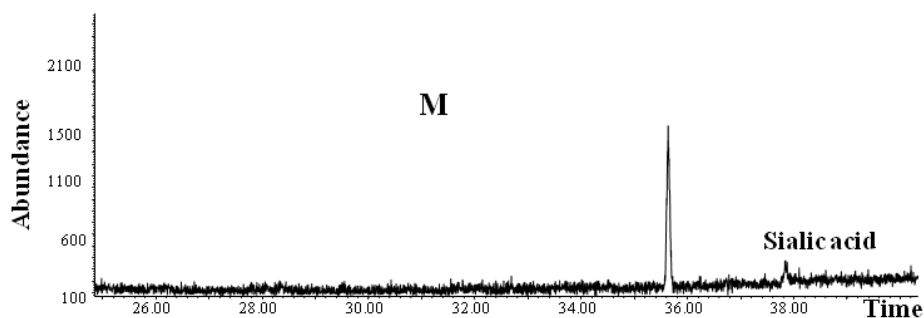


Figure 26: Expansion of GC-MS chromatogram of acetylated O-methyl glycosides of M

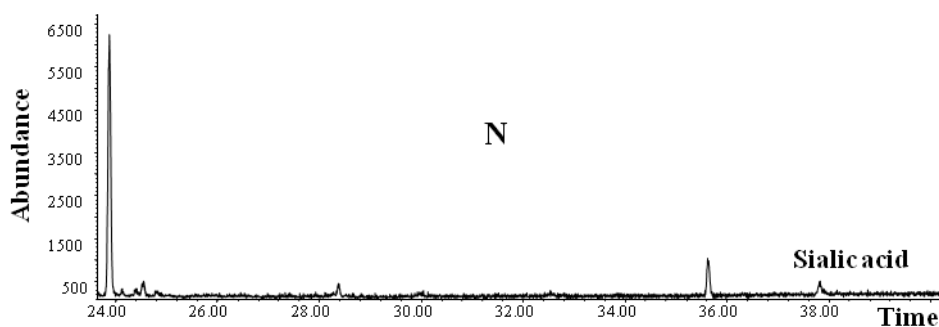


Figure 27: Expansion of GC-MS chromatogram of acetylated O-methyl glycosides of N

### 3- Materials and Methods

#### 3.1 Isolations of Lipopolysaccharide and Capsular Polysaccharide

##### 3.1.1 Outer Membrane vesicles of *Neisseria meningitidis* serogroup B

Outer Membrane Vesicles preparations were dialysed and freeze dried prior extraction procedure. Vesicles were disrupted according to the water/phenol method (Westphal and Jann, 1965): dried vesicles were treated with 1 ml of water and an equal volume of 90 % phenol, solution was incubated at 68 °C for 15 minutes. Phenol-water phases separation was performed by spinning at 4 °C.

Dialysis (cut-off 3500 Da) was used for phenol removal from the extractions phases which were finally freeze-dried.

Water phases were obtained in yield of 0,3 mg/mg<sub>vesicle</sub> and phenol phases in yield of 0,7 mg/mg<sub>vesicle</sub> (average values).

### 3.2 General and analytical methods

#### 3.2.1 SDS-PAGE and chemical analyses of LOS and CPS from OMVs

SDS-PAGE (Laemmli, 1970) of samples was performed on Mini Protean III Bio-Rad system run at 150 constant voltage. Discontinuous gels were realized (5 % stacking gel, 15 % separating gel) and stained according to the silver stain procedure for lipopolysaccharide (Kittelberger and Hilbink, 1993) or with coomassie procedure for proteins (Zehr *et al.*, 1989). In order to determine the content of LPS and CPS outside vesicles, OMVs solutions were filtrated on vivaspin system (cut-off 10000 Da) collecting a volume of permeate equal to the half of initial volume. Permeates were dialysed (cut-off 1000 Da), freeze dried and extracted according to water/phenol protocol (section 3.1.1). Water and phenol extracts, after freeze drying (0.9 mg in average values), were screened through SDS-PAGE as described above. Water extracts were treated according to the procedure to perform the GC-MS analysis of sugars as acetylated *O*-methyl glycosides: samples were dried over P<sub>2</sub>O<sub>5</sub> for 1 h under diminished pressure and treated with methanolic HCl at 80 °C for 16 h. Solvent was dried and the methyl glycosides were acetylated with dry pyridine (100 µl) and Ac<sub>2</sub>O (50 µl) at 80 °C for 20 min. The reactives were removed by evaporation and the mixture of peracetylated methyl glycosides was analyzed by GC-MS with the temperature program: 150 °C for 3 min, 150→280 °C at 3 °C/min, 300 °C for 5 min.

GC-MS branching point analysis of monosaccharides was performed derivatizing monosaccharides as partially methylated alditol acetates (PMAA) (Ciucanu and Kerek, 1984).

2 mg of water phase was solubilized in dry DMSO (1 ml) and the addition of powdered NaOH (100 mg) promoted lipooligosaccharide deprotonation (3 h, 25 °C). Solution was treated with 200 µl iodomethane (from 0°C to 25 °C, 16 h) and per-*O*-methylated lipooligosaccharide was extracted by adding water and chloroform to the reaction mixture. The organic layer was washed with 50 ml of water, dried under vacuum, dissolved in 4 M TFA. After 4 h at 120 °C, it was dried and acid traces were removed by isopropanol washing and drying. Partially methylated monosaccharides were converted in alditols by reduction with NaBD<sub>4</sub> in ethanol (1 h, 25 °C), followed by borates treatment with methanol and AcOH. Methylated alditols were finally acetylated (150 µl of Py, 150 µl of Ac<sub>2</sub>O, 80 °C, 30 min.) and salts removed with water-chloroform extraction. PMAA derivates dissolved in acetone were analyzed with following temperature program: 150 °C for 3 min, 150 → 204 °C at 1.5 °C/min, 204 → 300 °C at 10 °C/min. GC-MS was an Hewelett-Packard 5890 instrument, equipped with a SPB-5 capillary column (Supelco, 30 m x i.d. flow rate, 0.8 mL/min, He as a carrier gas). EI mass spectra were recorded with an ionization energy of 70 eV and an ionizing current of 0.2 mA.

### 3.3 Preparations and Mass Spectrometry of Lipid A

#### 3.3.1 MALDI MS spectrometry of intact Lipid A from *N. meningitidis* serogroup B

Free lipid A was obtained after treatment of the water extract (2 mg) with 1% acetic acid (100 °C, 3 h). After centrifugation (8,000 g, 20 min, 4 °C), the lipid A was collected as precipitate, washed twice with water, and lyophilized (80 µg, average value).

MALDI-TOF analyses were performed on Applied BioSystems (Framingham, MA) Voyager STR instrument equipped with delayed extraction technology. Dried Lipids A were dissolved in a mixture of CHCl<sub>3</sub>:CH<sub>3</sub>OH:H<sub>2</sub>O (2:3:1 by volume) and the matrix, 2,5-dihydroxybenzoic acid, was dissolved in TFA 0.1 M and CH<sub>3</sub>CN (30:70 by volume) at a concentration of 20 mg/ml. A sample matrix solution mixture (1:1 v/v, 1 µl) was deposited on a stainless steel gold-plate 100 sample MALDI probe tip and dried at 25 °C. Ions formed by a pulsed UV laser beam (nitrogen laser, λ= 337 nm) were accelerated through 25 KV. Mass spectra were recorded in negative and positive linear ion mode, using a delay time of 200 ms, grid voltage of 0.5% and 500 shots/spectrum and laser intensity of 2200.

### 3.4 NMR spectroscopy

#### 3.4.1 Capsular polysaccharide of *Neisseria meningitidis* serogroup B

All spectra were acquired on a Bruker 600 MHz equipped with a cryo probe at 298 K in D<sub>2</sub>O.

Capsular polysaccharide (2 mg in 600 µl D<sub>2</sub>O) spectra were calibrated with internal acetone (<sup>1</sup>H at 2.225 ppm, <sup>13</sup>C at 31.45 ppm). Homonuclear <sup>1</sup>H-<sup>1</sup>H-COSY and heteronuclear <sup>1</sup>H-<sup>13</sup>C-HSQC spectra were recorded with 512 FIDs of 2048 complex data points, respectively with 8 and 16 scans per FID. <sup>1</sup>H-<sup>13</sup>C-HMBC was recorded with 256 FIDs of 2048 data points and 80 scans per FID.

Spectra of water phases A<sub>2</sub> and A<sub>3</sub> were calibrated on *N*-acetyl sialic acid signal (2.08 ppm).

For <sup>1</sup>H-<sup>13</sup>C-HSQC 256 FIDs of 2048 complex data points were collected with 160 scans per FID. DOSY spectra were acquired at 298 K with the Bruker sequence stebppp1s using data sets of 32K x 64 points, 8 scans were acquired for each increment, and the two key parameters Δ and δ (250 and 4.8 ms, respectively) were optimised on the 1D sequence.

In all cases the spectral width was set to 10 ppm for homonuclear and 180 ppm for heteronuclear and the frequency carrier was placed at the residual HOD peak. Data were processed and analyzed with Bruker TopSpin 2.1 program.

## References

- Akira, S., Uematsu, S., and Takeuchi, O. **2006**. Pathogen recognition and innate immunity. *Cell*. 124 (4):783-801.
- Alexander, C., and Rietschel, E.T. **2001**. Bacterial Lipopolysaccharides and innate immunity. *J. Endotoxin. Res.* 7 (3):167-202.
- Astronomo, R.D., Kaltgrad, E., Udit, A.K., Wang, S.K., Doores, K.J., Huang, C.Y., Pantophlet, R., Paulson, J.C., Wong, C.H., Finn, M.G., and Burton, D.R. **2010**. Defining criteria for oligomannose immunogens for HIV using icosahedral virus capsid scaffolds. *Chem. Biol.* 17 (4):357-370.
- Barua, S., Yamashino, T., Hasegawa, T., Yokoyama, K., Torii, K., and Ohta, M. **2002**. Involvement of surface polysaccharides in the organic acid resistance of Shiga Toxin-producing *Escherichia coli* O157:H7. *Mol. Microbiol.* 43 (3):629-640.
- Bergogne-Berezin, E., and Towner, K.J. **1996**. Acinetobacter spp. as nosocomial pathogens: microbiological, clinical, and epidemiological features. *Clin. Microbiol. Rev.* 9 (2):148-165.
- Berron, S., De La Fuente, L., Martin, E., and Vazquez, J.A. **1998**. Increasing incidence of meningococcal disease in Spain associated with a new variant of serogroup C. *Eur. J. Clin. Microbiol. Infect. Dis.* 17 (2):85-89.
- Bhattacharjee, A.K., Jennings, H.J., Kenny, C.P., Martin, A., and Smith, I.C. **1975**. Structural determination of the sialic acid polysaccharide antigens of *Neisseria meningitidis* serogroups B and C with carbon 13 nuclear magnetic resonance. *J. Biol. Chem.* 250 (5):1926-1932.
- Birnbaum, G., Roy, R., Brisson, J., and Jennings, H. **1987**. Conformations of ammonium 3-deoxy-d-manno-2-octulosonate (KDO) and methyl  $\alpha$ - and  $\beta$ -ketopyranosides of KDO: X-ray structure and 1 H NMR analyses. *J. Carbohydr. Chem.* 6 (1):17-39.
- Bock, K., and Pedersen, C. **1983**. Carbon-13 nuclear magnetic resonance spectroscopy of monosaccharides. *Adv. Carbohydr. Chem. Biochem.* 41:27-66.
- Bohin, J.P. **2000**. Osmoregulated periplasmic glucans in *Proteobacteria*. *FEMS Microbiol. Lett.* 186 (1):11-19.
- Brandt, B.L., Smith, C.D., and Artenstein, M.S. **1978**. Immunogenicity of serogroup A and C *Neisseria meningitidis* polysaccharide vaccines administered together in humans. *J. Infect. Dis.* 137 (2):202-205.
- Bruge, J., Bouveret-Le Cam, N., Danve, B., Rougon, G., and Schulz, D. **2004**. Clinical evaluation of a group B meningococcal N-propionylated polysaccharide conjugate vaccine in adult, male volunteers. *Vaccine*. 22 (9-10):1087-1096.
- Burton, D.R., Pyati, J., Koduri, R., Sharp, S.J., Thornton, G.B., Parren, P.W., Sawyer, L.S., Hendry, R.M., Dunlop, N., Nara, P.L., and Et Al. **1994**. Efficient neutralization of primary isolates of HIV-1 by a recombinant human monoclonal antibody. *Science*. 266 (5187):1024-1027.
- Byrd, J., Zeph, L., and Casida Jr, L. **1985**. Bacterial control of *Agromyces ramosus* in soil. *Can. J. Microbiol.* 31 (12):1157-1163.

- Calarese, D.A., Lee, H.K., Huang, C.Y., Best, M.D., Astronomo, R.D., Stanfield, R.L., Katinger, H., Burton, D.R., Wong, C.H., and Wilson, I.A. **2005**. Dissection of the carbohydrate specificity of the broadly neutralizing anti-HIV-1 antibody 2G12. *Proc. Natl. Acad. Sci. U S A* 102 (38):13372-13377.
- Calarese, D.A., Scanlan, C.N., Zwick, M.B., Deechongkit, S., Mimura, Y., Kunert, R., Zhu, P., Wormald, M.R., Stanfield, R.L., Roux, K.H., Kelly, J.W., Rudd, P.M., Dwek, R.A., Katinger, H., Burton, D.R., and Wilson, I.A. **2003**. Antibody domain exchange is an immunological solution to carbohydrate cluster recognition. *Science*. 300(5628):2065-2071.
- Casida, L.E. **1988**. Response in Soil of *Cupriavidus necator* and Other Copper-Resistant Bacterial Predators of Bacteria to Addition of Water, Soluble Nutrients, Various Bacterial Species, or *Bacillus thuringiensis* Spores and Crystals. *Appl. Environ. Microbiol.* 54 (9):2161-2166.
- Ciucanu, I., and Kerek, F. **1984**. A simple and rapid method for the permethylation of carbohydrates. *Carbohydr. Res.* 131 (2):209-217.
- Corsaro, M.M., Gambacorta, A., Iadonisi, A., Lanzetta, R., Naldi, T., Nicolaus, B., Romano, I., Ummarino, S., and Parrilli, M. **2006**. Structural Determination of the O-Chain Polysaccharide from the Lipopolysaccharide of the *Haloalkaliphilic Halomonas pantelleriensis* Bacterium. *Eur. J. Org. Chem.* 2006 (7):1801-1808.
- Corti, D., Langedijk, J.P., Hinz, A., Seaman, M.S., Vanzetta, F., Fernandez-Rodriguez, B.M., Silacci, C., Pinna, D., Jarrossay, D., Balla-Jhagjhoorsingh, S., Willems, B., Zekveld, M.J., Dreja, H., O'sullivan, E., Pade, C., Orkin, C., Jeffs, S.A., Montefiori, D.C., Davis, D., Weissenhorn, W., Mcknight, A., Heeney, J.L., Sallusto, F., Sattentau, Q.J., Weiss, R.A., and Lanzavecchia, A. **2010**. Analysis of memory B cell responses and isolation of novel monoclonal antibodies with neutralizing breadth from HIV-1-infected individuals. *PLoS One* 5 (1):e8805.
- De Castro, C., Fregolino, E., Gargiulo, V., Lanzetta, R., and Parrilli, M. **2008**. A novel capsular polysaccharide from *Rhizobium rubi* strain DSM 30149. *Carbohydr. Res.* 343 (9):1482-1485.
- De Castro, C., Molinaro, A., Lanzetta, R., Silipo, A., and Parrilli, M. **2008**. Lipopolysaccharide structures from *Agrobacterium* and *Rhizobiaceae* species. *Carbohydr. Res.* 343 (12):1924-1933.
- Defaye, J., and Wong, E. **1986**. Structural studies of gum arabic, the exudate polysaccharide from *Acacia senegal*. *Carbohydr. Res.* 150 (1):221-231.
- Dell, A., Oates, J., Lugowski, C., Romanowska, E., Kenne, L., and Lindberg, B. **1984**. The *Enterobacterial common antigen*, a cyclic polysaccharide. *Carbohydr. Res.* 133 (1):95-104.
- Ding, L., Seto, B.L., Ahmed, S.A., and Coleman, W.G., Jr. **1994**. Purification and properties of the *Escherichia coli* K-12 NAD-dependent nucleotide diphosphosugar epimerase, ADP-L-glycero-D-mannoheptose 6-epimerase. *J. Biol. Chem.* 269 (39):24384-24390.
- Dubois, M., Gilles, K., Hamilton, J., Rebers, P., and Smith, F. **1956**. Colorimetric method for determination of sugars and related substances. *Anal. Chem.* 28 (3):350-356.
- Endimiani, A., Luzzaro, F., Migliavacca, R., Mantengoli, E., Hujer, A.M., Hujer, K.M., Pagani, L., Bonomo, R.A., Rossolini, G.M., and Toniolo, A. **2007**. Spread in an Italian hospital of a clonal *Acinetobacter baumannii* strain producing the TEM-92 extended-spectrum beta-lactamase. *Antimicrob. Agents Chemother.* 51 (6):2211-2214.
- Erbel, P.J., Barr, K., Gao, N., Gerwig, G.J., Rick, P.D., and Gardner, K.H. **2003**. Identification and biosynthesis of cyclic *Enterobacterial common antigen* in *Escherichia coli*. *J. Bacteriol.* 185 (6):1995-2004.

- Fedonenko, Y.P., Konnova, O.N., Zdorovenko, E.L., Konnova, S.A., Zatonsky, G.V., Shashkov, A.S., Ignatov, V.V., and Knirel, Y.A. **2008**. Structural analysis of the *O*-polysaccharide from the Lipopolysaccharide of *Azospirillum brasilense* S17. *Carbohydr. Res.* 343 (4):810-816.
- Fischer, M., Carlone, G.M., Holst, J., Williams, D., Stephens, D.S., and Perkins, B.A. **1999**. *Neisseria meningitidis* serogroup B outer membrane vesicle vaccine in adults with occupational risk for meningococcal disease. *Vaccine.* 17 (19):2377-2383.
- Fournier, P.E., Vallenet, D., Barbe, V., Audic, S., Ogata, H., Poirel, L., Richet, H., Robert, C., Mangenot, S., Abergel, C., Nordmann, P., Weissenbach, J., Raoult, D., and Claverie, J.M. **2006**. Comparative genomics of multidrug resistance in *Acinetobacter baumannii*. *PLoS Genet.* 2 (1):62-72.
- Fregolino, E., Fugazza, G., Galano, E., Gargiulo, V., Landini, P., Lanzetta, R., Lindner, B., Pagani, L., Parrilli, M., and Holst, O. **2010**. Complete Lipooligosaccharide Structure of the Clinical Isolate *Acinetobacter baumannii*, Strain SMAL. *Eur. J. Org. Chem.* 2010 (7):1345-1352.
- Galanos, C., Luderitz, O., and Westphal, O. **1969**. A new method for the extraction of R Lipopolysaccharides. *Eur. J. Biochem.* 9 (2):245-249.
- Gamian, A., Romanowska, E., Romanowska, A., Lugowski, C., Dabrowski, J., and Trauner, K. **1985**. *Citrobacter* Lipopolysaccharides: structure elucidation of the *O*-specific polysaccharide from strain PCM 1487 by mass spectrometry, one-dimensional and two-dimensional <sup>1</sup>H-NMR spectroscopy and methylation analysis. *Eur. J. Biochem.* 146 (3):641-647.
- Gargiulo, V., De Castro, C., Lanzetta, R., Jiang, Y., Xu, L.H., Jiang, C.L., Molinaro, A., and Parrilli, M. **2008**. Structural elucidation of the capsular polysaccharide isolated from *Kaistella flava*. *Carbohydr. Res.* 343 (14):2401-2405.
- Gargiulo, V., Garozzo, D., Lanzetta, R., Molinaro, A., Sturiale, L., De Castro, C., and Parrilli, M. **2008**. *Rhizobium rubi*(T): a gram-negative phytopathogenic bacterium expressing the Lewis B epitope on the outer core of its lipooligosaccharide fraction. *Chembiochem.* 9 (11):1830-1835.
- Germida, J.J., and Casida, L.E. **1983**. *Ensifer adhaerens* Predatory Activity Against Other Bacteria in Soil, as Monitored by Indirect Phage Analysis. *Appl. Environ. Microbiol.* 45 (4):1380-1388.
- Gerwig, G.J., Kamerling, J.P., and Vliegenthart, J.F.G. **1978**. Determination of the and configuration of neutral monosaccharides by high-resolution capillary g.l.c. *Carbohydr. Res.* 62 (2):349-357.
- Goel, V.K., and Kapil, A. **2001**. Monoclonal antibodies against the iron regulated outer membrane Proteins of *Acinetobacter baumannii* are bactericidal. *BMC Microbiol.* 1:16.
- Griffin, P.M., and Tauxe, R.V. **1991**. The epidemiology of infections caused by *Escherichia coli* O157:H7, other enterohemorrhagic *E. coli*, and the associated hemolytic uremic syndrome. *Epidemiol. Rev.* 13:60-98.
- Habeeb, A.F. **1966**. Determination of free amino groups in proteins by trinitrobenzenesulfonic acid. *Anal. Biochem.* 14 (3):328-336.
- Hanuszkiewicz, A., Kaczyński, Z., Lindner, B., Goldmann, T., Vollmer, E., Debarry, J., Heine, H., and Holst, O. **2008**. Structural Analysis of the Capsular Polysaccharide from *Acinetobacter lwoffii* F78. *Eur. J. Org. Chem.* 2008 (36):6183-6188.

- Haseley, S.R., Holst, O., and Brade, H. **1998**. Structural studies of the *O*-antigen isolated from the phenol-soluble lipopolysaccharide of *Acinetobacter baumannii* (DNA group 2) strain 9. *Eur. J. Biochem.* 251 (1-2):189-194.
- Higgins, P.G., Wisplinghoff, H., Krut, O., and Seifert, H. **2007**. A PCR-based method to differentiate between *Acinetobacter baumannii* and *Acinetobacter* genomic species 13TU. *Clin. Microbiol. Infect.* 13 (12):1199-1201.
- Holst, O., Bock, K., Brade, L., and Brade, H. **1995**. The structures of oligosaccharide bisphosphates isolated from the lipopolysaccharide of a recombinant *Escherichia coli* strain expressing the gene *gseA* [3-deoxy-D-manno-octulopyranosonic acid (Kdo) transferase] of *Chlamydia psittaci* 6BC. *Eur. J. Biochem.* 229 (1):194-200.
- Holst, O., Brade, H., Opal, S., Vogel, S., and Morrison, D. **1999**. Chemical structure of the core region of Lipopolysaccharides. In *Endotoxin in Health and Disease*: Marcel Dekker Inc., NY.
- Holst, O., Brade, L., Kosma, P., and Brade, H. **1991**. Structure, serological specificity, and synthesis of artificial glycoconjugates representing the genus-specific lipopolysaccharide epitope of *Chlamydia* spp. *J. Bacteriol.* 173 (6):1862-1866.
- Jann, B., and Jann, K. **1990**. Structure and biosynthesis of the capsular antigens of *Escherichia coli*. *Curr. Top. Microbiol. Immunol.* 150:19-42.
- John, C.M., Liu, M., and Jarvis, G.A. **2009**. Natural phosphoryl and acyl variants of Lipid A from *Neisseria meningitidis* strain 89I differentially induce tumor necrosis factor-alpha in human monocytes. *J. Biol. Chem.* 284 (32):21515-21525.
- Joly-Guillou, M.L. **2005**. Clinical impact and pathogenicity of *Acinetobacter*. *Clin. Microbiol. Infect.* 11 (11):868-873.
- Kajimura, J., Rahman, A., and Rick, P.D. **2005**. Assembly of cyclic *Enterobacterial common antigen* in *Escherichia coli* K-12. *J. Bacteriol.* 187 (20):6917-6927.
- Kaplan, N., Rosenberg, E., Jann, B., and Jann, K. **1985**. Structural studies of the capsular polysaccharide of *Acinetobacter calcoaceticus* BD4. *Eur. J. Biochem.* 152 (2):453-458.
- Katzenellenbogen, E., Kocharova, N.A., Zatonksy, G.V., Witkowska, D., Bogulska, M., Shashkov, A.S., Gamian, A., and Knirel, Y.A. **2003**. Structural and serological studies on a new 4-deoxy-d-arabino-hexose-containing *O*-specific polysaccharide from the Lipopolysaccharide of *Citrobacter braakii* PCM 1531 (serogroup O6). *Eur. J. Biochem.* 270 (13):2732-2738.
- Kawahara, K., Brade, H., Rietschel, E.T., and Zahringer, U. **1987**. Studies on the chemical structure of the Core-Lipid A region of the Lipopolysaccharide of *Acinetobacter calcoaceticus* NCTC 10305. Detection of a new 2-octulosonic acid interlinking the core oligosaccharide and lipid A component. *Eur. J. Biochem.* 163 (3):489-495.
- Kittelberger, R., and Hilbink, F. **1993**. Sensitive silver-staining detection of bacterial Lipopolysaccharides in polyacrylamide gels. *J. Biochem. Biophys. Meth.* 26 (1):81-86.
- Kjaer, M., Andersen, K.V., and Poulsen, F.M. **1994**. Automated and semiautomated analysis of homo- and heteronuclear multidimensional nuclear magnetic resonance spectra of proteins: the program Pronto. *Method Enzymol.* 239:288-307.
- Kondakova, A., and Lindner, B. **2005**. Structural characterization of complex bacterial glycolipids by Fourier transform mass spectrometry. *Eur. J. Mass. Spectrom.* 11 (5):535-546.

- Kuhn, H.M., Brade, L., Appelmeik, B.J., Kusumoto, S., Rietschel, E.T., and Brade, H. **1992**. Characterization of the epitope specificity of murine monoclonal antibodies directed against lipid A. *Infect. Immun.* 60 (6):2201-2210.
- Kuhn, H.M., Meier-Dieter, U., and Mayer, H. **1988**. ECA, the *Enterobacterial common antigen*. *FEMS Microbiol. Rev.* 4 (3):195-222.
- Kulshin, V.A., Zahringer, U., Lindner, B., Frasc, C.E., Tsai, C.M., Dmitriev, B.A., and Rietschel, E.T. **1992**. Structural characterization of the Lipid A component of pathogenic *Neisseria meningitidis*. *J. Bacteriol.* 174 (6):1793-1800.
- Kwong, P.D., Wyatt, R., Robinson, J., Sweet, R.W., Sodroski, J., and Hendrickson, W.A. **1998**. Structure of an HIV gp120 envelope glycoprotein in complex with the CD4 receptor and a neutralizing human antibody. *Nature.* 393 (6686):648-659.
- Laemmli, U.K. **1970**. Cleavage of structural proteins during the assembly of the head of bacteriophage T4. *Nature.* 227 (5259):680-685.
- Leone, S., Sturiale, L., Pessione, E., Mazzoli, R., Giunta, C., Lanzetta, R., Garozzo, D., Molinaro, A., and Parrilli, M. **2007**. Detailed characterization of the Lipid A fraction from the nonpathogen *Acinetobacter radioresistens* strain S13. *J. Lipid Res.* 48 (5):1045-1051.
- Leontein, K., Lindberg, B., and Lonngren, J. **1978**. Assignment of absolute configuration of sugars by g.l.c. of their acetylated glycosides formed from chiral alcohols. *Carbohydr. Res.* 62 (2):359-362.
- Lior, H. **1994**. Classification of *Escherichia coli*. In Gyles, C. **1994**. *Escherichia coli* in domestic animals and humans.:31-72.
- Lukáčová, M., Barák, I., and Kazár, J. **2008**. Role of structural variations of polysaccharide antigens in the pathogenicity of Gram negative bacteria. *Clin. Microbiol. Infect.* 14 (3):200-206.
- Maclean, L.L., Perry, M.B., Chen, W., and Vinogradov, E. **2009**. The structure of the polysaccharide O-Chain of the LPS from *Acinetobacter baumannii* strain ATCC 17961. *Carbohydr. Res.* 344 (4):474-478.
- Männel, D., and Mayer, H. **1978**. Isolation and chemical characterization of the *Enterobacterial common antigen*. *Eur. J. Biochem.* 86 (2):361-370.
- Martin, D.R., Walker, S.J., Baker, M.G., and Lennon, D.R. **1998**. New Zealand epidemic of meningococcal disease identified by a strain with phenotype B:4:P1.4. *J. Infect. Dis.* 177 (2):497-500.
- Mata-Haro, V., Cekic, C., Martin, M., Chilton, P.M., Casella, C.R., and Mitchell, T.C. **2007**. The vaccine adjuvant monophosphoryl lipid A as a TRIF-biased agonist of TLR4. *Science.* 316 (5831):1628-1632.
- Mayer, L.W., Reeves, M.W., Al-Hamdan, N., Sacchi, C.T., Taha, M.K., Ajello, G.W., Schmink, S.E., Noble, C.A., Tondella, M.L., Whitney, A.M., Al-Mazrou, Y., Al-Jefri, M., Mishkhis, A., Sabban, S., Caugant, D.A., Lingappa, J., Rosenstein, N.E., and Popovic, T. **2002**. Outbreak of W135 meningococcal disease in 2000: not emergence of a new W135 strain but clonal expansion within the electrophoretic type-37 complex. *J. Infect. Dis.* 185 (11):1596-1605.
- Melton-Celsa, A., and O'Brien, A. **1998**. Structure, biology, and relative toxicity of Shiga toxin family members for cells and animals. *Escherichia coli* 0157: H7 and other Shiga toxin-producing *E. coli* strains, *Am. Soc. Microbiol.*:121-128.

- Miller, S.I., Ernst, R.K., and Bader, M.W. **2005**. LPS, TLR4 and infectious disease diversity. *Nat. Rev. Microbiol.* 3 (1):36-46.
- Min, H., and Cowman, M.K. **1986**. Combined Alcian blue and Silver staining of Glycosaminoglycans in polyacrylamide gels: application to electrophoretic analysis of molecular weight distribution. *Anal. Biochem.* 155 (2):275-285.
- Miyake, K. **2004**. Innate recognition of Lipopolysaccharide by Toll-like receptor 4-MD-2. *Trends Microbiol.* 12 (4):186-192.
- Nataro, J., and Kaper, J. **1998**. Diarrheagenic *Escherichia coli*. *Clin. Microbiol. Rev.* 11 (1):142.
- Neuhaus, F.C., and Baddiley, J. **2003**. A continuum of anionic charge: structures and functions of D-alanyl-Teichoic acids in Gram-positive bacteria. *Microbiol. Mol. Biol. Rev.* 67 (4):686-723.
- Pantophlet, R. **2008**. Lipopolysaccharides of *Acinetobacter* in *Acinetobacter* molecular biology. Caister Academic Press, Norfolk, UK, 2008, ch.3, pp. 61-98.
- Pantophlet, R., and Burton, D.R. **2006**. gp120: target for neutralizing HIV-1 antibodies. *Annu. Rev. Immunol.* 24:739-769.
- Peeters, C.C., Lagerman, P.R., De Weers, O., Oomen, L.A., Hoogerhout, P., Beurret, M., Poolman, J.T., and Reddin, K.M. **2003**. Preparation of polysaccharide-conjugate vaccines. *Methods Mol. Med.* 87:153-174.
- Peleg, A.Y., Seifert, H., and Paterson, D.L. **2008**. *Acinetobacter baumannii*: emergence of a successful pathogen. *Clin. Microbiol. Rev.* 21 (3):538-582.
- Perpelov, A., Senchenkova, S., Shashkov, A., Komandrova, N., Tomshich, S., Shevchenko, L., Knirel, Y., and Kochetkov, N. **2000**. First application of triflic acid for selective cleavage of glycosidic linkages in structural studies of a bacterial polysaccharide from *Pseudoalteromonas sp.* KMM 634. *J. Chem. Soc., Perkin Trans. 1* 2000 (3):363-366.
- Pon, R.A., and Jennings, H.J. 2008. *Carbohydrate-Based Antibacterial Vaccines, Carbohydrate-Based Vaccines and Immunotherapies*: John Wiley & Sons, Inc.
- Raetz, C.R., and Whitfield, C. **2002**. Lipopolysaccharide endotoxins. *Annu. Rev. Biochem.* 71:635-700.
- Ramos-Morales, F., Prieto, A., Beuzon, C., Holden, D., and Casadesus, J. **2003**. Role for *Salmonella enterica* Enterobacterial common antigen in bile resistance and virulence. *J. Bacteriol.* 185 (17):5328.
- Ramsay, M., Kaczmarski, E., Rush, M., Mallard, R., Farrington, P., and White, J. **1997**. Changing patterns of case ascertainment and trends in meningococcal disease in England and Wales. *Commun. Dis. Rep. CDR Rev.* 7 (4):R49-54.
- Rappuoli, R., and Covacci, A. **2003**. Reverse vaccinology and genomics. *Science.* 302 (5645):602.
- Rick, P.D., Hubbard, G.L., Kitaoka, M., Nagaki, H., Kinoshita, T., Dowd, S., Simplaceanu, V., and Ho, C. **1998**. Characterization of the lipid-carrier involved in the synthesis of enterobacterial common antigen (ECA) and identification of a novel phosphoglyceride in a mutant of *Salmonella typhimurium* defective in ECA synthesis. *Glycobiology.* 8 (6):557-567.
- Rietschel, E.T. **1976**. Absolute configuration of 3-hydroxy fatty acids present in lipopolysaccharides from various bacterial groups. *Eur. J. Biochem.* 64 (2):423-428.

- Rinno, J., Golecki, J., and Mayer, H. **1980**. Localization of *Enterobacterial common antigen*: immunogenic and nonimmunogenic *Enterobacterial common antigen*-containing *Escherichia coli*. *J. Bacteriol.* 141 (2):814.
- Roberts, I.S. **1996**. The biochemistry and genetics of capsular polysaccharide production in bacteria. *Annu. Rev. Microbiol.* 50:285-315.
- Romanowska, E., Romanowska, A., Dabrowski, J., and Hauck, M. **1987**. Structure determination of the O-specific polysaccharides from *Citrobacter* O4- and O27-Lipopolysaccharides by methylation analysis and one- and two-dimensional <sup>1</sup>H-NMR spectroscopy. *FEBS Lett.* 211 (2):175-178.
- Romanowska, E., Romanowska, A., Lugowski, C., and Katzenellenbogen, E. **1981**. Structural and serological analysis of *Citrobacter*-036-specific polysaccharide, the homopolymer of  $\beta$ -(1 $\rightarrow$ 2)-linked 4-deoxy-D-arabinohexopyranosyl units. *Eur. J. Biochem.* 121 (1):119-123.
- Seydel, U., Oikawa, M., Fukase, K., Kusumoto, S., and Brandenburg, K. **2000**. Intrinsic conformation of Lipid A is responsible for agonistic and antagonistic activity. *Eur. J. Biochem.* 267 (10):3032-3039.
- Silipo, A., De Castro, C., Lanzetta, R., Molinaro, A., and Parrilli, M. **2004**. Full structural characterization of the Lipid A components from the *Agrobacterium tumefaciens* strain C58 Lipopolysaccharide fraction. *Glycobiology.* 14 (9):805-815.
- Silipo, A., Lanzetta, R., Amoresano, A., Parrilli, M., and Molinaro, A. **2002**. Ammonium hydroxide hydrolysis: a valuable support in the MALDI-TOF mass spectrometry analysis of Lipid A fatty acid distribution. *J. Lipid Res.* 43 (12):2188-2195.
- Silipo, A., Molinaro, A., Comegna, D., Sturiale, L., Cescutti, P., Garozzo, D., Lanzetta, R., and Parrilli, M. **2006**. Full Structural Characterisation of the Lipooligosaccharide of a *Burkholderia pyrrocinia* Clinical Isolate. *Eur. J. Org. Chem.* 2006 (21):4874-4883.
- Sillman, C., and Casida Jr, L. **1986**. Isolation of non obligate bacterial predators of bacteria from soil. *Can. J. Microbiol.* 32 (9):760-762.
- Silvestri, L.J., Hurst, R.E., Simpson, L., and Settine, J.M. **1982**. Analysis of Sulfate in complex carbohydrates. *Anal. Biochem.* 123 (2):303-309.
- Somogyi, M. **1952**. Estimation of sugars by colorimetric method. *J. Biol. Chem.* 200:245.
- Staaf, M., Hoog, C., Stevansson, B., Maliniak, A., and Widmalm, G. **2001**. Conformational investigation of a cyclic *Enterobacterial common antigen* employing NMR spectroscopy and molecular dynamics simulations. *Biochemistry.* 40 (12):3623-3628.
- Takeda, K., and Akira, S. **2005**. Toll-like receptors in innate immunity. *Int. Immunol.* 17 (1):1-14.
- Tozzi, A., Caprioli, A., Minelli, F., Gianviti, A., De Petris, L., Edefonti, A., Montini, G., Ferretti, A., De Palo, T., and Gaido, M. **2003**. Shiga toxin-producing *Escherichia coli* infections associated with hemolytic uremic syndrome, Italy, 1988–2000. *Emerg. Infect. Dis.* 9 (1):106.
- Turton, J.F., Woodford, N., Glover, J., Yarde, S., Kaufmann, M.E., and Pitt, T.L. **2006**. Identification of *Acinetobacter baumannii* by detection of the blaOXA-51-like carbapenemase gene intrinsic to this species. *J. Clin. Microbiol.* 44 (8):2974-2976.
- Urwin, R., Russell, J.E., Thompson, E.A., Holmes, E.C., Feavers, I.M., and Maiden, M.C. **2004**. Distribution of surface protein variants among hyperinvasive meningococci: implications for vaccine design. *Infect. Immun.* 72 (10):5955-5962.

- Van Der Ley, P., Steeghs, L., Hamstra, H., Ten Hove, J., Zomer, B., and Van Alphen, L. **2001**. Modification of Lipid A biosynthesis in *Neisseria meningitidis* lpxL mutants: influence on Lipopolysaccharide structure, toxicity, and adjuvant activity. *Infect. Immune*. 69 (10):5981.
- Van Looveren, M., and Goossens, H. **2004**. Antimicrobial resistance of *Acinetobacter* spp. in Europe. *Clin. Microbiol. Infect.* 10 (8):684-704.
- Vinogradov, E.V., Brade, L., Brade, H., and Holst, O. **2003**. Structural and serological characterisation of the O-antigenic polysaccharide of the Lipopolysaccharide from *Acinetobacter baumannii* strain 24. *Carbohydr. Res.* 338 (23):2751-2756.
- Vinogradov, E.V., Duus, J.O., Brade, H., and Holst, O. **2002**. The structure of the carbohydrate backbone of the Lipopolysaccharide from *Acinetobacter baumannii* strain ATCC 19606. *Eur. J. Biochem.* 269 (2):422-430.
- Vinogradov, E.V., Knirel, Y.A., Thomas-Oates, J.E., Shashkov, A.S., and L'vov V, L. **1994**. The structure of the cyclic *Enterobacterial common antigen* (ECA) from *Yersinia pestis*. *Carbohydr. Res.* 258:223-232.
- Vinogradov, E.V., Pantophlet, R., Brade, H., and Holst, O. **2001**. Structural and serological characterisation of the O-antigenic polysaccharide of the Lipopolysaccharide from *Acinetobacter* strain 96 (DNA group 11). *J. Endotoxin Res.* 7 (2):113-118.
- Vinogradov, E.V., Petersen, B.O., Thomas-Oates, J.E., Duus, J., Brade, H., and Holst, O. **1998**. Characterization of a novel branched tetrasaccharide of 3-deoxy-D-manno-oct-2-ulopyranosonic acid. The structure of the carbohydrate backbone of the Lipopolysaccharide from *Acinetobacter baumannii* strain nctc 10303 (atcc 17904). *J. Biol. Chem.* 273 (43):28122-28131.
- Vodopija, I., Baklaic, Z., Hauser, P., Roelants, P., Andre, F.E., and Safary, A. **1983**. Reactivity and immunogenicity of bivalent (AC) and tetravalent (ACW135Y) meningococcal vaccines containing O-acetyl-negative or O-acetyl-positive group C polysaccharide. *Infect. Immun.* 42 (2):599-604.
- Vollmer, W. **2008**. Structural variation in the glycan strands of bacterial peptidoglycan. *FEMS Microbiol. Rev.* 32 (2):287-306.
- Vollmer, W., Blanot, D., and De Pedro, M.A. **2008**. Peptidoglycan structure and architecture. *FEMS Microbiol. Rev.* 32 (2):149-167.
- Walker, L.M., Phogat, S.K., Chan-Hui, P.Y., Wagner, D., Phung, P., Goss, J.L., Wrin, T., Simek, M.D., Fling, S., Mitcham, J.L., Lehrman, J.K., Priddy, F.H., Olsen, O.A., Frey, S.M., Hammond, P.W., Kaminsky, S., Zamb, T., Moyle, M., Koff, W.C., Pognard, P., and Burton, D.R. **2009**. Broad and potent neutralizing antibodies from an African donor reveal a new HIV-1 vaccine target. *Science*. 326 (5950):285-289.
- Wang, J.F., Caugant, D.A., Li, X., Hu, X., Poolman, J.T., Crowe, B.A., and Achtman, M. **1992**. Clonal and antigenic analysis of serogroup A *Neisseria meningitidis* with particular reference to epidemiological features of epidemic meningitis in the People's Republic of China. *Infect. Immun.* 60 (12):5267-5282.
- Wang, L., and Reeves, P. **1998**. Organization of *Escherichia coli* O157 O antigen gene cluster and identification of its specific genes. *Infect. Immun.* 66 (8):3545.
- Westphal, O., and Jann, K. **1965**. Bacterial lipopolysaccharides. Extraction with phenol-water and further applications of the procedure. *Meth. Carbohydr. Chem.* 5: 83-91.

- Whitfield, C., and Roberts, I.S. **1999**. Structure, assembly and regulation of expression of capsules in *Escherichia coli*. *Mol. Microbiol.* 31 (5):1307-1319.
- Wyatt, R., Kwong, P.D., Desjardins, E., Sweet, R.W., Robinson, J., Hendrickson, W.A., and Sodroski, J.G. **1998**. The antigenic structure of the HIV gp120 envelope glycoprotein. *Nature.* 393 (6686):705-711.
- Zähringer, U., Lindner, B., and Rietschel, E. **1999**. Chemical structure of Lipid A: recent advances in structural analysis of biologically active molecules. In *Endotoxin in Health and Disease*: Marcel Dekker Inc., NY.
- Zehr, B.D., Savin, T.J., and Hall, R.E. **1989**. A one-step, low background coomassie staining procedure for polyacrylamide gels. *Anal. Biochem.* 182 (1):157-159.
- Zeph, L.R., and Casida, L.E. **1986**. Gram-negative versus gram-positive (actinomycete) nonobligate bacterial predators of bacteria in soil. *Appl. Environ. Microbiol.* 52 (4):819-823.
- Zwick, M.B., Labrijn, A.F., Wang, M., Spenlehauer, C., Saphire, E.O., Binley, J.M., Moore, J.P., Stiegler, G., Katinger, H., Burton, D.R., and Parren, P.W. **2001**. Broadly neutralizing antibodies targeted to the membrane-proximal external region of human immunodeficiency virus type 1 glycoprotein gp41. *J. Virol.* 75 (22):10892-10905.